Master of Science Thesis - Hydraulic Engineering

Probabilistic downtime analysis for complex marine projects

Development of a modular Markov model that generates binary workability sequences for sequential marine operations

Willem Eduard Laurens Bruijn

October 2017

Probabilistic downtime analysis for complex marine projects

Development of a modular Markov model that generates binary workability sequences for sequential marine operations

by

Willem Eduard Laurens Bruijn

to obtain the degree of
Master of Science
in Civil Engineering (track Hydraulic Engineering)
at the Delft University of Technology.

Student number:	4103343	
Project duration:	February 13, 2017 – October 20, 2017	
Thesis committee:	Prof. dr. ir. S. N. Jonkman,	TU Delft, chair
	Prof. dr. ir. P. H. A. J. M. van Gelder,	TU Delft
	Dr. ir. O. Morales-Napoles,	TU Delft
	Ir. A. J. H. Hendriks	Royal Boskalis Westminster N.V.

This thesis is confidential and cannot be made public until October 20, 2018.

"The best way to predict
your future is to create it"
- Abraham Lincoln

Preface

The report laying in front of you is the result of an eight month research at Boskalis, the Netherlands. Written as the completion of my study Civil Engineering at the Delft University of Technology, this master thesis is conducted in partnership with the Department of Hydraulic Engineering and Boskalis. I got inspired by this topic during the graduation presentation of J. Rip, because the translation of statistical complexity into understandable concepts excites me. It was the challenging and exciting topic that really got me going. However, it goes without saying that it nonetheless took some pains to eventually complete this thesis. For that reason I would like to express my heartfelt thanks to all who helped and supported me.

I would like to thank my supervisor at Boskalis, ir. A.J.H. Hendriks, for his support and the fruitful brainstorm discussions. My sincere thanks goes to prof. dr. ir. S.N. Jonkman for directing me in achievable goals, and preventing me for setting too many ambiguous goals. I also would like to thank prof. dr. ir. P.H.A.J.M. van Gelder for his creative ideas, particularly when it comes to statistics. I am grateful to dr. ir. O. Morales-Napoles for his help, especially in terms of mathematics. Last but absolutely not least, I would like to thank my friends, girlfriend and family (thanks Dad for borrowing your car) for their support throughout my thesis. Enjoy reading!

Willem Eduard Laurens Bruijn
Rotterdam, October 2017

Abstract

A complex marine project consist of series of operations, with each operation subject to a predefined operational limit and duration, depending on the equipment being used. If actual weather conditions exceed the operational limit, then the operation cannot be executed and hence downtime occurs. It is up to contractors, such as Boskalis, to accurately estimate the expected downtime in order to determine the project costs. Recently, anew tool has been developed to make downtime assessments by using the Markov theory: the so-called 'Downtime-Modular-Markov model' (DMM-model). It abstracts the actual metocean conditions by stochastically producing binary 'workability sequences' for each operation, where a distinction has been made between workable and non-workable states given an operational limit. The Markov statistics of the model are based on the characteristics of the observed metocean conditions. Complex marine project simulations are realizable based on these statistics. The purpose of this thesis is to develop the DMM-model for which a software-testing process is applied. In the verification phase the concept and the code of the model are checked on correctness, consistency and completeness. Subsequently, the validation phase addresses to the quality of the model. Three different metocean datasets are used to test the model and its individual modules whether they perform sufficiently accurate. The most important findings of both phases are tackled in the improvement & extension phase. Adjustments made during this last phase bring the DMM-model to a new state-of-the-art. It is recommended for further study to conduct an uncertainty analysis (quantify the model and parametric uncertainty).

Keywords: Complex marine project, operation, operational limit, downtime, Markov theory, Downtime-Modular-Markov model, workability sequences, simulation, software-testing, verification, validation, improvement, extension

Contents

1 Introduction **7**
- 1.1 Problem description . . . 7
  - 1.1.1 Background . . . 7
  - 1.1.2 Current approach of Boskalis . . . 8
  - 1.1.3 Downtime Modular Markov model . . . 12
  - 1.1.4 Problem statement . . . 14
- 1.2 Research description . . . 14
  - 1.2.1 Research objective . . . 14
  - 1.2.2 Research questions . . . 14
  - 1.2.3 Methodology . . . 15
  - 1.2.4 Thesis outline . . . 15

2 Downtime Modular Markov Model **17**
- 2.1 Markov theory . . . 17
  - 2.1.1 Introduction theory . . . 17
  - 2.1.2 Maximum likelihood estimate and transition matrix . . . 18
  - 2.1.3 Time-dependency . . . 19
  - 2.1.4 Chapman-Kolmogorov equations . . . 20
  - 2.1.5 Limiting probabilities . . . 22
- 2.2 Preliminaries . . . 22
- 2.3 Input data . . . 23
- 2.4 Module A: Seasonality . . . 23
- 2.5 Module B: Time-dependency . . . 25
- 2.6 Module C: Linked Markov chains . . . 25
- 2.7 Module D: Coupled operations . . . 27
- 2.8 Module E: Parallel operations . . . 28
- 2.9 Outcome . . . 29
- 2.10 Project example . . . 30
- 2.11 Conclusion . . . 31

3 Simulation **35**
- 3.1 Overview of other metocean parameter generators . . . 35
  - 3.1.1 Gaussian based models . . . 36

3.1.2 Re-sampling models . . . 36
3.1.3 Parametric models . . . 37
3.2 Uncertainty . . . 39
3.2.1 Types of uncertainty . . . 39
3.2.2 Uncertainty in models . . . 41
3.2.3 Uncertainty quantification . . . 42
3.3 Conclusion . . . 44

4 Software-testing **47**
4.1 Verification . . . 49
4.2 Validation . . . 50

5 Verification **53**
5.1 Conceptual verification . . . 53
5.1.1 Module A: Seasonality . . . 53
5.1.2 Module B: Time-dependency . . . 54
5.1.3 Module C: Linked Markov chains . . . 55
5.1.4 Module D: Coupled operations . . . 57
5.2 Model verification . . . 59
5.2.1 Module A: Seasonality . . . 59
5.2.2 Module B: Time-dependency . . . 60
5.2.3 Module C: Linked Markov chains . . . 61
5.2.4 Module D: Coupled operations . . . 61
5.3 Conclusion . . . 62

6 Validation **65**
6.1 Input data . . . 65
6.2 White-box validation . . . 67
6.2.1 Module A: Seasonality . . . 67
6.2.2 Module B: Time-dependency . . . 68
6.2.3 Module C: Linked Markov chains . . . 72
6.2.4 Module D: Coupled operations . . . 73
6.3 Data validation . . . 75
6.4 Black-box validation . . . 80
6.4.1 Different geographical locations . . . 80
6.4.2 Different project . . . 84
6.4.3 Different data . . . 86
6.5 Conclusion . . . 89

7 Extensions & Improvement **91**
7.1 Rectifications . . . 91
7.1.1 Influence period . . . 91
7.1.2 Persistency calibration . . . 93

7.1.3 Sequentially coupled operations . . . 96
7.1.4 Result . . . 97
7.2 New coding methods . . . 99
7.2.1 Initializing . . . 99
7.2.2 Generating time-series . . . 100
7.2.3 Missing data imputation . . . 100
7.2.4 Data compression . . . 107
7.2.5 Small validation . . . 108
7.3 Conclusion . . . 114

8 Synthesis **117**
8.1 Conclusions . . . 117
8.2 Recommendations . . . 120
8.3 Discussion . . . 121

A Algorithm block schemes **123**

B Improving points **127**

C Relation between P_{ij}^{pq} and π_j^q **129**

D Hypothesis testing **137**

E Validation **139**

F Extensions & Improvement **151**

Bibliography **159**

List of Figures **161**

List of Tables **161**

Nomenclature

Terminology

Actual duration	The duration to execute an operation, with delays.
Boundary states	The last state in workability sequence A, and the first state in workability sequence B.
Code uncertainty	Numerical errors and algorithmic mistakes in the source code.
Complex project	A project consisting of multiple operations (and multiple weather windows).
Continuous operation	An operation without a fixed net duration and no weather window is required, and that can be suspended if the operational limits are exceeded.
Coupled operation	If operation B must start directly when operation A has completed, then operation A is referred to as a coupled operation. If operation C must start directly after operation B has been completed, then operation A and B are coupled operations. This process can continue itself. This applies for example on the sequence of decommissioning a topside. Then operation A is cutting the legs of the jacket, followed by operation B is hoisting the topside. The topside will then be placed on a barge (operation C), followed by sea fastening the topside on the barge (operation D). For each operation a different operational limit (see below) is used and no downtime is allowed in between the operations. In this example operation A, B and C are coupled operation.
Cross-transition probability	If no influence period is scheduled, the cross transition probability determines the start state of the next operation, this is defined as the probability of having downtime at the start of a new operation.
Downtime	This can be calculated as follows: Actual duration minus net duration. Downtime can be a result of bad weather.
HADDOCK	The software program used by Boskalis to make risk assessments based on metocean data.

Influence period	See $D(p, q)$.
Marine operation	Operation of a limited defined duration related to handling of object(s) and/or vessel(s) in the marine environment.
Model uncertainty	Non-statistical errors in a simulations due to abstraction.
Net duration	The duration to execute an operation, without delays.
Observational errors	Mistakes in a data collection, which are induced by human/devices.
Operation	Similar to marine operation.
Operational limit	Some operations have an operational limit, which means they cannot be performed if this limit is exceeded. In marine operations these limits are mostly metocean parameter related, the most common limits are wave height, wave period and wind speed.
Parallel operation	If two operations are performed simultaneously.
Parametric uncertainty	The uncertainty related to the estimation of the input parameter(s) of a stochastic model.
Percentile value	The Pxx percentile duration indicates a chance of xx%, that the duration will less or equal to the Pxx value.
Persistency	Persistency refers to the time period a parameter remains below the operational limit. Several operations require a long-lasting weather window to be performed.
Project	A single operation or a series of operations which include all the operations to be executed.
Simulation uncertainty	The uncertainty related to the number of replications.
Uncoupled operation	If operation B must not necessarily start directly when operation A is completed, then operation A is referred as an uncoupled operation.
Undoubted periods	Specific states which must be workable or non-workable at time step t, because a state of a preceding operation was workable or non-workable.
Warranty window	A certain weather window, before permission is granted to start the operation, mainly used for requirements by the Marine Warranty Surveyor (MWS).
Weather window	The duration of how long a metocean parameter will remain below a critical value.
Workability	The amount of workable time steps in a time-series.

Symbols

Symbol	Unit	Description
BS^{qp}	-	The states of the first time step in the workability sequence of operation q and the last time step in the workability sequence of operation p.
$D(p,q)$	h	Influence period: the minimum number of workable time steps (hours) in operation q after a $1/0$ crossing in operation p that preceded [45], also denoted as $D^1(p,q)$.
$D^0(p,q)$	h	The non-workable influence period is equal to the minimum number of non-workable time steps (hours) in operation q after a $0/1$ crossing in operation p that preceded.
H_s	m	Significant wave height.
m	-	The month in the workability sequence $m = 1, ..., 12$.
N_i^*	-	The number of observed transitions starting from state $i \in S$ to state $j \in S$.
N_{ij}^{pq}	-	The number of observed transitions starting from state $i \in S$ in operation p to state $j \in S$ in operation q.
$N_{ij}^{\mathbf{X}}$	-	Due the implementation of the undoubted periods and influence periods, the number of transitions are defined as this parameter where $\mathbf{X}$ can be: $\mathbf{C}$ denoting the counted transitions starting from state i, $\mathbf{E}$ the expected number of transitions starting from state i and $\mathbf{P}$ the to be place number of transitions start from state i.
n_s	-	The number of states in S.
$P_{ij}, P_{ij}(t)$	-	The transition probability of moving from state $i \in S^u$ to state $j \in S$.
P_{ij}^{pq}	-	The cross transition probability of moving from state i in operation p to state j in operation q [45].
Q_{ij}	-	The transition probability matrix of the Markov Dependency method.
S	-	State space of the Markov chain.
t	-	The time step in the workability sequence $t = 1, ..., T$.
T_p	s	The peak wave period.
u	-	The order of the Markov chain.
U	m/s	The wind speed.
$U(p,q)$	h	Undoubted period: The number of time steps (hours) that are implemented for a succeeding operation, because specific time steps cannot be any other state.
v	m/s	Surface current velocity.
X_t	-	The state of workability sequence of the discrete random variable X at time step t.

α	-	The significance value; 0.05 assumed in this thesis.
π_j	-	Limiting probability of state $j \in S$: the probability that workability sequence is in state $j \in S$ independent of a previous state.
χ^2	-	The Chi-squared statistic used for hypothesis tests.

Abbreviations

ARMA	Autoregressive moving-average
DWK inequality	Dvoretzky-Kiefer-Wolfowitz inequality
DMM-model	Downtime Modular Markov model
ECDF	Empirical cumulative distribution function
HED	Hydronamic Engineering Department (of Boskalis)
MetOcean	Meteorology & Oceanography
MD	Markov Dependency
MP	A monopile for the foundation an offshore wind turbine
MLE	Maximum likelihood estimate of the transition probabilities $\hat{P}_{ij}$
MWS	Marine Warranty Surveyor
NTH	Non-time homogeneous
O	Order of the Markov chain
PWTH	Piece-wise time homogeneous
RMSE	Root mean square error: measure for the difference between values in the observed and predicted by the model or estimator.
TP	A transition piece for the foundation an offshore wind turbine
UCMP	Updated Conditional Markov Probability
V&V	Verification & Validation
WoDS	West of Duddon Sands (project)

Executive summary

A complex marine project consist of series of operations, for instance the installation of an offshore windmill foundation: sailing to project site, installing the monopile, placing the transition piece, sailing to harbor. Each operation is subject to a predefined operational limit and duration, depending on the equipment being used. An operational limit is for example $H_s \leq 1.5$ m, which means the operation can only be executed if the significant wave height is below 1.5 meters. If actual weather conditions exceed the operational limit, then the operation cannot be executed and hence downtime occurs. It is up to contractors, such as Boskalis, to accurately estimate the expected downtime in order to determine the project costs. Boskalis' current method to make these downtime assessments is by means of an in-house software tool: HADDOCK. HADDOCK is a simulation tool performed directly upon observed/hindcast data. In other words, it simulates projects on the past and no information is provided about the future, which means the number of project realizations is equal to the number of available years in data. Recently anew tool has been developed, which is called the 'Downtime-Modular-Markov model' (DMM-model) to make downtime assessments. It is a stochastic model that produces synthetic time-series with the same characteristics of the observed/hindcast metocean conditions. With the DMM-model more project simulations are possible, which reduces the simulation uncertainty. However, by using a stochastic simulation model other uncertainties are introduced (Chapter 3):

- Simulation uncertainty: the uncertainty related to the number of project simulation replications. The more project replications, the lower simulation uncertainty.
- Parametric uncertainty: the uncertainty related to the estimation of the input parameter(s) of the stochastic model [20]. The more input parameters and/or the less data on which the parameters are estimated, the higher the parametric uncertainty.
- Model uncertainty: the uncertainty described by non-statistical errors in abstraction [61]. The more complex the model, the higher the uncertainty.
- Observational errors: mistakes in data collection.
- Code uncertainty: the numerical uncertainty related to errors and algorithmic mistakes. The less errors, the lower the uncertainty.

The first three uncertainties describe the main uncertainties, which are recommended to quantify. Observational errors are not considered to influence downtime estimations and code errors should rather be rectified instead of quantified. However, the model-user should be aware of these uncertainties. The purpose of this thesis is to develop the DMM-model for which a software-testing process consisting of 3 phases is applied. In the verification phase the concept and the code of the model are checked on correctness, consistency and completeness. Subsequently, the validation phase addresses to the quality of the model. Three different metocean datasets are used to test the model and the individual modules its based on whether they perform sufficiently accurate. The most important findings of both phases are tackled in the improvement & extension phase. Adjusting the DMM-model during this last phase brings the model to a new state-of-the-art.

The DMM-model is a discrete-time 2-state-Markov model, which abstracts the actual metocean conditions into workable states '1' and non-workable states '0' depending on the operational limit. A so-called 'workability-array' is created from the hindcast data and the operational limit, which consists only of binary data. Hence, the information about the actual metocean parameter is lost. Based on the statistics within the 2-state workability-array, the model is able to produce stochastically binary 'workability sequences' for each operation. Even when an operation is limited to two or more parameters, the model is still able to produce binary time-series for the specific operation and no dependencies need to be modelled.

Figure 1 represents how the 'transition probabilities' P_{ij} are defined for a 1st-order Markov chain with the workability states $\{0, 1\}$. It shows that the next state j at time step $t+1$ is depended on the current state i at time step t. These transition probabilities can be estimated on the created workability-array. Additional to the transition probabilities, there are some modules created which form the complete DMM-model. When a module is being used, depends on the operations in the project and the metocean dataset. In the following, the use of each module will be explained with some important findings of the verification and validation phase.

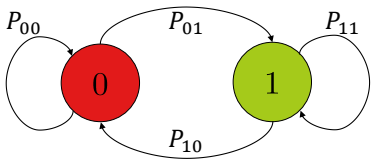

Figure 1: A 1st-order Markov chain example with 2 states and the transition probabilities P_{ij}

- *Module A: Seasonality.* In order to take seasonality into account, probabilities are varied over the year. This happens either 'piece-wise time homogeneous', where the probabilities are constant per month or this happens 'non-time homogeneous', where the probabilities are constant per day. Despite some small coding errors this module works sufficiently accurate, however it can be extended by including weekly or seasonal homogeneous probabilities.

- *Module B: Time-dependency.* The next state X_{t+1} could also be dependent on the current state X_t and even more previous states $X_{t-1}, X_{t-2}, ..., X_0$. The Markov

chain order determines on how many states the next state is based. It captures the autocorrelation of the metocean parameter and in the validation phase it is found that the 'persistency' is also more accurately preserved by increasing the Markov chain order. Increasing the Markov chain order is only possible in the piece-wise time homogeneous function, since the non-time homogeneous function is limited to the 1st-order.

- *Module C: Physical feasibility in linked chains.* If an operation is finished, a link must be formed between the finished operation and the succeeding operation in order to continue the project evolution. For that purpose the 'influence period' $D(p, q)$ is applied, which is defined as the time period between the 1/0 crossing of operation p till the 1/0 crossing of operation q. From all the observed influence periods in hindcast data, the 'reasonably' smallest (where the exceedance probability equals 0.98) is implemented. It denotes the minimum amount of workable states for the next operation. This happens for example in case the first operation has a limit of $H_s \leq 1$ m and the succeeding operation has a limit of $H_s \leq 3$ m. The influence period avoids that the next time step $t + 1$ of the succeeding operation can be a non-workable state, when the current time step t of the current operation was a workable state. That would mean that the sea conditions change within an hour from below a significant wave height of 1 meter, to above a significant wave height of 3 meters, which is unrealistic. In case the influence period is zero, the 'cross-transition probability' P_{ij}^{pq} is being used, which is estimated similar as the 'regular' transition probabilities on hindcast data.

- *Module D: Coupled operations.* Between the coupled operation and the succeeding operation *no* downtime is allowed, i.e. the succeeding operation *must* start *directly* when the current operation has finished. It is validated that this module does not work at all. In advance it needs to be determined how many (sequentially) coupled operations are present in the project. These (sequentially) coupled operations need to be simulated simultaneously, so that a calm weather window can be found where no downtime occurs in between the operations.

- *Module E: Parallel operations.* This module has been disregarded as Boskalis does not perform parallel operations.

Next to the DMM-model two other approaches have been studied, which segregate the generation of time-series and the project simulation: the 'Updated Conditional Markov Probabilities' (UCMP) and the 'Markov Dependency' (MD). The main advantage of these methods is that coupled operations can be simulated and any start date can be chosen; the DMM-model is bounded to a specific start date. Based on a small validation with 5 operational limits (H_s, T_p and U, and combinations of these) on an offshore location, it can be concluded that the UCMP method did not show any promising results. This in contrast to the MD method, which yielded in promising results in terms of persistency preservation. However, here, the workability percentage is less accurate preserved. Therefore

it is recommended to continue studying the MD method and to improve the workability percentage preservation.

The conclusions and recommendation considered to be most important are:

- Section 5.1.3 explains the mistakes of the influence period in the old model. Therefore it is redefined in Section 7.2, which explains that in the improved model the 'reasonably' smallest influence period is implemented instead of a randomly chosen influence period from the exceedance probability curve.
- A higher Markov chain order resulted in a better preservation of persistency (Section 7.1.2), while the old model was limited to a 2nd-order.
- The coupled operation module did not work at all, and the theory of solving this is provided in Section 7.1.3. It is recommended to recode this module to make it workable.
- It is recommended to quantify the model and parametric uncertainty; Section 3.2.3 creates a basis for this purpose.

The added value of the DMM-model regarding downtime analysis in general, is that there was no stochastic model in current literature to simulate complex marine projects. It is still believed that the reduced simulation uncertainty has more value than the increased parametric and model uncertainty in the DMM-model. These other 2 uncertainties can be controlled by means of the model settings.

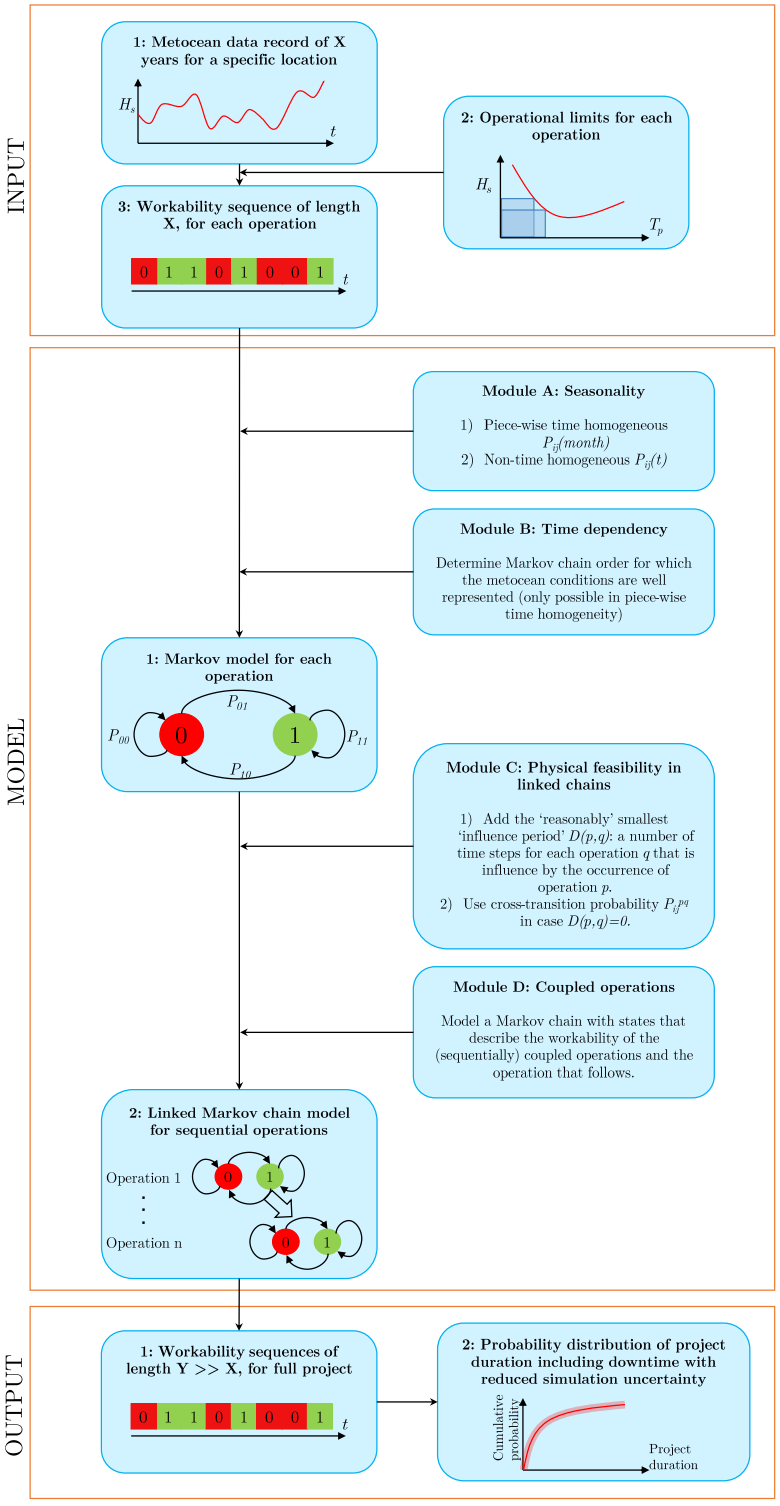

Figure 2: The new breakdown of the DMM-model for complex marine projects based on Rip [45].

1 Introduction

1.1 Problem description

Section 1.1.1 will start with the background of this thesis. Section 1.1.2 describes how Boskalis is currently conducting risk assessments. Section 1.1.3 introduces a new model which makes risk assessments.

1.1.1 Background

Marine projects are usually acquired by means of tenders which include the project cost. The project cost is related to the project duration. The longer the project takes, the more it costs logically. The project duration is in turn dependent on, amongst others, the intended equipment, the project location and the sequence of operations. For example, it can be imagined that heavier equipment speeds up the project, but at the same time the costs go up because heavier equipment is more expensive. Also, a far distant location results in more sailing hours and critical operations, such as lifting a topside which must be executed with caution, can influence the project duration.

Figure 1.1 depicts a project flowchart, from the project planning to execution. In the beginning of a project a deterministic planning is made, which is only dependent of the sequence of operations, the equipment that is intended and the project location. The deterministic planning does not contain weather risks. Bad weather may influence certain operations (e.g. if the wind blows too hard, hoisting activities cannot be executed). To incorporate the risks, a probabilistic project planning is made. Within the risk model a distinction is made between external (e.g. bad weather) and inherent (e.g. engineering complexity) uncertainties of activities. As a project manager strives to reduce weather risks, based on the risk model the sequence of operations or the intended equipment can be adapted in order to optimize the probabilistic project planning. He could hire more advanced equipment or start the project earlier, so that the specific operations could be performed in calmer periods. After the project is executed the actual duration and actual cost are known. The aim of the project planning is to estimate these as accurate as possible. The result of the probabilistic project planning is not a single project duration, in contrast to the deterministic project planning, but the result is rather a probability distribution of possible durations.

In the weather risk assessments '**downtime**' is estimated. Downtime is expressed as the time an operation cannot be executed due to unfavorable weather conditions. By estimating an accurate project downtime (consult Section 1.1.2 for more information about downtime), a better cost estimate can be made. For example, if *less* downtime occurs than expected, the project duration in the tender is too long and the tender price too high. This could lead to a 'lost' tender. On the flip side, if this leads to an acquired tender, more costs are saved. And the other way around, if *more* downtime occurs than expected, the project duration in the tender is too short and the tender price too low. Either way, an inaccurate downtime estimation can result in a bad outcome and therefore downtime assessments are important for any marine contractor.

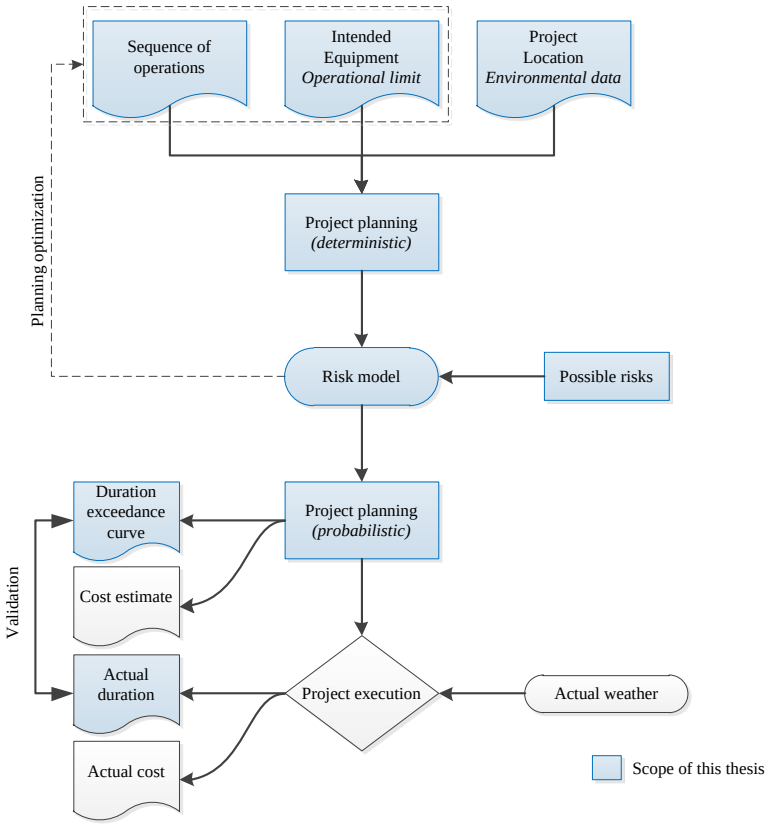

Figure 1.1: From deterministic to probabilistic project planning to project execution [45]

1.1.2 Current approach of Boskalis

Royal Boskalis Westminster (hereinafter referred to as 'Boskalis') is a global maritime services company, executing projects relating to the construction and maintenance of

maritime infrastructure. The expansion of the Suez Canal or the installation of the Veja Mate offshore wind farm are two examples of projects executed by Boskalis. Boskalis uses the Design-Bid-Build[1] method for projects, also known as Design-Tender method. The in-house engineering department Hydronamic Engineering Department (HED), has a dedicated Metocean (Meteorology & Oceanography) & Data Engineering team to perform weather risk assessments, which are instructed by the Tender Department.

The software package HADDOCK is used to perform the weather risk assessments for Boskalis. It simulates a sequence of operations and their operational limits using historical weather data (hindcast data). This is explained with Figure 1.2. In this example there is an '**operational limit**' of $H_s = 2$ m. Whenever a significant wave height is larger than 2 meters, the operation cannot be (safely) executed with the intended equipment. For a lower significant wave height, vice versa. For the given time steps the binary '**workability sequences**' are given. The dataset is dichotomized by denoting a '1' for the workable time steps, and a '0' for non workable time steps. In HADDOCK the workability percentage is calculated as follows:

$$Workability = \frac{\text{no. of workable time steps (green)}}{\text{total length of time series}} * 100\% = \frac{9}{20} = 45\% \qquad (1.1)$$

In this example 120 hours of 6-hourly data is evaluated for only one metocean parameter (H_s). In real projects datasets consisting of more metocean parameters of approximately 20 years are used. Depending on the project that needs to be performed, more operational limits can be set (e.g. wind speed, wave direction, current velocity, etc.); even combinations of metocean parameters are possible for a single operation. In this thesis the operational limits are given by Boskalis. The determination of these limits is not within the scope.

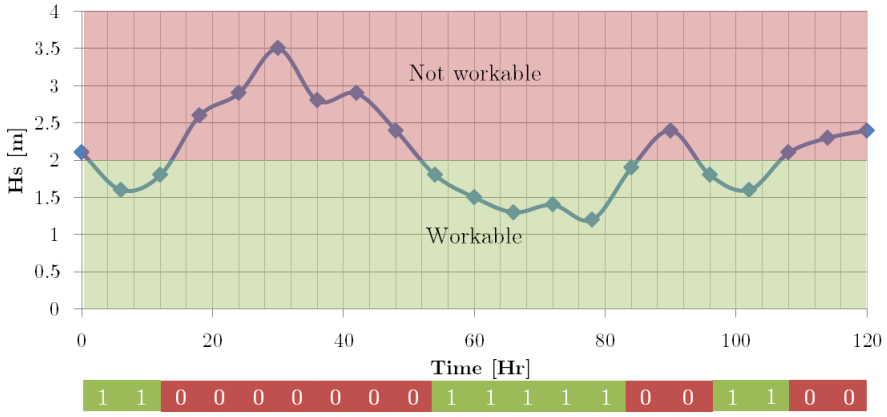

Figure 1.2: An example of how to get from an operational limit to a workability sequence

[1]Design-Bid-Build method is a traditional method to deliver a project and consist of three sequential phases: designing phase, bidding (tender) phas and the construction phase.

Boskalis distinguishes three types of projects: continuous projects, single weather window project and complex projects. A '**continuous project**' is a project with an operational limit which can be interrupted due to weather downtime. Dredging or rock dumping activities are examples of a continuous project. For this type of projects the weather risk is expressed as workability. The '**net duration**' is defined as the time required to complete an operation without any delay. Suppose the net duration is 24 hours in the example from Figure 1.2, which is equal to 4 workable time steps (each time step is 6 hours). The result is that the operation is finished after 66 hours (11 time steps), this is defined as the '**actual duration**' (duration with weather delay). This means that 42 hours of '**downtime**' (actual duration – net duration) has occurred and the workability is changed to: $\frac{4}{11} = 36\%$. Note that the workability percentage will change if the operation is started at a different time step.

A '**single weather window project**' is required for projects that need at least a predetermined period to execute the operation given that the operational limit will not be exceeded during this period (e.g. heavy-lifts or offshore piling). If the weather conditions are in a workable state but the forecasted conditions are not sufficient for the net duration, the operation will not be executed ('**waiting time**' occurs). In Figure 1.3 an example of a single weather window is given (the net duration is 4 time steps in this example). The operation cannot be executed any earlier, considering the two non-workable time steps. The workability percentage does not correspond with the actual downtime for these type of projects. The downtime for this type of projects is referred as '**persistency**'. It corresponds to the occurrence of long-lasting (persistent) good weather conditions [56].

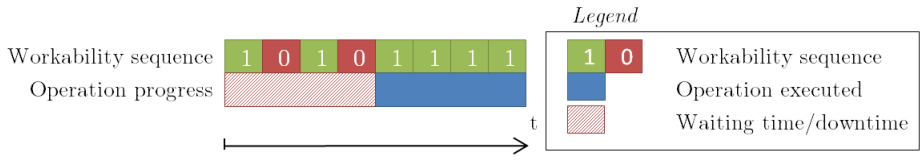

Figure 1.3: Hypothetical example of a single weather window project with a net duration of 4 time steps adopted from Rip [45]

In this thesis the main focus is on '**complex projects**'. Complex projects consist of series of operations, for example the installation of the foundation of an offshore wind farm. In this project the operations can be as follows:

1. load up foundations from quay onto vessel
2. sailing to installation site
3. jack-up
4. install foundation
5. jack-down
6. sail back to port

In case of installation of multiple foundations (multiple operations are repeated) for the wind turbines, one speaks of '**cyclic projects**'. In complex projects more operations are executed, therefore multiple weather windows need to be available, i.e. multiple durations of

(a) metocean parameter(s) have to remain below a critical value(s).

In case an operation *must* start *directly* after completing the preceding operation, it is referred as a '**coupled operation**'. For example after placing a transition piece (TP) on a monopile (MP) for an offshore wind turbine, the TP has to be grouted immediately. In other words, the placing of the TP is not allowed to start, if the operational limit of grouting the TP is exceeded after placing it. An '**uncoupled operation**' is an operation which does not necessarily have to be followed directly by the next operation, like jacking up. Coupled operations result in more downtime, since longer weather windows are needed.

A Marine Warranty Surveyor (MWS) is an independent third-party who provides '**warranty windows**'. A warranty window is defined as the minimum hours that need to be available before permission is granted to start an operation. The warranty windows are usually based on safety reasons or contingencies that may occur during an operation. Therefore, the warranty window is longer than the net duration.

To clarify some of the aforementioned definitions, an example of a hypothetical complex project is used which is shown in Figure 1.4. On the left three different operations are given, each with a different operational limit. Operation 1, which is a coupled operation, has a net duration of five time steps. Considering it is a coupled operation, it could not start any earlier, else operation 2 would encounter downtime. After completing operation 1, operation 2 can start directly. Operation 2 is an uncoupled operation and has a net duration of three time steps. After completion of operation 2, operation 3 cannot start directly because the operational limit was exceeded which resulted in the non-workable state. The MWS provided a warranty window of three time steps for operation 3, while the net duration was only two time steps. For these reasons operation 3 experiences two time steps of downtime. The total downtime in this hypothetical project is seven time steps.

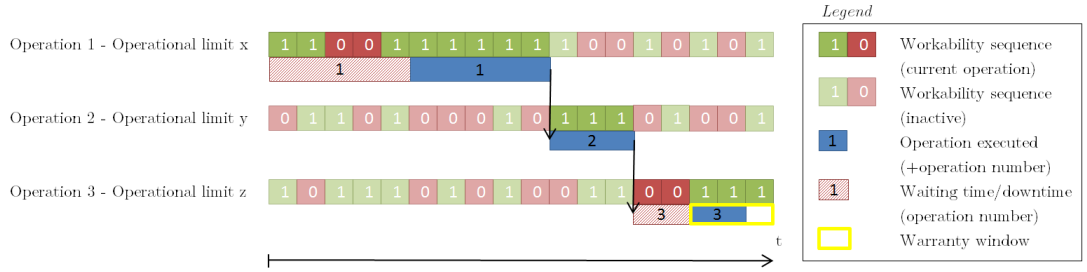

Figure 1.4: Hypothetical example of a complex project with a coupled operation 1 and uncoupled operation 2 and a warranty window provided for operation 3 [56]

For complex projects the total downtime of the project is assessed, as in the example above. It is also interesting to have a closer look at the downtime of each operation apart. In this way one can tell which operation is most vulnerable to downtime. In the same manner downtime per cycle can be assessed, and it can be determined which cycle was the most vulnerable to downtime. The way to describe downtime for complex projects is based on '**percentile values**'. A percentile value gives the chance that the project duration is less or

equal than the given value, based on the duration realizations. Hence, a P50 means there is 50% chance the duration of the project is less or equal than the P50 value. The P50 value can be expressed in any time unit (e.g. hours, days). The percentile graph (Figure 1.5) depicts the cumulative probability distribution: $P(duration \leq P50) = 0.5$. Generally, the P50 or P80 values are used to determine the project duration, the choice is up to the client. Additionally, a persistence table and a graph describing the influence of the start date can be delivered as output for a project.

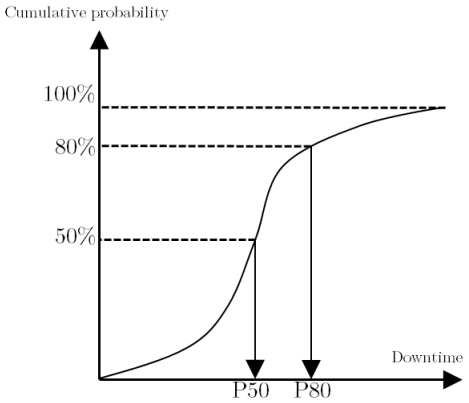

Figure 1.5: Hypothetical example of the cumulative distribution of downtime of a project (P50 and P80 indicated)

1.1.3 Downtime Modular Markov model

The current method Boskalis uses for the determination of workability is analytical, while the determination of downtime happens through simulation. First, a distinction has to be made between simulation and analytical methods. Analytical methods use anything from algebra to differential equations, but no probability/statistics is used. The solutions of analytical methods are typically exact solutions, where the parameters correspond directly to physical processes. There are some analytical methods available in literature to assess downtime of complex projects [5], but these are disregarded in this thesis since they can become very complex with multiple operations subject to multiple operational limits. Simulation on the other hand, approximates analytical problems by means of probability/statistics. Boskalis uses hindcast data in order to obtain the workability/persistency/downtime of complex projects. Simulation is a technique of conducting realizations using a model to figure out the behavior at different environments. The selection of a method depends on several factors, such as the available hindcast data, desired accuracy and available time to do the analysis. These factors must be discussed and weighed between the Tender Department and Hydronamic Department, in order to choose which type of downtime method should be used. For complex projects the use of simulation technique is preferred because of the analytical complexity as explained. The downside of these simulations on hindcast datasets is that these datasets only consist of 10-25 years of data. This may sound like a big dataset, but

the opposite is true for complex projects. Due to the presence of seasonality effects a project has to start each year at the same date of the year. This results in the same number of project realizations as the number of available years in the dataset. Simulating this number of project realizations will give a large probability distribution of the project durations. The more years available, the more accurate the probability distribution can be estimated. This principle is referred to as '**simulation uncertainty**'. It can be compared to coin tossing: if the coin is tossed 10 times, the outcome does not have to be 5 times heads and 5 times tails, knowing that the probability a head/tail appears is 0.5 of a fair coin. When the coin is tossed a 1000 times, the probability of a head or a tail will be close to 0.5. For this reason, a stochastic data generator, the so-called 'Downtime Modular Markov model', is modelled to augment the existing datasets in order to obtain more project realizations.

The Downtime Modular Markov model (hereinafter referred to as DMM-model) is a model that estimates the project duration and the downtime for projects of Boskalis. The basis for the DMM-model has already been programmed in Rip [45]. This model abstracts the actual metocean conditions by producing binary workability sequences for a single operation and for series of operations (complex projects). By means of the Markov theory a dataset of metocean parameters is statistically enlarged. With a larger dataset more project simulations can be realized, thereby a more accurate result for the expected project downtime can be estimated (this is schematized in Figure 1.6). Several modules have been made in order to make the model more realistic (e.g. introducing seasonality). In Chapter 2 the DMM-model will be further discussed.

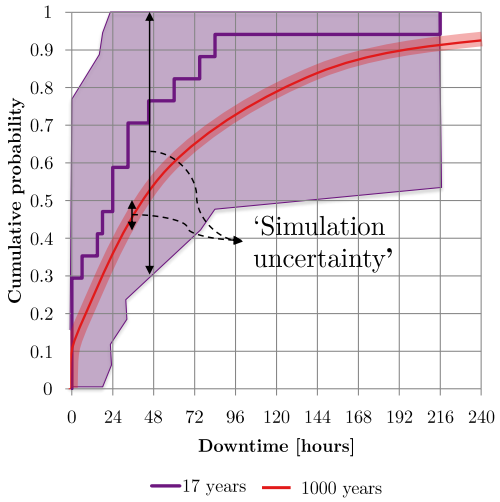

Figure 1.6: Hypothetical example of the purpose of the DMM-model; by enlarging the dataset, the simulation uncertainty reduces

1.1.4 Problem statement

In tender phases of projects accurate information about downtime is important (as explained in Section 1.1.1). The current approach of Boskalis is to simulate complex projects directly on the hindcast data, which causes a high simulation uncertainty. Recently, the DMM-model is created in order to reduce this uncertainty, by stochastically producing workability sequences for sequential operations in complex projects. The first study of this model yielded in promising results to assess the project duration/downtime. However, an extensive validation study is needed before such a new model can be practically implemented. A software-testing process is applied for that purpose (Chapter 4). Such a process consists of a verification and validation phase (Chapter 5 and 6). The verification process assesses the DMM-model on its correctness, consistency and completeness, where the validation process analyzes whether the DMM-model works sufficiently accurate. From this study the model can be further improved and extended, hence the reliability of a computer model increases and it brings the DMM-model one step closer to implementation.

1.2 Research description

1.2.1 Research objective

The basis of the DMM-model is readily available. The objective of this thesis is to further develop it. It needs to be determined whether the theories are correctly implemented and whether the model and its modules are working sufficiently accurate. Recommendations need to be made on how to further improve the model, and it needs to be concluded whether it is still believed that the model is of additional value regarding weather risks.

1.2.2 Research questions

1. Literature study:
   (a) How can downtime be analyzed with the current DMM-model?
   (b) Which methods for metocean parameter generators can be found in literature?
   (c) Is it possible to quantify uncertainties concerning the DMM-model?
2. Verification:
   (a) Is the concept and the model code of the current DMM-model correct, consistent and complete?
3. Validation:
   (a) Do the DMM-model and its individual modules perform sufficiently accurate?
4. Improvement and extensions:
   (a) How can the current DMM-model be improved/extended?

1.2.3 Methodology

In order to answer the research questions from above, this thesis will be conducted in the following steps (in Figure 1.7 these steps are indicated blue encircled numbers):

1. Understanding of the work methods of Boskalis regarding workability and downtime.
2. Analyzing the current DMM-model and the underlying Markov theory it is based on.
3. Creating an overview of other stochastic metocean parameter generators, like the DMM-model.
4. Analyzing other uncertainties that are present in the model and its parameters.
5. Conducting a concept and model verification of the DMM-model per module.
6. Validating the modules of the DMM-model separately (White-box validation).
7. Validating the total DMM-model, based on its input data and output (downtime distribution).
8. Analyzing the results of the verification and the validation phase. From these results improvements and extensions are made regarding the model.
9. Making recommendations about the improvement of the DMM-model and conclude whether the model is valuable for Boskalis to perform weather risk assessments.

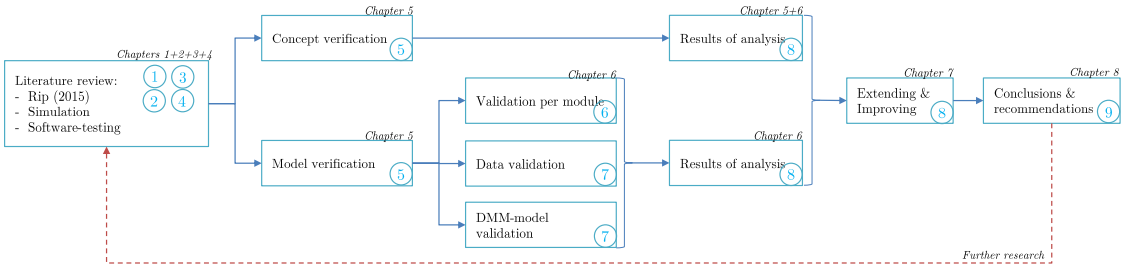

Figure 1.7: Framework of the methodology of this thesis combined with the chapter layout. The red line indicates the same methodology can be applied for further research. The blue encircled numbers indicate the steps from above.

1.2.4 Thesis outline

To answer the research questions and the set goals, this thesis is organized in the following way: Chapter 1 describes the problem definition with its research questions and introduces the work-methods to analyze downtime for marine projects. In a previous study another model (the DMM-model) is developed to estimate downtime based on the Markov theory.

Chapter 2 describes the Markov theory and analyzes the DMM-model. It is recommended to understand the basis of the DMM-model while reading this thesis, therefore it is essential that this chapter is well-understood. An overview of other metocean parameter generators (such as the DMM-model) is given in Chapter 3 as part of the literature study. The purpose of this thesis is to further develop the DMM-model. By doing so, a software-testing process is followed, which is explained in Chapter 4. It starts with a verification of the software, which is conducted in Chapter 5. Thereafter, a validation is conducted in Chapter 6. Based on the results of the verification and validation process improvements and extensions can be made for the DMM-model, which are clarified in Chapter 7. Lastly in Chapter 8, conclusions of the thesis and recommendations for further research are provided.

2 Downtime Modular Markov Model

This chapter aims to answer the research question No. 1a: '*How can downtime be analyzed with the current Downtime Modular Markov model?*'. The DMM-model is a computer model with algorithms and equations based on the Markov theory that tries to capture the downtime behaviour of marine projects. The Markov theory will be introduced in Section 2.1. Several assumptions and requirements are stated in order to make the DMM-model functional (Section 2.2). The input data consists of metocean historical datasets near the project locations (Section 2.3). Subsequently, each module on which the DMM-model is based will be outlined in Sections 2.4 - 2.8. In Section 2.9 is explained what the output is of the DMM-model. In order to visualize how projects are simulated, an example is provided in Section 2.10. In final Section 2.11 an answer is given to the research question.

2.1 Markov theory

Markov analysis is a probabilistic method which can be compared to decision analysis[1]. The difference lies in that Markov analysis provides probabilistic information about the decision, which helps the decision maker in making a decision. In Section 2.1.1 the introduction of the Markov theory will be described, and in Section 2.1.2 the maximum likelihood estimate is described. Finally, the time-dependency, the Chapman-Kolmogorov equations and the limiting probabilities are described in Section 2.1.3, 2.1.4 and 2.1.5 respectively.

2.1.1 Introduction theory

The Markov process is a type of stochastic or random process, that has the property to make the next value of the process dependent of the current value. This theory is explained by using the book of Ross [47] and Taylor III *et al.* [53]. Consider that $X = (X_t : t \in T)$ is a stochastic process on a probability space, with discrete time step $t = 0, 1, 2, ..., T$. Random variable X_t can be interpreted as the 'state' of the system at time step t, within 'state space' S. The most simple example of the Markov chain is with two states $S = \{0, 1\}$,

[1] Decision analysis: the discipline compromising the philosophy, methodology, a collection of systematic procedures to address complex decisions in a formal manner [26].

where state 0 denotes non-workable and state 1 denotes workable. Between these states transition probabilities are present, P_{ij}, such that the current state is i and the next state is j. More than two states are possible too, then the transition probabilities are given as: $P_{ij}, \quad \forall i, j = 0, 1, ..., N$.

$$P\{X_{t+1} = j | X_t = i, X_{t-1} = i_{t-1}, ..., X_1 = i_1, X_0 = i_0\} = P_{ij} \quad \forall i, j \in S, t = 0, 1, ..., T \tag{2.1}$$

Equation 2.1 states that the future state X_{t+1} is independent of the past states $X_0, X_1, ..., X_{t-1}$ and solely depends on the present state X_t. The Markov chain constitutes a collection $X_t, t \geq 0$ having the transition probabilities $P_{ij}, \quad \forall i, j = 0, 1, ..., N$. Figure 2.1 clarifies the two state example with the workable and non-workable states. The transition probabilities are indicated with arrows. The first subscripted number is the start state and the second subscripted number is the end state.

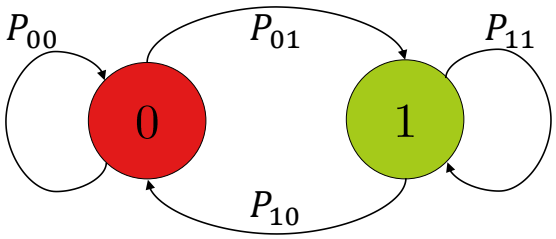

Figure 2.1: A first-order Markov chain example with 2 states and the transition probabilities P_{ij}

2.1.2 Maximum likelihood estimate and transition matrix

The transition probabilities P_{ij} can be estimated from the observed transitions [52]. The *maximum likelihood estimate* (MLE)[2] of the transition probabilities can be computed as follows:

$$\hat{P}_{ij} = \frac{N_{ij}}{N_i^*}, \quad \forall i, j \in S \tag{2.2}$$

In this equation the N_{ij} is the number of transitions from state i to state j and N_i^* is equal to the total number of transitions that start from state i. The transition matrix can be obtained from the given transition probabilities. In Equation 2.3 a two state (left) and any higher order state (right) transition matrix is given:

[2]The most likelihood estimation is a statistical method of estimating population characteristics given a sample by finding the parameter values that maximize the probability of getting the particular sample actually obtained from the population [18].

$$P_{ij} = \begin{bmatrix} P_{00} & P_{01} \\ P_{10} & P_{11} \end{bmatrix} \qquad P_{ij} = \begin{bmatrix} P_{00} & P_{01} & P_{02} & \dots \\ P_{10} & P_{11} & P_{12} & \dots \\ \vdots & \vdots & \vdots & \\ P_{i0} & P_{i1} & P_{i2} & \dots \\ \vdots & \vdots & \vdots & \end{bmatrix} \tag{2.3}$$

Given that probabilities are positive and the process must be in some state after leaving state i, the following holds:

$$\sum_{j \in S} P_{ij}(t) = 1, \qquad \forall i, j \in S \tag{2.4}$$

In Section 1.1.2 is explained that the workability is defined binary over time. The information about the wave height or any other metocean parameter is disregarded because it is irrelevant. The only relevant information is whether, under the metocean conditions, the operation can be performed or not; this binary workability indicates the 'states'. This principle is also used in stock market analysis, where the price is not relevant but only the change of the price (the stock price might go up or down). Based on a hypothetical metocean historical dataset, the following workability sequence is observed:

0 0 1 1 0 0 0 1 1 0 0 0 0 1 1 1 0 1 1 1 1

With $N_{00} = 6$; $N_{01} = 4$; $N_{10} = 3$; $N_{11} = 7$ and $N_1^* = 10$; $N_0^* = 10$ the maximum likelihood estimate can be calculated: $P_{00} = \frac{6}{10}$; $P_{01} = \frac{4}{10}$; $P_{10} = \frac{3}{10}$; $P_{11} = \frac{7}{10}$. Note that the last state is not included in the number of start states. With these probabilities the following transition matrix (Equation 2.3) is defined:

$$P_{ij} = \begin{bmatrix} 0.6 & 0.4 \\ 0.3 & 0.7 \end{bmatrix} \tag{2.5}$$

The summation of each row equals a probability of 1. The table can be interpreted as follows: if the current time step is non-workable, the probability to stay in a non-workable state equals 0.6 (transition probability P_{00}) and to go to a workable state equals 0.4. In the same manner the transition probabilities for a workable sea state are indicated.

2.1.3 Time-dependency

A Markov chain can be *time-dependent*, unless the observations are independent of the past or present. In that particular case, the given time independent sequence is for example a random walk. This can be interpreted as a model for an individual walking on a straight line, who at each time step either takes a step to the right with probability p or a step to the left with probability $1 - p$. For metocean parameters this does not hold; they are time-dependent. This dependency is determined on how many time steps influence the next

transition, thereby the 'order' of the Markov chain is introduced. By increasing the Markov chain order (i.e. making the next state dependable of more time steps), the autocorrelation is captured. Figure 2.1 presents a 1-time step dependency, where the next time step is influenced by the current time step. Suppose that state 1 is a rainy day and state 0 a sunny one. Now suppose that the transition probability to go to a sunny day starting from a rainy day (P_{10}) is α and to go to a rainy day starting from a sunny day (P_{01}) is β. Then, the left transition matrix in Equation 2.3 can be filled in, with the remaining probabilities $(1-\alpha, 1-\beta)$. The time-dependency can be extended, if for example the next sunny/rainy day is dependent on the past 2 (or more) days. By increasing the time-dependency, the transition matrix increases as well. The left matrix in Equation 2.3 is a 1st-order chain, where X_{t+1} only depends on the value of X_t. Higher order chains can be obtained, where X_{t+1} depends on $X_t, X_{t-1}, ..., X_{t-(u-1)}$ with u denoting the number of the order chain. The most likelihood of Equation 2.2 changes to:

$$\hat{P}_{ij....kl} = \frac{N_{ij...kl}}{N^*_{ij...k}}, \quad \forall i, ..., k \in S \tag{2.6}$$

Consider the aforementioned hypothetical observed workability sequence and suppose that the time-dependency is of order 2. This implies that the next state depends on the past 2 states (X_t, X_{t-1}). The following transitions can be observed: $N_{000} = 3, N_{001} = 3, N_{010} = 0, N_{011} = 4, N_{100} = 2, N_{101} = 1, N_{110} = 3, N_{111} = 3$. The following 2-start-states can be observed: $N^*_{00} = 6, N^*_{01} = 4, N^*_{10} = 3, N^*_{11} = 6$. From these observations the maximum likelihood estimate (Equation 2.6) can be calculated: $P_{000} = \frac{3}{6}, P_{001} = \frac{3}{6}, P_{010} = 0, P_{011} = 1, P_{100} = \frac{2}{3}, P_{101} = \frac{1}{3}, P_{110} = \frac{3}{6}, P_{111} = \frac{3}{6}$. The resulting transition matrix of the 2nd-order Markov chain can be indicated as follows:

Table 2.1: Transition matrix of 2nd-order Markov chain

	Next time step:			
Current time step:	00	01	10	11
00	P_{000}	P_{001}	0	0
01	0	0	P_{010}	P_{011}
10	P_{100}	P_{101}	0	0
11	0	0	P_{110}	P_{111}

Note that, the summation of probabilities on each row equals 1 again.

2.1.4 Chapman-Kolmogorov equations

With the Chapman-Kolomogorov equations the limiting probabilities (Section 2.1.5) can be obtained. In the foregoing one-step transition probabilities P_{ij} have been used. The n-step

transition probabilities P_{ij}^{n}, the probability that a process in state i will be in state j after n transitions, are defined by the Chapman-Kolmogorov equations:

$$\begin{aligned} P_{ij}^{n+m} &= P\{X_{n+m} = j | X_0 = i\}, \\ P_{ij}^{n+m} &= \sum_{k \in S} P_{ik}^{n} P_{kj}^{m} \quad \forall n, m \geq 0, \forall i, j \in S \\ P_{ij}^{n+m} &= P_{ij}^{n} \cdot P_{ij}^{m} \end{aligned} \tag{2.7}$$

This can be interpreted as going from state i to state j in $n+m$ steps (with an intermediate stop in state k after n steps. Summing over all possible k values gives P_{ij}^{n+m}.

By multiplying the transition matrix P_{ij} n times by itself the n-step transition matrix is obtained. This is clarified with the two-state example of Table 2.1. Suppose that the current state is workable '1'. In Figure 2.2 the transition probabilities are visualized for the current and next time steps ($t, t+1$ and $t+2$). The transition probabilities at time step: $t+2$ become 0.49, 0.21, 0.12 and 0.18. Note that the summation of these probabilities is equal to 1 again. The probability that the state after 2 time steps is workable again is 0.49 + 0.12 = 0.61 and non-workable 0.21 + 0.18 = 0.39. The following n-step transition matrix is obtained (with $n = 2$ in this case). In the lower row of the matrix the two transition probabilities starting from a workable state are given. The same approach can be applied with a non-workable starting state.

$$P^{(2)} = \begin{bmatrix} 0.48 & 0.52 \\ 0.39 & 0.61 \end{bmatrix} \tag{2.8}$$

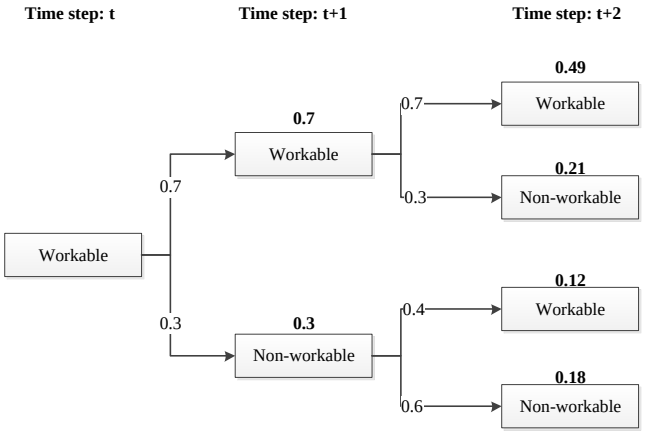

Figure 2.2: 2-Step schematization of transition probabilities from $X_t = 1$, hence the summation of the workable states equal $P_{11}^{(2)}$ and the summation of the non-workable states equal $P_{10}^{(2)}$ in Equation 2.8

2.1.5 Limiting probabilities

With the knowledge from Section 2.1.4 and keep on multiplying the transition matrix P_{ij} many times ($n \to \infty$) by itself, it seems that P_{ij}^n is converging to a limiting probability π_j. For example, if we keep on tossing a fair coin, the $\lim_{n\to\infty} P_{ij}^n$ will eventually get 0.5. This limiting probability can be computed given that the Markov chain is ergodic[3].

$$\begin{aligned} \pi_j &= \sum_{i \in S^u} \pi_i P_{ij}, \quad \forall j \in \\ \sum_{j \in S} \pi_j &= 1 \end{aligned} \tag{2.9}$$

This results in the following limiting probabilities from our two state example.

$$\begin{aligned} \pi_0 &= P_{00}\pi_0 + P_{10}\pi_1 \\ \pi_1 &= P_{01}\pi_0 + P_{11}\pi_1 \\ \pi_0 + \pi_1 &= 1 \end{aligned} \tag{2.10}$$

Rewriting the equations above results in:

$$\pi_0 = \frac{P_{10}}{P_{01} + P_{10}}, \quad \pi_1 = \frac{P_{01}}{P_{01} + P_{10}} \tag{2.11}$$

By increasing the schematization in Figure 2.2 the changes in the state probabilities will converge, until they result in the limiting probabilities and there is no change at all. The limiting probability is the probability that the process is in state j after large number of transitions, independently of the initial state. The 1st-order limiting probability is equal to the workability percentage. This probability will be used later on for the estimation of the first state of a project simulation in the DMM-model, since that state cannot be based on any earlier states. The foregoing assumes a 1st-order Markov chain, the limiting probabilities for higher orders (u) are calculated with:

$$\hat{\pi}_{jk..l} = \frac{1}{T-u} \sum_{t=1}^{T-u} \mathbf{1}_{\{X_t=j, X_{t+1}=k, \ldots, X_{t+u-1}=l\}} \tag{2.12}$$

2.2 Preliminaries

The following requirements and assumptions are set (adopted from Rip [45] and extended).
Requirements The generated dataset with the Markov theory should preserve the same characteristics as the original dataset.

- Seasonality is respected.
- Persistency of sequential workable/non-workable time steps is respected.

[3] Positive recurrent and aperiodic states are called ergodic

- The overall and monthly workability is respected.

Assumptions

- There is no trend in the observed data (no climate change); just seasonality affects are considered.
- The net duration of an operation is deterministic.
- The operational limit is fixed per operation (hard boundary): a time step is either workable or not.
- The statistics within the original dataset are assumed to be representative for the truth.

2.3 Input data

Metocean historical (hindcast) datasets near project locations used for the DMM-model and HADDOCK are obtained from the in-house global offshore database. These datasets consist mostly of hourly, 3-hourly or 6-hourly data (depending on how it is measured) and they consist of approximately 10-25 years of data. The parameters in the metocean dataset are for example the significant wave height H_s, wave peak period T_p, the wave zero-crossing period T_z, wind speed U, wave direction $\theta_{\text{wave dir.}}$, etc.

The metocean parameters which constitute an operational limit for the projects are interpolated to hourly data. The MATLAB function `interp1` with 'spline' method is used for this purpose. The spline method in MATLAB is the 'piecewise cubic spline interpolation', which makes a cubic polynomial curve fit between three data points (x_{t-1}, x_t, x_{t+1}). Rip [45] concluded that this approach distorts the exceedance probability distribution of weather windows (i.e. the persistency), and consequently the downtime distribution may be effected.

After interpolating to hourly-time series of the metocean parameters, the '**binary workability sequences**' are created similarly as in Figure 1.2. Where every workable time step is denoted with a 1 and every non-workable time step is denoted with a 0. Each operation is assigned to a column in a matrix (the so-called 'workability-array'). The obtained 'workability-array' is schematized in Table 2.2.

2.4 Module A: Seasonality

Seasonality takes place due to the earth's orbit and its declination. The Northern Hemisphere is closer to the sun in our summer (July) than the Southern Hemisphere, which means it is summer on the whole Northern Hemisphere. During our winter (December) the Southern Hemisphere is closer to the sun, than the Northern Hemisphere. For the people living on the Southern Hemisphere the seasons are the other way around. Generally, sea states are calmer during summer than winter, meaning that the workability percentages would be larger. If the transition probabilities are called *time homogeneous* or *stationary*, it is assumed

Table 2.2: A hypothetical example of a 'workability-array', where the first column represents the time steps and all the other columns represent the binary workability sequences for all operations.

Time step	Operation 1	Operation 2	···	Operation N
01-01-1991 0:00	1	1	···	0
01-01-1991 1:00	1	0	···	0
01-01-1991 2:00	1	1	···	1
01-01-1991 3:00	0	1	···	1
01-01-1991 4:00	0	1	···	0
···	···	···	···	···
31-12-2015 23:00	0	0	···	1

that they do not vary over the year, but in reality seasons do influence these transition probabilities. It is probable that the transition to a workable state is higher during summer, than during winter (on the Northern Hemisphere). Therefore, two approaches to include seasonality are introduced: the *piece-wise time homogeneous* (PWTH) method and the *non-time homogeneous* (NTH) method.

Piece-wise time homogeneous This approach is also called 'monthly stationary' in this thesis, as it assumes monthly piece-wise stationarity probabilities. The dataset is split into periods and for these periods the transition probabilities are assumed to be constant. For the piece-wise time homogeneous process the metocean data is split into 12 monthly ($m = 1, 2, ..., 12$) datasets. The split datasets consist of the number of years available in hindcast data disjoint time-series. In the split datasets the number of transitions (state i to j) are counted and subsequently the transition probabilities $\hat{P}_{ij}(m)$ are computed (with equation 2.2). This calculation accepts a small inaccuracy due to the transitions spanning different years.

Non-time homogeneous The probabilities of this approach are also called 'inhomogeneous' or 'non-stationary' probabilities in this thesis. The non-time homogeneous method in the DMM-model allows the one-step transition probabilities to vary over time, as the transition probabilities are calculated per day, $\hat{P}_{ij}(t)$. I.e. the non-time homogeneous Markov process is considered, where the transition probabilities vary over the year (depending on the day of the year). For this method the transition probabilities are calculated by using a discrete non-parametric kernel function, that gives more weightage to transitions near the calendar day of interest within a certain bandwidth. Days exceeding the bandwidth are disregarded. By means of a least squared cross validation (LSCV) the kernel bandwidths are chosen. This process will not be used for higher order chains, due to the computational complexity. To clarify both methods Figure 2.3 is presented with both methods.

Hypothesis tests as defined in Section 6.2.2, the homogeneity test, determine which method is more accurate to perform the simulation of the DMM-model with.

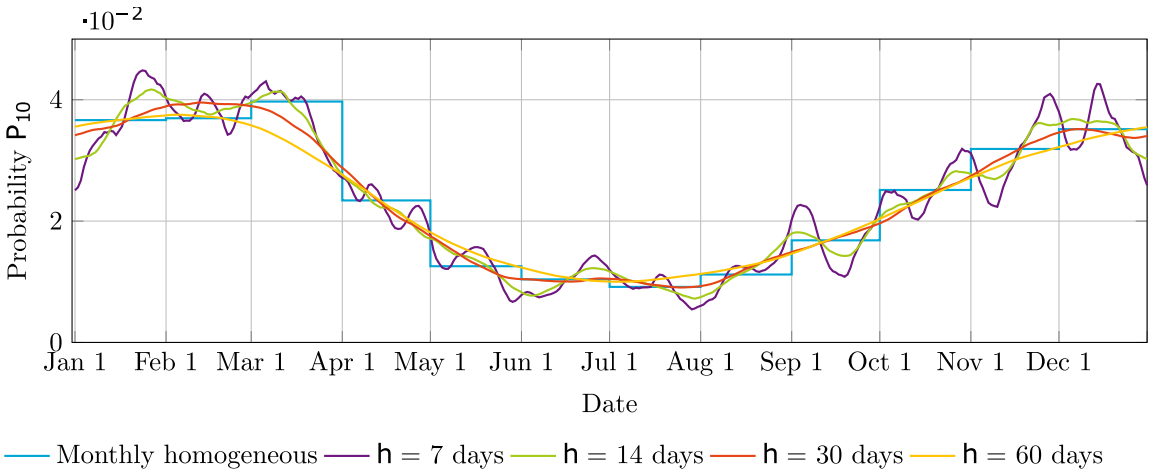

Figure 2.3: Comparison between the piece-wise time homogeneous and the non-time homogeneous processes (with different bandwidths (h)) for the transition probability P_{01} extracted from Rip [45].

2.5 Module B: Time-dependency

By time-dependency the order of the chain is meant, as Section 2.1.3 explains this theory. If a higher order is used, more 'memory' is built in the model, and more accurate predictions can be made. However, the additional history ('memory') grows exponentially with the order, which is equal to $(n_s - 1)n_s^u$. Where n_s and u denote the number of states and the order respectively. The parametric uncertainty (Section 3.2 addresses to the uncertainties) increases as more parameters need to be estimated. Hypothesis tests as defined in Section 6.2.2, the order test, are built in order to determine which Markov chain order is most accurate. The non-time homogeneous method can only be performed in a 1st-order Markov chain, but the piece-wise time homogeneous method can be performed in a 1st- and 2nd-order Markov chain.

2.6 Module C: Linked Markov chains

With the modules C, D and E the model is made applicable for sequential operations as well. In this module the '*influence period*', $D(p, q)$, and the '*cross-transition probability*', $\hat{P}_{ij}^{pq}$, are introduced, which form a link between 2 different Markov chains. These parameters ensure that the modelled time steps are physically feasible.

Influence period This method overcomes that the model produces unrealistic changes in between 2 succeeding operations. For example, a workable 1 state is produced at time step t of operation p with an operational limit of $H_s \leq 0.5$ m, and at the next time step $t+1$ non-workable 0 state is produced of operation q with an operational limit of $H_s \leq 3$ m. If the time step is one hour, this implies that the sea states changes in one hour from $H_s \leq 0.5$ m to $H_s > 3$ m, which is not realistic. It determines the duration the next operation(s) *has*

to be workable, after a workable time step of the current operation. The influence period is defined as the time period from the moment that an operation becomes non-workable (i.e. the 1/0 boundary of the first operation is passed), until the time step the succeeding operation becomes non-workable (i.e. the 1/0 boundary of the second operation is passed). Figure 2.4 presents an example of two different influence periods for an operation with limit $H_s \leq 0.5$ m followed by an operation with limit $H_s \leq 1$ m.

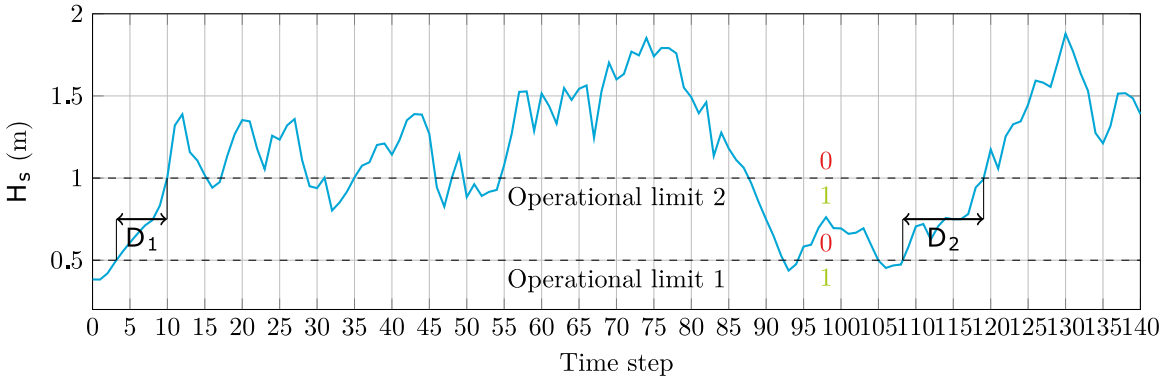

Figure 2.4: An example of two influence periods (D_1 and D_2) for an operational limit $H_s \leq 0.5$ m following operational limit $H_s \leq 1$ m; extracted from Rip [45]

Note that the last observed 1/0 crossing of operation 1 before the 1/0 crossing of operation 2 determines the influence period $D(p, q)$, as time step 94 is not counted for any influence period. Similarly, only the first 1/0 crossing of operation 2 that follows after a 1/0 crossing of operation 1 determines the influence period. From all of the observed influence periods D in the hindcast data an exceedance probability curve can be made, as depicted in Figure 2.5. The exceedance probability curve decreases as the influence period increases.

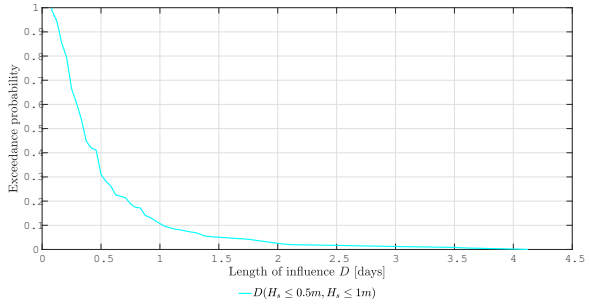

Figure 2.5: An exceedance probability curve of the influence period $D(H_s \leq 0.5$ m, $H_s \leq 1$ m)

After completing an operation the DMM-model draws an exceedance probability $P(D \geq d)$ from an uniform distribution [0,1]. Where d corresponds to the influence period of the drawn probability $P(D \geq d)$ of all the operations that follow. Each influence period is scheduled at the starting time step $t + 1$, if the current operation is completed at time step t. Figure 2.8 shows a simulation example wherein the influence period is applied.

Cross-transition probability In case there is no influence period $D(p, q)$ scheduled, which might occur when the next operational limit is stricter than the current operational limit, then the cross-transition probability is used. The Markov chain order determines how many states are needed to produce the new state. For example, if the chain order is two, it means that two time steps are looked back. Suppose that states $\{A_t = 1, A_{t-1} = 1\}$ are generated and operation A is finished. In the observed metocean dataset is counted how many times a $\{A_t = 1, A_{t-1} = 1\}$ is followed by a $B_{t+1} = 0$ or 1. This approach is similar as the most likelihood estimate of the regular transition probabilities (Equation 2.2). The cross-transition probability is defined as:

$$\hat{P}_{ij}^{pq} = \frac{N_{i^p j^q}}{N_{i^p}^*}, \quad \forall i, j \in S \tag{2.13}$$

Where $N_{i^p j^p}$ is the number of observed transitions which start from state i in the workability sequence of operation p to state j in the workability sequence of operation q. And, $N_{i^p}^*$ is the number of transitions that start from state i in the workability sequence of operation p ($N_{i^p}^* = \sum_{j^q} N_{i^p j^q}, \quad \forall j^q \in S$).

2.7 Module D: Coupled operations

If operation B *must* start *directly* when operation A has been completed, then operation A is referred to as a coupled operation. This definition is already introduced in Section 1.1.2. Coupled operations are more sensitive to encounter downtime than an uncoupled operation, because a larger weather window is needed which suits both operations executed consecutively. In the model, the workability sequence for both operations are generated simultaneously, which means four states, $S = \{0, 1, 2, 3\}$ can be defined (see Table 2.3). The model checks whether both operations can be performed without downtime in between them.

Table 2.3: Workability states for a coupled operation

Coupled operation	Subsequent operation	Modelled state value
0	0	0
0	1	1
1	0	2
1	1	3

In the model the transition probabilities between the four states are estimated from the input data with the maximum likelihood estimate (Equation 2.2). It might happen that specific states will never be visited. If the operational limit of the 'coupled operation' is stricter than the subsequent operation (e.g. coupled operational limit: $H_s \leq 0.5$ m and subsequent operational limit: $H_s \leq 3$ m), than state two ($S = 2$) will never be visited. Vice versa, state one ($S = 1$) will never be visited. In these scenarios the state that is never visited will be denoted with a probability of 0. Note that Module C is not used being used for the coupled operation, because it is incorporated in Module D.

2.8 Module E: Parallel operations

'Parallel operations' are defined as performing two operations simultaneously. This theory is not (yet) incorporated in the DMM-model. Two types of parallel operations can be distinguished. Type 1: the operations *must be* executed simultaneously with the same net duration. Type 2: the operations *may be* executed simultaneously (i.e. a new operation may start when only one operation of the parallel operations has finished). Initially, the same states as determined for coupled operations (Table 2.3) are created $S = \{0, 1, 2, 3\}$.

Type 1 For the first type the unnecessary operational limits need to be disregarded. For example, operation A has operational limits of $H_s \leq 1$ m and $U \leq 10$ m/s and operation B has operational limits of $H_s \leq 2$ m and $T_p \leq 7$ s, then the determining operational limits will be $H_s \leq 1$ m, $U \leq 10$ m/s and $T_p \leq 7$ s. The operational limit $H_s \leq 2$ m is disregarded, since it will always hold if $H_s \leq 1$ m holds. In Figure 2.6 the first example (above) schematizes the first type. Both operations have the same net duration (three time steps). Operation 1 could start one time step earlier, but both operations must start simultaneously and therefore it starts one time step later (more downtime is observed). I.e. a workable weather window where $S = 3$ is searched which is sufficiently long to fit the net duration.

Type 2 The approach from above cannot be applied for the second type. In Figure 2.6 the second example (below) a type 2 process is schematized. Operation 1 has a net duration of three time steps and operation 2 has a net duration of four time steps. Operation 1 starts when the weather window is sufficiently long enough. A single time step later operation 2 can be executed, both operations are executed simultaneously for two more time steps till operation 1 has finished. Finally, operation 2 needs two more time steps to finish. I.e. a workable weather window where $S = \{2, 3\}$ is searched which is sufficiently long to fit the net duration of operation 1 and a workable weather window where $S = \{1, 3\}$ is searched which is sufficiently long to fit the net duration of operation 2.

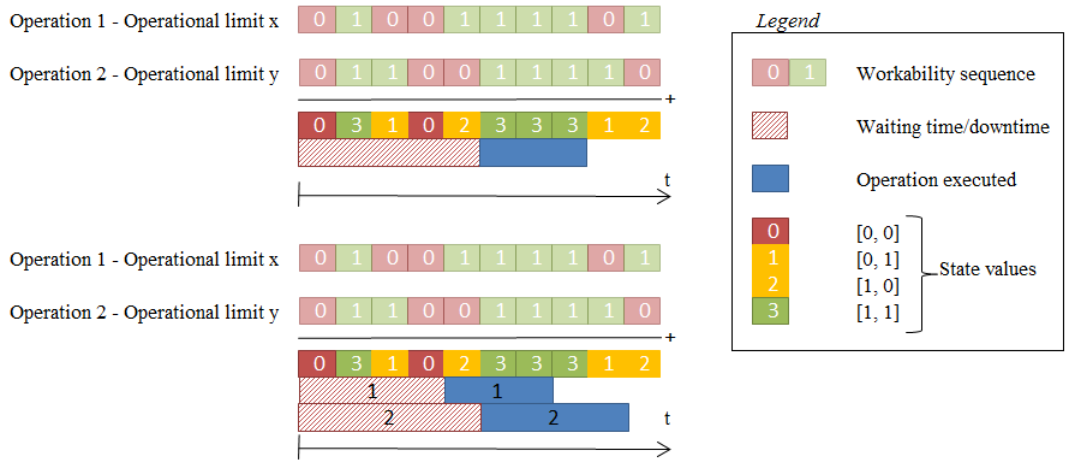

Figure 2.6: Schematizations of a type 1 (above) and a type 2 (below) parallel operations

2.9 Outcome

The outcome of the DMM-model is the distribution of the project duration and downtime duration. These can be described by an empirical cumulative distribution function (ECDF), which is defined as:

$$\hat{F}_n(x) = \frac{1}{n}\sum_{i=1}^{n} \mathbf{1}\{X_i \leq x\}, \tag{2.14}$$

where

$$\mathbf{1}\{X_i \leq x\} = \begin{cases} 1 & if X_i \leq x \\ 0 & \text{otherwise} \end{cases} \quad . \tag{2.15}$$

The model-user is free to choose how many years need to be simulated. By increasing the number of years, the simulation uncertainty decreases (Section 1.1.3) which is quantified by the Dvoretzky-Kiefer-Wolfowitz (DKW) inequality[4] to obtain the confidence bands for $\hat{F}_n$. With $\hat{F}_n$ the lower (L) and upper (U) confidence bands are defined as follows [13]:

$$\begin{aligned} L(x) &= max\left\{\hat{F}_n(x) - \sqrt{\frac{1}{2n}ln(\frac{2}{\alpha})}, 0\right\}, \\ U(x) &= min\left\{\hat{F}_n(x) + \sqrt{\frac{1}{2n}ln(\frac{2}{\alpha})}, 1\right\}, \end{aligned} \tag{2.16}$$

Then, for *any* CDF F and *all* n

$$\mathbb{P}(L(x) \leq F(x) \leq U(x)) \geq 1 - \alpha \quad \forall x \in \mathbb{R} \tag{2.17}$$

Where $1-\alpha$ is the probability at each point x that $F(x)$ does not lie within the confidence bands. In Figure 2.7 is shown that increasing the sample size n (number of generated years), results in smaller maximum distances between $\hat{F}_n(x)$ and $L(x)$ and $U(x)$. Note that, the larger the sample value n develops, the less important the α-value gets as the lines converge. It is suggested to create a 1000 project realizations (sample n) with the DMM-model, because this reduces the uncertainty to a value below the 5%. In Figure 1.6 is presented how this influences the confidence bands on the project duration.

[4] $\mathbb{P}\left(\sup_{x\in\mathbb{R}} |\hat{F}_n(x) - F(x)| \geq \epsilon\right) \leq 1 - 2e^{-2n\epsilon^2}$ for any $\epsilon, n > 0$

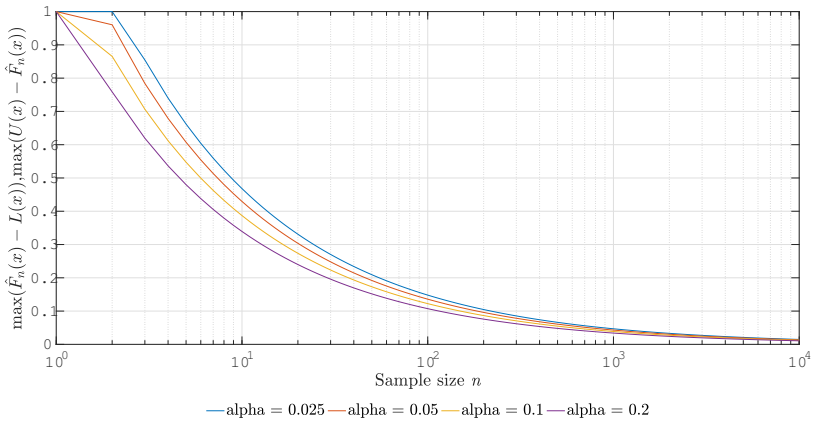

Figure 2.7: By increasing the sample size n the maximum distance between $\hat{F}_n(x)$ and $L(x)$ or $U(x)$ decreases for multi α-values

2.10 Project example

The DMM-model will be explained by the following hypothetical project in Figure 2.8, where the blue circles correspond with the numbered list below. In this small project 1st-order Markov chain is assumed.

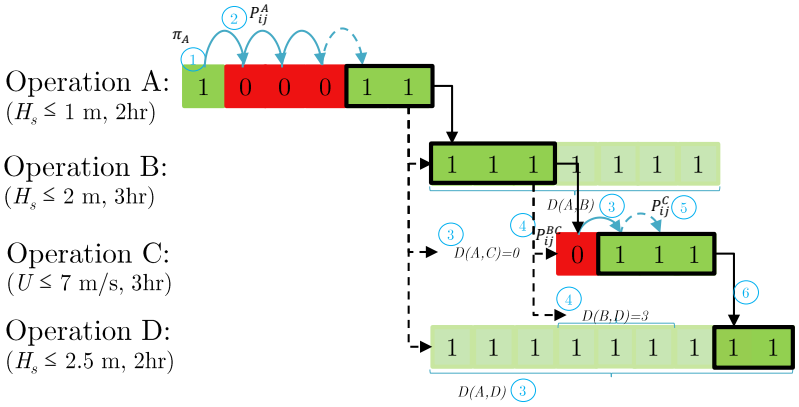

Figure 2.8: Visual clarification of the DMM-model simulation procedure with a hypothetical project.

1. The first symbol is produced with the limiting probabilities for operation A, as can be calculated with Equation 2.11.

2. The workability sequence continues with the transition probabilities of operation A, as can be with Equation 2.2, until the net duration of two hours is reached. The completion of the operation is framed with a black rectangle.

3. For all succeeding operations the influence period of operation A is determined. Operation B is influenced 7 time steps and operation D is influenced 9 time steps. Operation C is not influence at all, which can be explained by its different parametric unit. The influence period is determined with the exceedance probability as explained in Section 2.6. The net duration of operation B (indicated with a black rectangle) is within the influence period. From this time step the project continues.

4. For all succeeding operations the influence period of operation B is determined. This is only the case for operation D, but it does not create any new states. Operation C does not have a generated state by the influence period, hence the cross-transition probability is used P_{ij}^{BC} which results in a non-workable state. The cross-transition probability is calculated with Equation 2.13.

5. The workability sequence continues with the transition probabilities P_{ij}^{C}, until the net duration of 3 hours is reached. The completion is framed with a black rectangle.

6. The influence period of operation A was sufficiently long for operation D, that the net duration fits within this period. No new states have to be generated with the transition probabilities of operation D.

These steps summarize how 1 project is simulated, which resulted in a project duration of 15 time steps. The downtime is calculated by subtracting the total net duration of the project duration which is $15 - 10 = 5$ time steps. The more projects are simulated, the less the simulation uncertainty.

2.11 Conclusion

In this chapter the Markov theory and the DMM-model are analyzed. The actual metocean conditions are abstracted to binary workability sequences. Based on the statistics from these sequences a stochastic simulation is possible with the Markov theory. New binary workability sequences are generated for each operation in the project. On these grounds many project simulations are possible, causing a lower simulation uncertainty. While, HADDOCK is only able to simulate a number of projects equal to the number of available years in the metocean hindcast dataset (approximately 10-25 years).

The *settings* of the DMM-model are determined by the hindcast data, project start date, years to simulate, Module A and Module B. In Module A hypothesis tests are built which determine the seasonality that can be piece-wise time homogeneous or non-time homogeneous. And, in Module B hypothesis tests are built to determine the time-dependency of Markov chain. Module C and Module D are not part of the settings, but they will be activated in case needed (depending on the operations within the project). Module C links two Markov chains with the influence period or the cross-transition probability. Module D ensures the operation following a coupled operation does not encounter downtime. This summarizes the work-method of the DMM-model and answers research question No. 1a: '*How can downtime be analyzed with the current Downtime Modular Markov model?*'.

Figure 2.9 presents a breakdown of the DMM-model for visualization purposes. The upper box presents how the binary workability sequences are created. The metocean dataset together with the operational limit determine the workability state sequences, which are in turn the input for the Markov model. The middle box presents the Markov model with the different modules. Modules A and B are performed on the created binary workability sequences. Thereafter the new states are generated with the Markov theory. These newly generated states are linked by using the other modules (C,D and E) in order to create projects. Since more projects can be realized with the newly generated data, the probability distribution of the project duration and downtime duration is narrower (more accurate).

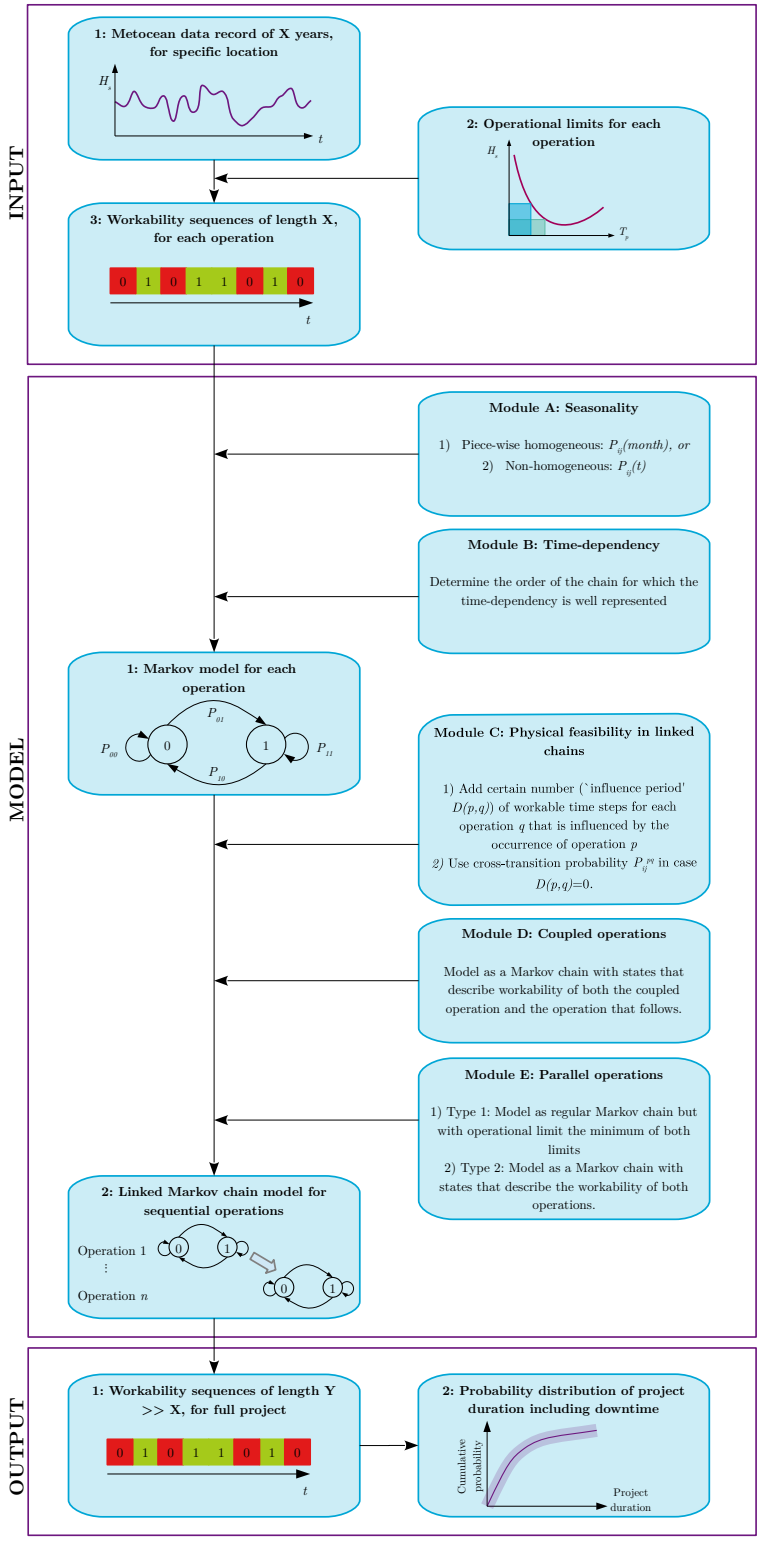

Figure 2.9: Breakdown of the DMM-model for complex marine projects extracted from Rip [45]

3 Simulation

A model tries to represent the real-world, where the model-user can compare the results of the model with his expectations. A simulation is defined as the operation of the model representing the real-world [32]. The operation of the DMM-model is an example of such a simulation, with the actual project duration and downtime distribution as output. This leads to the following research question No. 1b: '*Which methods for metocean parameter generators can be found in literature?*'. This is addressed in Section 3.1.

According to Box "*All models are wrong, but some are useful*" [11], because all models try to approximate the real-world but not one model can duplicate the *exact* real-world. Each model has its uncertainty, and the model-user should be aware of these uncertainties. In Section 3.2 uncertainties concerning computerized simulations are addressed, and it aims to answer research question No. 1c: '*Is it possible to quantify uncertainties concerning the DMM-model?*'. In Section 3.3 both research questions will be answered.

3.1 Overview of other metocean parameter generators

Metocean parameter generators are statistical models that try to produce realistic random sequences of meteorological and oceanic variables (e.g. wave height (H_s), wave period (T_p), temperature) for a set location. Many of these generators are used for water engineering design, agricultural, ecosystem and hydrological impact studies [60]. The DMM-model applies a Monte-Carlo[1] simulation which comprises the statistical metocean data. For similar models one should realize the output of these models are not forecasts, but rather a distribution of possible scenarios. Monbet *et al.* [34] conducted a survey into stochastic models and methods for sea state time-series, with a particular focus on simulation. The following Sections review examples of these generators. It is scoped to time-series for a given location only, where other models make use spatio-temporal[2] information (e.g. in [1] the datasets along a maritime line are extrapolated). Furthermore, in this review it is assumed that there is no over-year trend in the data, as was also given as assumption in Section 2.2.

[1] Random samples from a known population of simulated data to track statistical behaviour [36].
[2] Relates to space and time.

3.1.1 Gaussian based models

Metocean datasets cannot be assumed to be Gaussian distributed, but it is possible to transform the time-series into time-series with Gaussian marginal distributions. The Box-Jenkins and the Translated Gaussian process describe how this is conducted.

Box-Jenkins method In the book of Jenkins *et al.* [12] several models are described that can generate time-series. The autoregressive (AR), the moving-average (MA) and the autoregressive moving-average (ARMA) model can be used to simulate time-series for hydrological events [63]. A prerequisite of the Box-Jenkins model is that the input data (metocean datasets) have to be stationary and normally distributed with a constant mean and variance. However, these long-term datasets are nonstationary and therefore this prerequisite is not met. The datasets can be transformed to a more or less stationary time-series by using the method of Bruce (1982), the method of Box-Cox (1964) or the modified Box-Cox method by Guedes Soares and Ferreira (1995) [63]. Once the transformation is applied, an ARMA model can be used to the transformed time-series to generate time-series. Several studies have done this approach for generating H_s, a bivariate time-series (H_s, T), and also for wind U processes [34]. The main drawback is that the metocean datasets consist of more parameters than 1 or 2, which are correlated with one another. Therefore, generating time-series for all these parameters is rather complex. In these cases, the transformed set must be multi-variate normal, which means that any relationship between the transformed variables must be linear [41] and thereafter the ARMA model can be used.

Translated Gaussian Process The Translated Gaussian Process (TGP) is much like the Box-Jenkins method. Given that the metocean datasets are non-stationary, the TGP reduces the data to stationarity via filtering, de-trending and normal scores transformation. Subsequently, time-series are generated for the transformed data with a Gaussian correlated simulation method. And finally, by inverse operations the non-stationary non-Gaussian trending characteristics of the original metocean dataset is recaptured [59]. Walton and Borgman generated time-series only for H_s by using Inverse Discrete Fourier Transformation (IDFT). This method can produce time-series fast and the results mimic the original dataset reasonably. The same procedure is used for more parameters in [10] and [14] to multivariate time-series (H_s, T, θ_m). In case strong dependence is apparent between the parameters (like the correlation between wave height and wave period), another transformation to restore the original distributions has to be used. Instead, the Rosenblatt transformation is then used, this is done for (H_s, T),(H_s, θ_m),(U, Φ) according to [34]. Apparently, it has not been done for more than 2 metocean parameters yet, while the Rosenblatt transformation is capable of doing it for more variables.

3.1.2 Re-sampling models

The principle of re-sampling is randomly sampling the original metocean dataset, and thereby generating new time-series. Following this theory it might be possible that at time t the wave height is 3 m and the next hour $(t + 1)$ the wave height is 0.5 m, which is not realistic. This is where the block-resampling and the Markov chains re-sampling come in.

Block re-sampling New time-series are generated by randomly sampling block lengths l_i and time locations t_i. For a given time-series X_t, blocks are defined as [34]:

$$B_i = \{X_{t_i}, X_{t_i+1}, ..., X_{t_i+l_i}\} \tag{3.1}$$

This approach is not appropriate for metocean data to determine persistency. If blocks are too small the same problem occurs, as re-sampling without blocks (as earlier explained). And the other way around, if blocks are too long the new generated time-series will tend to mimic the hindcast data and no innovation is brought in [34]. However, when the metocean dataset is transformed into the workability-array as in Section 2.3, block re-sampling might work. In this approach the autocorrelation functions may be difficult to preserve.

Markov chains re-sampling The essence of re-sampling Markov chains is to build non parametric estimators of the transition probabilities. The DMM-model is based on this technique. In literature similar methods are found [28] [44] [35] [16].

3.1.3 Parametric models

In the sequel various parametric models are gathered.

Finite state space Markov chain In the article of Sahin [48] hourly wind speed data is synthetically generated by using a 1st-order Markov chain with 8 states. The states are defined by means of the mean and multiple standard deviations. With a uniform random number generated transitions between successive time steps are obtained, similarly as the DMM-model. It is concluded that a 1st-order does not preserve sufficiently accurate the statistics of the wind speed; higher orders are recommended. The drawback of this approach is that many parameters need to be estimated, but there are approaches to overcome this.

Copula model In [29] time-series are constructed for significant wave height and wind speed by using copulas. Copulas are applicable for models when multiple variables are correlated with one another. It can be imagined that a stronger wind results in a higher wave. Copulas are functions that join multivariate distributions to their one-dimensional marginal distribution functions, which are uniformly distributed between [0,1]. The procedure to generate time-series is as follows:

1. By using a random number generator the first wind speed value is created.
2. With the first wind speed, the wind speed values are calculated by solving the inverse conditional Gaussian copula.
3. Subsequently, significant wave heights are computed for each wind speed with the inverse conditional Gumbel copula.
4. The inverse cumulative distribution function is applied to transform the significant wave heights and wind speeds to their original values.

5. The generated values are combined per month to include seasonality. Hence, whole years are generated.

In article of Jäger *et al.* [23] is described how synthetic hourly time-series of significant wave heights (H_s) and the corresponding mean zero-crossing periods (T_{m02}) are characterized. Time-series with the duration of an oceanographic winter are simulated by means of vine-copulas so that the joint dependencies between the variables are captured. In this manner time-series are generated for two parameters, while for complex marine projects often more parameters are needed.

Multivariate distributions Most of the aforementioned methods are limited to a one or two parameters, while the existing metocean datasets consist of more parameters. In [19] a method is described to model multivariate distributions of n metocean parameters. That method aims at modeling of seasonal joint distributions of these parameters. First the seasonal variations are captured through a harmonic representation of the mean values and the standard deviations of the considered n variables. Seasonal dependency was then removed by de-trending the data, allowing the method to provide more data. With this transformation the nature of the joint probability distributions remain unchanged. A four-parameter gamma distribution was used to model the probability density function for each metocean parameter, and subsequently transformed into a stationary Gaussian distribution (this is referred to as the Nataf transformation). The time-series are retransformed into standard normal distributions via so-called diffeomorphism. Eventually, the multivariate probability distribution functions are obtained by means of multinormal distribution. The correlation between the metocean variables is then reproduced.

In [19] the described method was able to model seasonal information on the joint occurrences of mean wind velocity, significant wave height and mean wave period. Because of the interest in weather persistency, several mathematical persistence models were made, which are able to extrapolate information about the occurrences of weather windows. Most of the marine operations have two operational limits and the third parameters is defined as the minimum duration of the weather windows (persistency). This model can consider the frequency of occurrence of the required weather window as a function of the two operational limits. The presence of seasonality is herein taking into account. Following the same steps as described above, it was observed that the seasonal trends and the duration dependence are well captured by the model. For simplicity this method has only been tested for significant wave height and mean wind velocity at 10 m elevation. Therefore, more validation is needed for this method for multiple parameters.

Nonlinear autoregressive models Literature provides several models based on 'Artificial Neural Networks' which are able to model the wind speed (U) [37] or significant wave height (H_s) combined with wave period (T) [31]. However, these models are currently used for short-term prediction. Furthermore, there are several models based on time-varying autoregressions to model the wind speed (U) [22] or wave height (H_s) [51]. Where the AR-model of wind speed is given by Equation 3.2 and the AR-model of significant wave height is given by Equation 3.3.

$$U_t = \sum_{i=1}^{r} a_{t,i} U_{t-i} + \epsilon_t \tag{3.2}$$

$$H_t = \sum_{i=1}^{r} a_i^{S_t} H_{t-i}^{S_t} + b^{S_t} + \sigma^{S_t} \epsilon_t \tag{3.3}$$

Yet again only 1 or 2 parameters are generated, while complex projects require more parameters.

3.2 Uncertainty

In practice it is difficult to determine downtime for complex projects analytically, therefore simulation/sampling studies are performed. These computerized simulations/sampling studies are representations of real-world processes and with the results, downtime distributions can be obtained. Such a stochastic process is bounded by probabilistic rules to generate new synthetic time-series with the same characteristics of the observed data. These principles introduce uncertainties [27].

3.2.1 Types of uncertainty

In general there are two types of uncertainty: inherent/aleatory uncertainty and knowledge/epistemic uncertainty. Aleatory uncertainty dictates the natural randomness in the states of system, as one can never know the exact outcome with for example coin tossing. Epistemic uncertainty is caused by the lack of knowledge/data. It can be reduced by increasing the amount of knowledge/data. Van Gelder [57] framed different types of uncertainties in the block scheme of Figure 3.1. Where the inherent uncertainty could exist in space or time. The epistemic uncertainty is subdivided into model and statistical uncertainty. The model uncertainty arises through imperfectly knowing/understanding the processes or phenomena in the model. Statistical uncertainty is the uncertainty that originates from the chosen statistical function which might not describe the process or phenomenon adequately. It is subdivided in the distribution type and the parameters of this distribution. The less knowledge/data, the larger the uncertainty of the parameters. The distribution type uncertainty represents the uncertainty of distribution, as it is not precisely known for example whether the occurrences of the water level in the North sea is exponential or Gumbel distributed or differently distributed. The three most important uncertainties within the DMM-model are assigned to the classifications within this framework. Below, these uncertainties are further elaborated.

In Section 1.1.3 the term '**simulation uncertainty**' has been introduced already, which relates the uncertainty to the number of replications. For the DMM-model this corresponds to the number of project simulations; the more project simulations, the less the simulation uncertainty. In literature this uncertainty is often referred to as *aleatoric uncertainty* [61] (in time) for parameters. In simulation studies the probabilistic rules are often determined

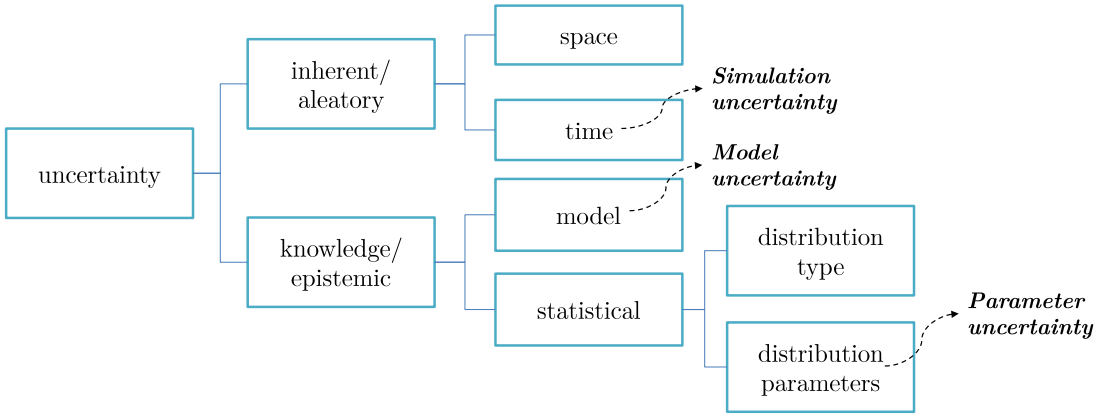

Figure 3.1: Classification of different types of uncertainty [57], with the main uncertainties of the DMM-model assigned to their corresponding uncertainty classification.

by the mean and variance of (a) parameter(s). The newly generated synthetic time-series are simulated according to their *a priori* distributions. Since it is logically impossible to simulate the exact future, the simulated parameter(s) include some uncertainty and hence the downtime prediction is not exact. However, by repeating the prediction the simulation/aleatoric uncertainty decreases.

The '**parametric uncertainty**' is the uncertainty related to the estimation of the input parameter(s) of the stochastic model [20]. In literature this is often referred to as the *epistemic uncertainty* [20]. For example, a die is rolled 4 times and the following numbers were observed: 1,2,2,4. It is known that a fair die has 6 sides with each the same probability. In this example, we cannot determine these probabilities due to lack of data. The parametric uncertainty decreases if the parameters are based on more data, because the *a priori* distributions are more certain. In case more input parameters have to be simulated, the parametric uncertainty increases. Additionally, datasets could consist of '**observational errors**', which is described as mistakes in the data collection and part of 'missing' data. This is sometimes referred to as noisy data. In the die example, a 5 could be recorded when actually a 4 was observed. Datasets are collected by devices or humans, hence they are prone to errors. Enlarging your dataset will reduce the uncertainty induced by observational errors. The available hindcast datasets consist of approximately 20 years of data, hence it is believed that the uncertainty induced by observational errors is low. The parametric uncertainty is associated with the observational errors, as the input parameters are calculated with the recorded datasets.

The '**model uncertainty**' describes non-statistical errors in abstraction [61] and is also part of the *epistemic uncertainty*. The more input parameters are used, the more complex the model gets and the lower the model uncertainty gets. For example, by modelling an open ocean with only wave height and wave period will give a simplistic result, but when the wave direction, wind speed, current velocity are included as well, the model will give a

more detailed representation of the reality. Including all parameters will make the model more realistic, hence the model uncertainty decreases. This uncertainty is conflicting with the parametric uncertainty, as more parameters need to be estimated.

The '**code uncertainty**' is also known as the numerical uncertainty, which is defined as the numerical errors and algorithmic mistakes. The more complex the model, the more vulnerable it is to coding errors. The more a model is validated the lower the code uncertainty.

3.2.2 Uncertainty in models

In this Section the aforementioned uncertainties will be discussed for both models (HADDOCK and DMM-model), with its purpose to identify the reasons that cause the uncertainties.

- Simulation uncertainty:
  - HADDOCK: available hindcast datasets of approximately 10-25 years
  - DMM-model: number of project realizations as required (1000 is suggested in Section 2.9)

The simulation uncertainty is dependent on the replications of project simulations. HADDOCK uses the hindcast dataset for the simulation, hence the number of project simulations is equal to the number of available years in hindcast data. This causes a high simulation uncertainty. The DMM-model generates a predetermined number of stochastic project realizations based on the statistics of the hindcast data in order to reduce this uncertainty. The more project realizations, the less the simulation uncertainty.

- Parametric uncertainty:
  - HADDOCK: interpolation
  - DMM-model: interpolation (same) + estimation of input parameters

In HADDOCK the output is fully determined by the hindcast data. There is no kind of some inherent randomness in the model, this results in no parametric uncertainty. Unless, the dataset needs to be interpolated to 1-hourly data. In that case parameters are estimated by interpolation techniques, which introduces parametric uncertainty. The DMM-model applies the same interpolation step. Besides, the DMM-model has to estimate the input parameters, such as the transition probabilities $\hat{P}_{ij}$ and the limiting probabilities π_i, that are needed for the simulation. The parametric uncertainty increases by threefold as more parameters need to be estimated: (1) using a higher-order Markov chain; (2) using the non-time homogeneity; (3) generation of coupled operations.

- Model uncertainty:
  - HADDOCK: basis
  - DMM-model: basis (same) + statistical deviations

In both methods there is some 'basis' model uncertainty, as not all factors contributing to downtime are accounted for (e.g. breakdowns, crew transfers). The DMM-model increases the model uncertainty, due to the abstraction of real metocean conditions to binary workability sequences. Deviations in workability percentage or persistency are likely to occur because of the abstraction. The aforementioned threefold that increases the parametric uncertainty will reduce the model uncertainty, because these deviations will be reduced.

- Code uncertainty:
  - HADDOCK: code-errors
  - DMM-model: code-errors (higher)

The code uncertainty is unknown for HADDOCK, but since it has been extensively validated, it is believed that this uncertainty is low. A software-testing process (see Section 4) can be used in order to assess this uncertainty. The DMM-model is going through a software-process in this thesis, and there are (some fatal) errors found in the algorithm (this is elaborated in Chapters 5 and 6). Therefore, the code uncertainty is higher in the DMM-model than in HADDOCK. The more errors are rectified, the lower the code uncertainty.

- Observational errors:
  - HADDOCK: mistakes in data collection
  - DMM-model: mistakes in data collection (same)

It is believed that the observational errors are small in the hindcast datasets. The 3rd party selling the datasets validates them in order to filter outliers. Moreover, the dimension of errors induced by devices are too small to determine whether an operational limit is exceeded or not. The observational errors are the same for both models, since the same datasets are used.

3.2.3 Uncertainty quantification

As described in the previous Sections, HADDOCK and the DMM-model are prone to a variety of uncertainties. The model-user should be aware of these uncertainties, else critical and expensive decisions with unfounded confidence are made. The essence of the DMM-model is to reduce the simulation uncertainty, but simultaneously a stochastic process introduces new uncertainties. By means of the DKW inequality (Section 2.9) confidence bands are defined to quantify the simulation uncertainty. In order to make reliable decisions based on your model, the model-user should be familiar with the other uncertainties as well. This Section provides a first step in quantifying the parametric and model uncertainty. The code errors should rather be rectified than quantified, therefore this uncertainty is not further considered. The observational errors are considered to be too small to influence the project downtime, hence the observational errors are also not further considered. This Section aims to give quantification possibilities regarding the parametric and model uncertainty. Once these are quantified a visualization, such as a bar chart, can be obtained.

Parametric uncertainty The piecewise cubic spline interpolation creates a smooth line between the data points, while in reality these data points are more spiky. The quantification of the uncertainty regarding the interpolation method can be studied by comparing an original hourly dataset with an hourly interpolated dataset. Additional parametric uncertainty is introduced by estimating the input parameters: $\hat{P}_{ij}$, π_i, $\hat{P}_{ij}^{pq}$, $D(p,q)$. The more parameters need to be estimated, the higher the parametric uncertainty. A lower parametric uncertainty comes at the expense of a higher model uncertainty. The following parameters are used in the DMM-model:

- Transition probability $\hat{P}_{ij}$:
  These are calculated with the most likelihood estimator (Equation 2.2), which has its mean $\bar{P}_{ij}$ and variance $Var[P_{ij}]$, defined as [40]:

$$\begin{aligned} \bar{P}_{ij} &= \frac{N_{ij}+1}{N_i+N} \\ Var[P_{ij}] &= \frac{\bar{P}_{ij}(1-\bar{P}_{ij})}{N_i+N+1} \end{aligned} \tag{3.4}$$

  Where N_{ij} denotes the number of transitions starting from state i to state j, N_i denotes the number of transition starting from state i, and N denotes the total number of transitions. The more observations available, the more accurate the most likelihood estimate is, as the variance decreases. Hence, the monthly stationary transition probabilities will be very accurate, as they are based on many observations. However, these are used throughout the whole month for every time step, which causes model uncertainty. In Figure 2.3 can be seen that these probabilities remain the same for the whole month. In reality however, the transition probabilities on the first day of the month will definitely not be the same as the last day of the month. The non-time homogeneous function overcomes this problem, as it calculates daily transition probabilities by means of kernel functions. For that method fewer observations are used, hence the variance increases.

- Limiting probability π_i:
  These can be calculated with Equation 2.11 or 5.1. The latter indicates that the limiting probabilities are equal to the workability percentage. A standard deviation can be computed from the workability percentage, and with it uncertainty is quantified.

- Cross-transition probability $\hat{P}_{ij}^{pq}$:
  The cross-transition probability is nearly similar to the regular transition probability. The difference lies in that transitions spanning different operations are used, which makes it a bit more complex. However, the same approach can be applied as the regular transition probability to quantify the mean and variance.

- Influence period $D(p,q)$:
  The influence period is determined from an exceedance curve, which is the inverse of a

cumulative probability curve. Therefore, the DKW inequality can also be used for the influence period in order to quantify the uncertainty related to it.

Model uncertainty The model uncertainty is nil when all the parameters influencing downtime are known. HADDOCK and the DMM-model only comprise metocean conditions related to operations; other influences, such as breakdowns and crew transfers, are not incorporated. In reality there is also a distribution in the net durations and operational limits, where the models apply deterministic values for it. It is the captain his call whether the operation will be executed or not, and some crews could execute certain operations faster than others. These influences comprise the 'basis' model uncertainty and these are difficult to quantify, but structured expert judgement could be useful tool for it. From real executed projects can be studied how much percentage of downtime is related to non-metocean parameters.

Furthermore, additional model uncertainty is introduced in the DMM-model by abstracting metocean data to binary states. The information of the metocean parameter is lost, as it cannot be determined whether the value is close or far off the operational limit. Deviations in workability and persistency could arise as a result from this. The chi-squared and the two-sample Kolmogorov-Smirnov test, as given in Section 6.3, could be used to quantify the uncertainty related to the persistency deviation.

3.3 Conclusion

In the beginning of this Chapter the research question: '*Which methods for metocean parameter generators can be found in literature?*' was asked. Monbet *et al.* conducted a survey of stochastic models for wind and sea state time-series, which is extended in this thesis in Section 3.1. Gaussian based models such as the 'Box-Jenkins method' and 'Translated Gaussian Process'; re-sampling models such as 'Block re-sampling' and 'Markov chain re-sampling'; Parametric models such as 'Finite state space Markov chain', 'Copula method', 'Multivariate distribution method' and 'Nonlinear autoregressive models' are the described generators. The past decades copula-based approaches have become more popular to generate time-series for sea states. However, the main drawback of all models is that they are limited to a few number of parameters, mostly just 1 or 2, that are generated. Fouques [19] proposed a method for multivariate distributions, but nevertheless it is only validated for 2 variable. Some of these models are applicable for scheduling marine operations based on persistency if the operations are only subject to the generated parameters. Validating the DMM-model with one of the mentioned models is questionable, because each model has its limitations and uncertainties. For validation purposes it is therefore recommended to compare the generated time-series with the observed/hindcast data.

Furthermore, several types of uncertainties concerning computerized simulations are laid out in Section 3.2 in order to answer research question No. 1c: '*Is it possible to quantify uncertainties concerning the DMM-model?*'. Section 3.2.3 aims to answer this research question. The code uncertainty and observational errors are disregarded in answering this

question, as it is believed that code errors can be rectified and mistakes in data collection will not influence the downtime duration. The essence of the DMM-model is to reduce the simulation uncertainty, which is quantified by the DKW inequality. The quantification of the other uncertainties is not as straightforward as the simulation uncertainty. The parametric uncertainty can be quantified in a way, as each estimated input parameter has some uncertainty. Also, the model uncertainty can be quantified by the deviations from reality in terms of workability percentage and persistency. These deviations are due to the abstraction of metocean data into binary data. The interpolation uncertainty and 'basis' model uncertainty do not necessarily have to be quantified, because they are the same for both methods.

4 Software-testing

The last few decades the reliability of computer predictions is a matter that grows in interest. This also applies to simulation of metocean parameters, considering the amount of available data is growing each day. Questions that arise are "can the computer prediction be used as decision? What is the accuracy of the computer prediction? How can the validity be assessed of the computer prediction?" The answering of these questions is addressed to model verification and validation (V&V) [6]. Answers to questions like aforementioned are needed regarding the DMM-model, observed that the DMM-model is programmed only once. It may therefore still contain several errors or limitations. There are no grounds to place confidence on for the model, when there has not been conducted a thorough V&V process. The terms 'verification' and 'validation' are often used in the software testing and software engineering world, but the definition of both terms are mostly vague. In the following sections the differences between verification and validation are attempted to define as clear as possible.

Figure 4.1 maps how V&V is related in a modelling process, based on [46]. The V&V process starts when the understanding of the real world and the problem is tackled. Subsequently, a conceptual model is built, followed by the computer model. The first version of the computer model is ready to perform downtime simulations, which is done in Rip [45] (indicated with the blue lines). Enough hindcast datasets are available to develop and use the model.

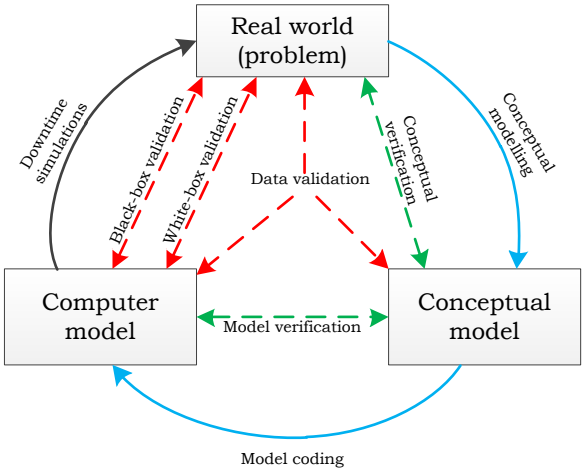

Figure 4.1: Schematized map of relation between real world, concept and computer model. Blue lines indicate how a model is built. Green lines indicate the verification phase. Red lines indicate the validation phase.

In this map the blue lines indicate the 'conceptual modelling' describes the theoretical concepts where the model is based on, and the 'model coding' describes the coding of the theories in MATLAB. 'Downtime simulations' describes the generated output of the DMM-model, which represent the real-world. These 3 steps can be compared by a simple example where the bed sediment movement is modelled. The concept focuses on the theories, such as the Shields parameter. The model coding addresses to modelling the situation and relevant equations. The output of such a model is the volume of moved sediment. In Figure 4.1, it can be noted that there are two types of verification (green lines), defined as follows:

1. Conceptual verification: determining that the conceptual model contains all necessary input and details in order to conduct the downtime simulation.
2. Model verification: determining the relation between the concept and the computer model.

Furthermore, there are various forms of validation (indicated with red lines in Figure 4.3), which are defined as follows:

1. Data validation: determining that the hindcast data required to make downtime simulations is sufficiently accurate and determine how many years are needed to simulate.
2. White-box validation: determining that the modules of the DMM-model represent the real world with sufficient accuracy.

3. Black-box validation: determining that the overall DMM-model represents the real world with sufficient accuracy.

The V&V process is an on-going development throughout the life-time of the DMM-model, and it should not be conducted just once. In the beginning of this process the conceptual and model verification are more relevant, because in this phase the errors and limitations can be easier identified. In a later stage white and black-box validation is more relevant, since the model is complete. Often the real world data is inaccurate, and that is where the data validation comes in, with its purpose is to better understand the data. The cyclic software development process of the DMM-model is visualized in Figure 4.2. It starts with understanding the DMM-model, followed by the verification phase and the validation phase. In the final phase the findings of previous phases are improved and the model is developed to a new-state-of-the-art.

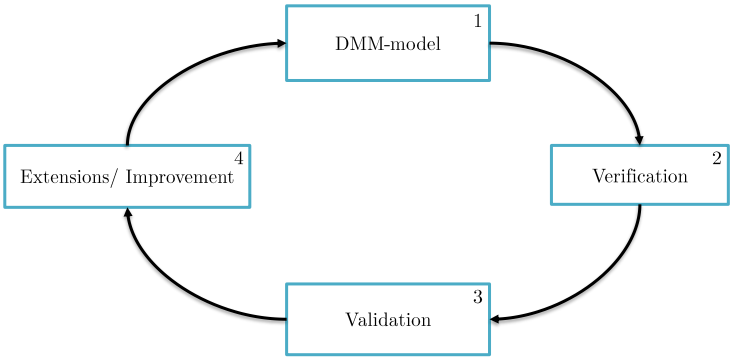

Figure 4.2: The cyclic software-testing process of the DMM-model.

4.1 Verification

At the starting of the software testing/software engineering process, a verification study has to be conducted first. Verification addresses to the numerical treatment of the model, i.e. it is concerned with whether the model is well-programmed and error-free. It answers the main question: "Are we building the model the right way?" [9]. Small model errors can cause major model failures, therefore this process is very important. The DMM-model will be checked whether it is consistent, complete and correct.

The verification process is divided into two approaches; the conceptual verification and the model verification. The concept verification determines that the theories and assumptions underlying the DMM-model are correct. It includes the reasonableness of the model structure, logic and mathematical relationships. While, model verification determines the correctness of the computer programming and implementation of the DMM-model. The concept and model verifications will be conducted per module, and for the correctness and consistency of

the DMM-model relations in between modules are verified. This is schematized in Figure 4.3. Although model verification and white-box validation are often treated simultaneously, they are not treated together in this thesis. The used methods for model verification are 'checking the code' and 'visual checks'. Checking the code means the verifier reads the code and ensures the right logic and date is used, this is mostly done for complex models like the DMM-model. Visual checks are done by running the code and check whether different elements/variables behave logically [46].

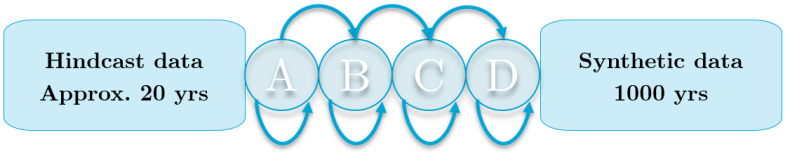

Figure 4.3: Schematization of the verification process, where A B C D denote the different modules.

4.2 Validation

Validation is done at the end of the software testing process, after the verifications are completed. Validation addresses to the quality of the model, i.e. it is concerned with checking that the right model is programmed instead of checking whether the model is programmed the right way. It answers the main question: "Are we building the right model?" [9]. The correctness of the final output of the DMM-model with respect to the specified requirements has to be determined. If some errors are missed in the verification process, they can be caught as failures in the validation process. The DMM-model is developed for the specific purpose to assess more accurately downtime of complex marine projects. Its validity is determined with respect to that purpose [49]. Several evaluations have to be conducted until sufficient confidence is obtained that the model can be considered valid for its intended purpose.

As aforementioned, three forms of validation will be conducted (data, white-box and black-box validation). The used data in the DMM-model is extracted from the real world and used as input for the conceptual model and computer model. The assessing of the input data is beyond the scope of this thesis. The data validation is concerned with how many years are required as input/output of hindcast data to obtain a realistic sea state based on workability percentage and persistency. Inaccurate input data can cause significant inaccuracy of output data. The white-box validation is concerned with the output of each module in comparison with the real world. The used method for white-box validation will be 'inspecting outputs'. Inspecting outputs can be done for each module, where the actual and the expected results are compared [46]. And finally, the black-box validation is concerned with the overall behavior of the DMM-model. Two forms of black-box validation are available. The output of the DMM-model, which comprehends the downtime duration distribution or the actual project duration distribution, can be compared with the same

distributions simulated by HADDOCK. And, the output distributions can be compared with similar simulations models, such as Copula [29]. However, in Section 3.3 it is concluded that only the hindcast data will be used in this thesis. In Figure 4.4 the validation process is schematized. The red arrows indicate the white-box validation, the black arrows indicate the black-box validation and the green ellipse indicates the data validation.

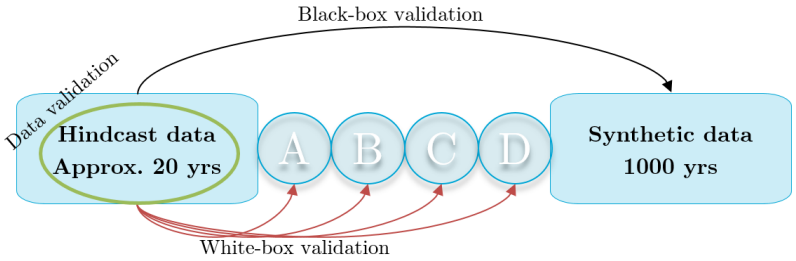

Figure 4.4: Schematization of the validation process, where A B C D denote the different modules.

5 Verification

This chapter tries to answer the research question No. 2a: '*Is the concept and the model code of the current DMM-model correct, consistent and complete?*' It is assumed that the reader understands the work methods of the different modules of the DMM-model as explained in Chapter 2. In this chapter a verification will be done by means of 'verification-testing'. The verification will be conducted with multiple tests for the modules of the DMM-model, and they are regarded separately in the following sections. The verification-testing is meant to determine whether the DMM-model meets the specified requirements in the model. The concept and the model code are treated separately in Sections 5.1 and 5.2. These are verified whether they are error-free, consistent or contain any limitations. Initially, it is assumed that the DMM-model performs incorrectly, until evidence indicates otherwise. Conclusions are drawn in Section 5.3, which refocuses the purpose of this chapter. It reveals a synopsis of what was found and leads into the implications of the findings, which will be observed again in Chapter 6 and 7.

5.1 Conceptual verification

5.1.1 Module A: Seasonality

Weather conditions vary over the year (seasonality), therefore transition probabilities of the DMM-model will vary over the year. It is conceivable that during the winter more severe conditions are present, than during the summer. This results in more workable states during summer, than during winter. Two methods to take seasonality into account are piece-wise time homogeneous and non-time homogeneous. For verification of Module A, piece-wise time homogeneous method and non-time homogeneous method are treated separately. For further research it is recommended to compare the methods below with the methods introduced by Trahan [55].

Piece-wise time homogeneous This theory is based on the article of Anastasiou and Tsekos [3], who partitioned the hindcast data into two seasons (summer and winter). Where the piece-wise time homogeneous function in the DMM-model is only able to partition the hindcast data into monthly workability sequences. Hence, for the sake of completeness, the DMM-model can be improved by making the piece-wise time homogeneous function also applicable for seasons or weeks. The monthly stationarity is derived by initially splitting

the hindcast dataset into 12 monthly workability sequences, which are in turn used for the calculation of the transition probabilities $\hat{P}_{ij}$, the limiting probabilities π_i and the cross-transition probabilities $\hat{P}_{ij}^{pq}$. The cross-transition probabilities are verified in Section 5.1.3.

As the theory describes in [45], the monthly time-series of each year are concatenated. This accepts a small inaccuracy spanning different years, because the concatenation of the monthly datasets adds a transition between the different years which did not occur in reality. More specifically, with this theory there exists a transition between the last time step of the last day of each month and the first time step of the first day of each month. For clarification of this error consult Figure 5.1, where the blue boxes indicate the workability sequences of January months over multiple years and the arrows indicate the newly added transitions. The error influences monthly transition probabilities $\hat{P}_{ij}(m)$ and limiting probabilities $\pi_i(m)$.

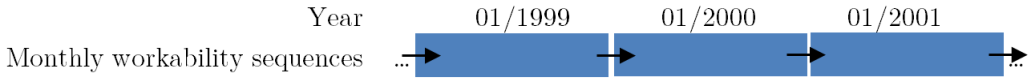

Figure 5.1: Schematization of the non-existing transitions (indicated with the arrow) in between different years for the same month for the piece-wise time homogeneous method. The blue boxes depict workability sequences for January over multiple years.

Non-time homogeneous This theory is based on Rajagopalan *et al.* [44], who used non-parametric kernel estimators to determine the transition probabilities of precipitation data. The same methodology is also applicable on metocean hindcast data to determine the transition probabilities per day $\hat{P}_{ij}(t)$. It is noted that the theory of the DMM-model has an erronious assumption of 366 days per year, which is obviously only true for leap years. Therefore, the correctness of the transition probabilities before and after the leap-day will be checked in the model verification (Section 5.2.2).

Furthermore, it is concluded that the transition probability is the only parameter modelled non-time homogeneously. It is inconsistent to predicate the other parameters (the limiting probability and the cross-transition probability) upon monthly datasets, once the non-time homogeneous function is being used. The other parameters can be calculated by using the same kernel bandwidths in the determination of the transition probabilities.

5.1.2 Module B: Time-dependency

Module B determines the order of the chain as explained in Section 2.5. Using a higher order chain results in a larger transition matrix (Table 2.1 presents the 2nd-order transition matrix). It is concluded in Rip [45] that higher order chains are solely used in the piece-wise time-homogeneous function, because of the complexity in determination of the transition probabilities for higher order chains in the non-time homogeneous function. And, because it is believed that the increase parametric uncertainty (consult Section 3.2 for uncertainty explanations) does not weigh up against the achieved lower model uncertainty. However, the piece-wise time homogeneous function is limited to a 2nd-order Markov chain. It will

be validated in Chapter 6 whether the use of higher order chains result in more accurate workability sequences.

5.1.3 Module C: Linked Markov chains

Influence period The influence period $D(p,q)$ implements a number of time steps at once in contradiction to the Markov theory, which will only generate single time steps (as explained in Section 2.6). The implemented time steps by the influence period are theoretically a block repetition of the hindcast data with a determined length based on the exceedance probability. After implementing the influence period in operation q, the regular Markov transition probabilities continue for operation q. No literature has been found for such a concept. It is concluded that this concept is *not correctly* implemented. The left boundary of the influence period is defined by the 1/0 crossing of operation p and the right boundary of the influence period is defined by the 1/0 crossing of operation q. First of all the influence period is implemented after an operation is finished and not after the 1/0 crossing of operation p is observed. Secondly, only workable time steps are implemented in operation q without the boundary of the 1/0 crossing in operation q (i.e. a non-workable state should have been placed after the influence period). The following two scenarios will explain more clearly why it is incorrect.
Scenario 1: After the implementation of the influence period, the DMM-model continues with the regular transition probabilities P_{ij}^{q}, when actually a 0 should have appeared based on the hindcast data. This is because the influence period is a block of 1s, until a 0 appears in the workability sequence of operation q (the 1/0 boundary of operation q). By continuing with the regular transition probabilities P_{ij}^{q}, there is a highly likely chance another set of 1s is going to appear (since the transition probability P_{11} is large in many cases). This results in a too high persistency of workable time steps in the workability sequence of operation q, and thus less downtime occurs.
Scenario 2: In case the randomly chosen influence period is zero time steps ($D(p,q) = 0$), which might occur when operation p and operation q are having different parametric operational limits. Then there are no workable time steps scheduled for operation q (i.e. in hindcast data a transition is observed from a workable state in operation p to a non-workable state in operation q). Hence, a non-workable time step should be generated in the workability sequence of operation q. However, the DMM-model uses the cross-transition probability instead to generate a state for operation q, which offers again the possibility to generate a workable time step in the workability sequence operation q. Therefore, the probability of generating a non-workable time step has become too low and the possibility of generating a 1 too high. This scenario also results in a too high workable persistency and thus less downtime.

In Section 7.1.1 will be explained how these scenarios are solved. Furthermore, the theory of the DMM-model describes that the exceedance curves of the influence period are yearly based, which will result in a too conservative downtime approximation for the summer months. This can be solved by introducing seasonal or monthly exceedance curves. And, it is noted that the influence period works only one-way. It implements workable time steps

in the workability sequence of operation q, when the preceding operation p has a stricter operational limit. Theoretically, this can also be applicable the other way around. In case the first operation p with a less strict operational limit observes a *non-workable* time step and crosses the 0/1 boundary, then operation q with a stricter operational limit cannot be workable either for a certain period. This introduces the non-workable influence period, $D^0(p, q)$, and is illustrated in Figure 5.2.

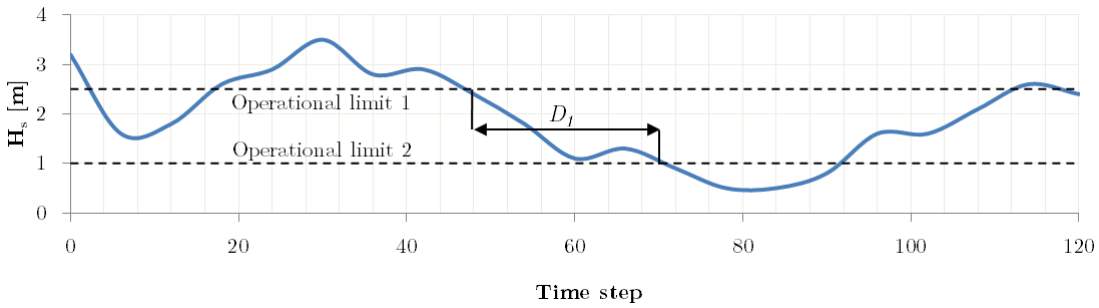

Figure 5.2: Schematization of the non-workable influence period, where the periods D are defined by the passages of the 0/1 boundary of operation 1 and the 0/1 boundary of operation 2.

A situation might occur as presented in Figure 5.3, where operation A becomes workable after 4 time steps and finishes within 3 time steps. The DMM-model would use the cross-transition probability P_{ij}^{AB} to generate the first state of operation B as indicated with an arrow. This time step could be a workable or non-workable state. Given that operation A was not workable at the 4th time step with an operational limit of $H_s \leq 3$ m, then it is also known that operation B cannot be workable for a certain period. This means that there is a non-workable influence period, which could overlap the state that is going to be generated by the cross-transition probability. The horizontal red bracket indicates the non-workable influence period.

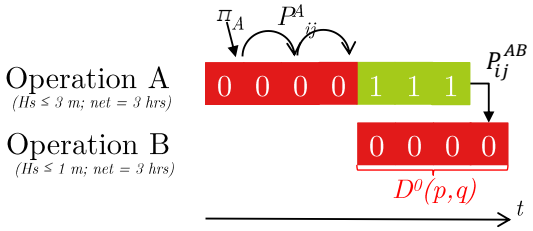

Figure 5.3: A hypothetical situation where the non-workable influence period overlaps the state that is generated by the cross-transition probability.

Cross-transition probability No literature have been found for this concept. The concept is based on the same idea of the regular transition probabilities, however these

transitions are in between different operations. Metocean parameters are correlated to each other, some less distinct than others, but there is a natural correlation. Therefore, applying the concept of the most likelihood estimation on the 'cross-transition probability' makes sense. As explained in Section 5.1.1, the DMM-model is limited to piece-wise stationarity in determining the cross-transition probability, which would be inconsistent if the seasonality in Module A is assigned to non-time homogeneity. In theory, it would be possible to make the cross transition probability non-time homogeneous. In that case the same kernel bandwidths should be used, which were predetermined in Module A for each specific operation. As it is anew concept, the mathematical relation between $\hat{P}_{ij}^{pq}$ and π_j^q is derived in order to indicate the cross-transition probability its order of magnitude. Consult Appendix C for the derivation and the results.

5.1.4 Module D: Coupled operations

Complex projects can consist of coupled operations, and the theory of Module D is correct for only 1 sequentially coupled operation. However, in reality more than one sequentially coupled operations are possible too. Multiple sequentially coupled operations apply to for example on the sequence of decommissioning a topside. Cutting the legs of the topside (operation A), followed by hoisting the topside (operation B). Subsequently, the topside is placed on a barge (operation C), followed by sea fastening the topside on the barge (operation D). Each operation has a different operational limit and no downtime is allowed in between the operations. In this example operation A, B and C are denoted as coupled operations.

An important conclusion can be drawn based on the theory of this module. There is a limit to sequentially coupled operations, due to parallel generation of the workability sequences of the coupled operations and of the operation that follows. For example, if there are 2 sequentially coupled operations (A and B), the workability sequences for operation A, B and C are generated in parallel. This introduces 8 different states ($S = 0, 1, 2, 3, 4, 5, 6, 7$) which are similarly created as in Table 2.3. Hence, 64 transition probabilities (assuming a 1st-order Markov chain) are possible between those states. The number of transition probabilities can be calculated with $\mathcal{O}((4^{n+1})^u)$, where n denotes the number of sequentially coupled operations and u the chain order. Note that this is a double exponential function, which means the number of transition probabilities grows quickly as the order or number of sequentially coupled operations grows (as presented in Table 5.1). For example, just 1 sequentially coupled operation with a 3rd-order Markov chain, results in 4096 transition probabilities ($(4^2)^3$). The more transition probabilities the more complex the DMM-model gets and the higher the parametric uncertainty (Section 3.2). Having too many transition probabilities would lead to copying the hindcast data, as the transition probabilities tend to values of 0 and 1. No new information is gained with DMM-model when hindcast data is exactly copied, making it worthless. The number of sequentially coupled operations is a fixed number, which is known prior to a project simulation, but the Markov chain order can be chosen. Therefore, an optimum analysis for the amount of transition probabilities that can be used to simulate reliable metocean parameters (consult the article of Jimoh

and Webster [24] for this purpose). In Section 7.1.3 is explained how sequentially coupled operations can be modelled in the current DMM-model.

Table 5.1: The amount of transition probabilities by varying the Markov chain order (first column) and the number of sequentially coupled operations (first row), which can be determined by $\mathcal{O}(4^{n+1})^u$.

		No. coupled operations			
		0	1	2	...
Order	1	4	16	64	...
	2	16	256	4096	...
	3	64	4096	262144	...
	4	256	65536	16777216	...
	...	...	...	...	...

Furthermore, it was already stated in Section 2.7 that Module C is not used when the coupled and its succeeding operation are simulated. An error could occur as presented in Figure 5.4. In this example a 1st-order Markov chain is applied and 4 time steps are generated. The influence period $D(A, B)$ *should* have been used after the transition 2nd transition, because operation A crosses the 1/0 boundary and the operational limit of operation A is stricter than operation B. Hence, operation B should be workable for a minimum number of time steps. Suppose the least observed influence period is $D(A, B) = 2$ time steps, as indicated in the figure, which means at least 2 workable states should be generated. However, in the 4th time step a non-workable state is generated in operation B, which is possible since a 1st-order is applied. This example shows that unrealistic workability sequences can be generated with the current approach. The module will be validated in Section 6.2.4, in order to find out whether these inconsistencies are occurring.

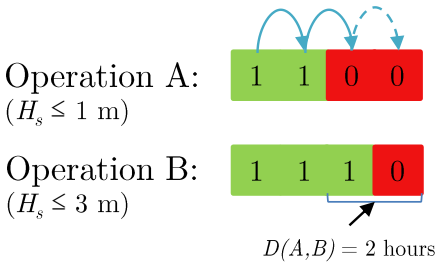

Figure 5.4: Hypothetical project simulation of a coupled operation and its succeeding operation, where the influence period should overlap the a generated state.

5.2 Model verification

5.2.1 Module A: Seasonality

Piece-wise time homogeneous In this model verification the $\hat{P}_{ij}(m)$ and $\pi_i(m)$ are checked. It is proved that the error described in the concept verification is taking place. It can be recovered by partitioning the monthly workability sequences per year. Subsequently, the transitions can be counted and the maximum likelihood estimate $\hat{P}_{ij}(m)$ can be calculated from these summations.

Furthermore, it is proved that in the monthly workability sequences of the DMM-model the first time step of the next month is included in the array of the current month. The reason for including this time step is to obtain the last transition of the month, as clarified in Figure 5.5. This makes sense for the calculation of the monthly transition probabilities, $\hat{P}_{ij}(m)$, however the limiting probabilities $\pi_i(m)$ are changed as well by this inclusion. These are calculated with the following formula:

$$\pi_i = \frac{N_i}{N_i + N_j}, \quad \forall i, j \in S \tag{5.1}$$

Where N_i and N_j denote the number of observed states per month. This formula is valid if only the states of the current month are taken into account, but due to the inclusion of the first time step of the next month a small error is made. The limiting probabilities are used in both seasonality methods. Separate monthly datasets excluding the first time step of the next month have to be made to recover this error.

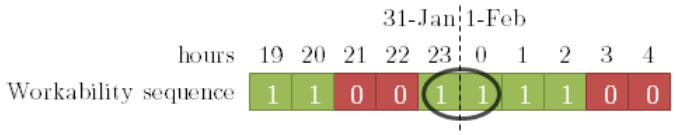

Figure 5.5: Schematization of the last transition of the month

Non-time homogeneous In this model verification the influence of the 366 days assumption on the transition probabilities is checked. The calculation of transition probabilities are correct for leap years. However, for non-leap years it is proved that most of the transition probabilities are miscalculated, except for the following days:

$$1\text{Jan} + \text{Kernel bandwidth} \leq \text{Correctly computed } \hat{P}_{ij} \leq 28\text{Feb} - \text{Kernel bandwidth} \tag{5.2}$$

The kernel bandwidth denotes a number of days determined in Module A (as explained in Section 2.4). The transition probabilities of the days not within the domain of Equation 5.2 are incorrectly computed due to the 366 days assumption. The DMM-model loops through the 366 days to determine the transition probabilities per day. As a result, data is

shifted due to the leap-day. Table 5.2 presents in the first column the loop-days and how they correspond to dates in reality.

Table 5.2: Comparison of the numbered days in the DMM-model and reality

Day in DMM-model	Date of leap year	Date of non-leap year
58	27-Feb	27-Feb
59	28-Feb	28-Feb
60	29-Feb	1-Mar
61	1-Mar	2-Mar
62	2-Mar	3-Mar

If the transition probabilities are computed on 61st day for example. Then it turns out that this day corresponds to 25% of the hindcast data with 1-March and 75% of the hindcast data with 2-March. This applies to all days onwards from the 60th day, due to the unsynchronized numbering of the dates from the leap-day. Equation 5.2 also includes the kernel bandwidth, because the kernel bandwidth is used for the calculation of the transition probabilities. The first few days of January are determined with the last few days of December because of the kernel bandwidth, which explains the left hand side of Equation 5.2. The right hand side of the equation can be explained similarly.

5.2.2 Module B: Time-dependency

The standard MATLAB code to construct a state-transition matrix for higher order Markov chains is not verified, but is assumed to be correct. The transition matrix indicates how many of each transition is observed. It is used as input for the limiting probabilities $\pi_i(m)$, the monthly transition probabilities $\hat{P}_{ij}(m)$ and the cross-transition probabilities $\hat{P}_{ij}^{pq}$. The code of the hypothesis tests are concluded to be incorrect (see Section 6.2.2 for explanation of the hypothesis tests). First the hypothesis test of seasonality has to be conducted for all operations. Piece-wise time homogeneity can be applied in case none of the hypothesis tests are rejected, else non-time homogeneity should be used. Secondly, the order test should only be conducted if the seasonality is determined to be piece-wise time homogeneous. A 2nd order should be assigned if none of the operations reject the hypothesis test, else a 1st order should be used. A pseudocode is given of this process in Listing 5.1.

Listing 5.1: Pseudocode: Redefining the hypothesis-tests

```
Test1 = SeasonalityTest(All operations)
if all(Test1) > α
    Seasonality = Piece-wise time homogeneous
else
    Seasonality = Non-time homogeneous
    Order = 1
end

if Order = 1
    continue
else
    Test2 = OrderTest(All operations)
    if all(Test2) > α
        Order = 2
    end
end
```

5.2.3 Module C: Linked Markov chains

Influence period Based on several checks it is concluded, that the function for the influence period is written correctly disregarding the wrong implementation as Section 5.1.3 describes. However, the function is being called for every operation transition for every year/project that is generated, which is very time consuming. The resulting exceedance curve is based on the hindcast data, therefore it has to be called just once for every possible operation combination, before looping in the generation of years/projects to make the DMM-model more efficient.

Cross-transition probability The same as the influence period holds for the cross-transition probability, as this function is being called for every year/project that is generated in case the influence period is not scheduled. The cross-transition probabilities are based on the (monthly) hindcast data, therefore they have to be determined before looping in the generation of years to make the DMM-model more efficient.

As aforementioned, the cross-transition probability is determined by piece-wise stationarity, which includes the error described in Section 5.1.1.

5.2.4 Module D: Coupled operations

The concept verification indicated that multiple sequentially coupled operations cannot be simulated. This Section addresses to the model verification. It is verified that the current DMM-model is only able to simulate coupled operations in piece-wise stationarity, and not in the non-time homogeneous function. Therefore, a more thorough validation is performed in Section 6.2.4, to find the limitations of this module.

5.3 Conclusion

Every module has been verified on its theoretical concept and model code. From the verification it is concluded that several limitations and errors were obtained in the modules, which are overviewed in Table 5.3. Research question No. 2a: '*Is the concept and the model code of the current DMM-model correct, consistent and complete?*' can be unfolded into three aspects (correctness, consistency and completeness). In terms of theoretical concepts of the DMM-model only the influence period is verified to be incorrect, the other theoretical concepts are verified to be correct, consistent and complete. In terms of the model code the DMM-model is verified to be is not correct, as errors have been found in for example the determination of the transition probabilities. Neither the model code is consistent, as for instance the cross-transition probabilities can only be determined monthly stationary. Nor the model is code is complete, as it is for example limited to a 2nd-order Markov chain. This answers the research question and the found limitations and errors will be validated or improved in the next chapters of this thesis.

Table 5.3: Summarized conclusions per module of the verification process

	Comment:
Module A:	Piece-wise time homogeneous: • The function makes a small error in the derivation of the $\hat{P}_{ij}(m)$ and $\pi_i(m)$, which can easily be recovered. The degree of this error is rather small. • The function is limited to monthly stationarity, while it can be extended to weekly or seasonal probabilities. Non-time homogeneous: • The function miscalculates the transition probabilities $\hat{P}_{ij}(t)$, due to leap-years. • The limiting probabilities π_i are based on monthly stationarity, while with the kernel bandwidth the limiting probabilities can also be determined for each day.
Module B:	The hypothesis tests had to be recoded, due to several errors. It needs to be validated whether higher orders are more accurate. Time-dependency can only be used for the piece-wise time-homogeneous function, while several hypothesis tests concluded that the non-time-homogeneous function matches better the hindcast data.
Module C:	Influence period: • The influence period is incorrectly implemented, as too many workable time steps are implemented. • The exceedance curves are yearly based, which can be too conservative. Therefore, the seasonal and monthly exceedance curves have to be validated. . • The influence period works only one-way. It implements only workable time steps for operation q, which follows from preceding operation p with a stricter operational limit. The influence period can be made two-way, where non-workable time steps are implemented. • It is concluded that the influence period can be coded more time efficient. Cross-transition probability: • This probability is limited to piece-wise stationarity, while in theory the same kernel bandwidth, predetermined in Module A for non-time-homogeneous function, can be used. • A small error is made in the derivation of the $\hat{P}_{ij}^{pq}$, because of an error in the piece-wise time-homogeneous function. The degree of this error is similarly small as the error of $\hat{P}_{ij}(m)$. • It is concluded that the cross-transition probability can be coded more time efficient.
Module D:	• The model is limited to one sequentially coupled operations, however in practice more sequentially coupled operations can be possible too. • The model is limited to piece-wise stationarity for coupled operations. In order to make the model more consistent coupled operations have to be made non-time-homogeneous as well.

6 Validation

In this chapter a software validation is conducted for the DMM-model. As explained in Chapter 4 the validation is performed after the verification process is finished. As Section 4.2 describes, the validation is divided into three parts: the 'white-box', 'data' and 'black-box' validations. These three validations are analyzed in Sections 6.2, 6.3 and 6.4 respectively. Three different datasets have been used for the validation, as given in Section 6.1. As a conclusion, in Section 6.5 an answer will be given to research question No. 3a: '*Do the DMM-model and its individual modules perform sufficiently accurate?*'. In Chapter 5 several errors, inconsistencies or limitations have been found and it is studied in this chapter what the influence is of these findings. With 'sufficiently accurate' is meant whether the model and its modules perform reliable despite the findings of the verification. After the validation a prioritization of the findings can be made. For example, in case a module does not perform sufficiently accurate the findings are assigned to a high priority to resolve.

6.1 Input data

The following three datasets are used for validation of the DMM-model in this Chapter.

- 'Gulf of Guinea dataset': consist of 23 years (from 1992 – till 2015) sampled with an interval of 3 hours. Coordinates: 0.5°N 4.5°E
- 'North sea dataset': consist of 23 years (from 1992 – till 2015) sampled with an interval of 3 hours. Coordinates: 57.83°N 0.5°W
- 'Tasman sea dataset': consist of 24 years (from 1992 – till 2016) sampled with an interval of 3 hours. Coordinates: 38.5°S 148°E

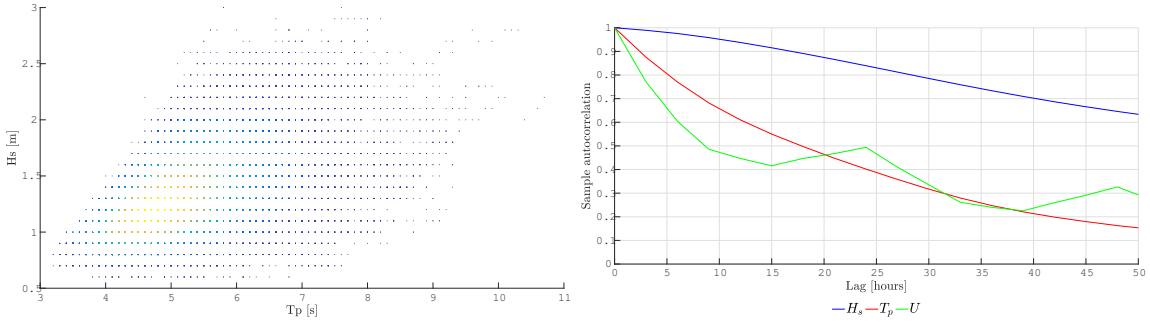

Figure 6.1: The H_s, T_p scatter (left) and the sample autocorrelation (right) for the Gulf of Guinea dataset.

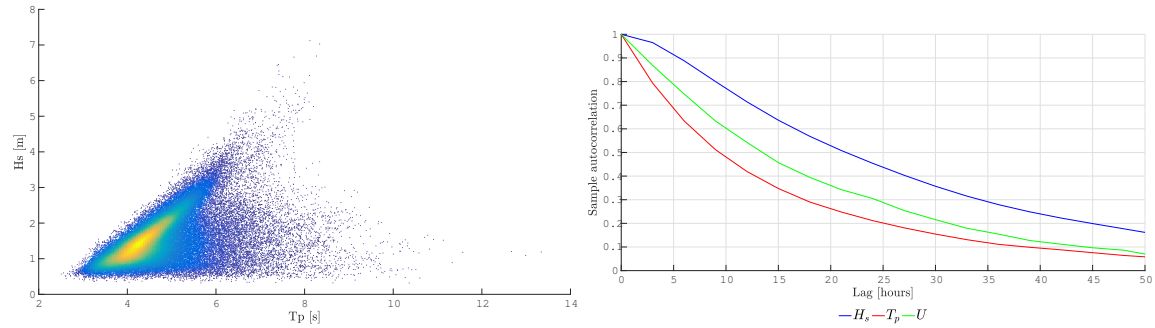

Figure 6.2: The H_s, T_p scatter (left) and the sample autocorrelation (right) for the Tasman sea dataset.

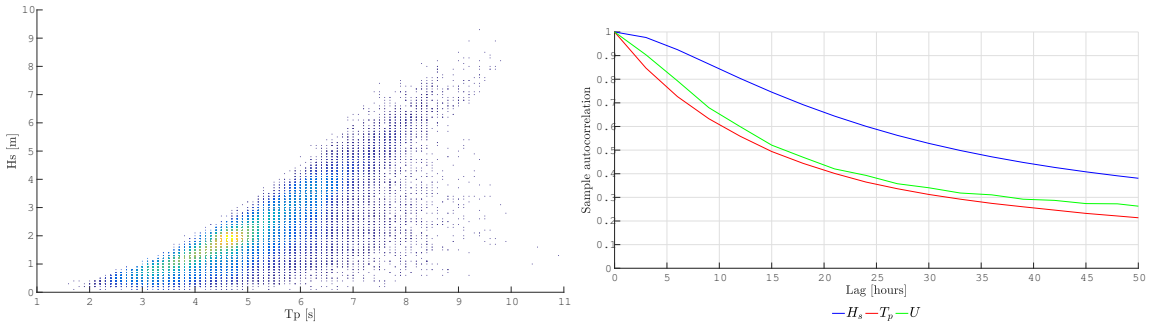

Figure 6.3: The H_s, T_p scatter (left) and the sample autocorrelation (right) for the North sea dataset.

The datasets are time-series consisting of observations (e.g. H_s, U, T_p), which can be considered as $x_1, ..., x_n$. The mean of the datasets is given by:

$$\bar{x} = \frac{1}{n} \sum_{t=1}^{n} x_t \tag{6.1}$$

The autocovariace is given by:

$$\hat{\gamma}(h) = \frac{1}{n} \sum_{t=1}^{n-|h|} (x_{t+|h|} - \bar{x})(x_t - \bar{x}) \tag{6.2}$$

The autocorrelation[1] is determined with the mean and the autocovariance as [8]:

$$\hat{\rho}(h) = \frac{\hat{\gamma}(h)}{\hat{\gamma}(0)} \tag{6.3}$$

6.2 White-box validation

The white-box validation determines whether the modules of the DMM-model represent the real world with sufficient accuracy.

6.2.1 Module A: Seasonality

In the verification of Module A an error is found in the piece-wise time homogeneous method and in the non-time homogeneous method. In this Section it is studied what the influence is of these errors.

The seasonality effects influence the transition probabilities as explained Section 2.5. In Figures 6.4a and 6.4b the transition probability P_{01} is presented for the piece-wise time homogeneous and the non-time homogeneous function. The left figure is based on a wave field in the North sea (Northern Hemisphere) and the right figure is based on a wave field between Australia and Tasmania (Southern Hemisphere). Both metocean datasets are subject to an operational limit of $H_s \leq 1.5$ m. It is clear that the transition probability of moving to a workable state is higher in the summer, than during winter on the Northern Hemisphere. Vice versa, the transition probability of moving to a workable state for the Southern Hemisphere is higher during winter months of the Northern Hemisphere.

From Figure 6.4 it can be observed that Module A works sufficiently accurate. The monthly homogeneous method results in a stationary probability for each month and by using a higher kernel bandwidth h a smoother line throughout the year is obtained. A stationary probability throughout the whole year would appear if a kernel bandwidth of 365 is chosen. The best proposed fit is determined with a least square cross validation procedure. The error found in the verification (Section 5.1.1) for the piece-wise homogeneous function is too small to have a noticeable influence on the results of the transition probabilities. This also holds for the found error during verification of the non-time-homogeneous function (Section 5.2.1). The results of the transition probability in Figure 6.4a have a large standard deviation in July for a kernel bandwidth of 7 days. This can be explained by analyzing the hindcast data in the specific month. It is concluded that 23-years of hindcast data is still a relatively small amount of data. If one-day observations deviate from the nearest days,

[1] The autocorrelation is the correlation of a function with a lagged version of itself. It illustrates how rapidly the time-series are expected to change [58].

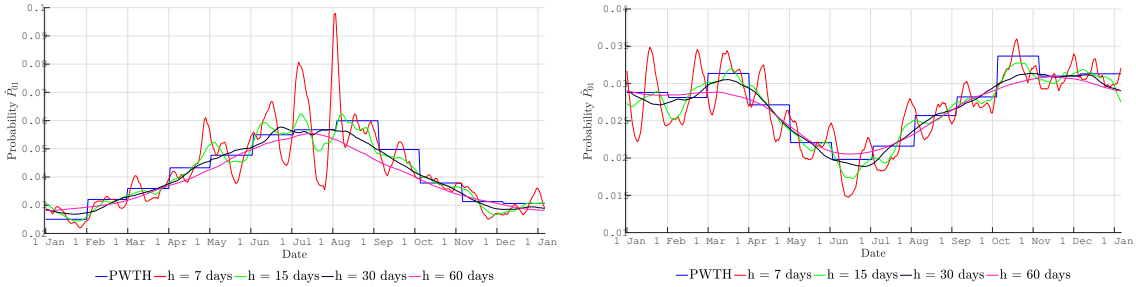

(a) Northern Hemisphere (North sea) **(b)** Southern Hemisphere (Tasman Sea)

Figure 6.4: Seasonality effects on both hemispheres presented with transition probability P_{01} subject to operational limit $H_s \leq 1.5$ m. Piece-wise time homogeneous method is indicated in blue and the non-time homogeneous method is performed with different kernel bandwidths h.

and thereby exceeding the operational limit, the transition probability P_{01} will decrease significantly. In this example the found error due to leap-days is not clearly noticeable, but it is recommended to recover the error anyway.

6.2.2 Module B: Time-dependency

In the verification of Module B it is recommended to validate the effect of time-dependency, because the current DMM-model is limited to a 2nd-order for the piece-wise time homogeneity and limited to a 1st-order for the non-time homogeneous method. This Section addresses to that purpose. In this validation it is studied which seasonality method is more accurate, and whether a higher order describes the hindcast more accurate than a 1st- or 2nd-order.

Two type of tests are conducted: the homogeneity-test and the order-test. The model code is verified to be incorrect (Section 5.2.2), therefore it is rewritten according to Listing 5.1 to perform the hypothesis tests. Consult Appendix D for explanation of hypothesis-testing and consult Appendix E.2 for the results. In this thesis a 95% confidence level ($\alpha = 0.05$) is used, which is a general guideline.

Homogeneity test [52] The transition probabilities per week within a month should be more or less the same, if the assumption of monthly piece-wise stationarity is correct. The monthly workability sequences are sub-divided into Y = 4 different sub-intervals (weeks per month). The transition probabilities per week (sub-interval) are tested with the transition probabilities per month. The following hypotheses are defined:

- $H_0 : P_{ij}(y) = P_{ij}(m) \quad \forall i, j \in S, y = 1, 2, 3, 4, m = 1, 2, ..., 12$
- $H_1 : P_{ij}(y) \neq P_{ij}(m) \quad \forall i, j \in S, y = 1, 2, 3, 4, m = 1, 2, ..., 12$

Where $P_{ij}(y)$ denotes the transition probability from state i at time t to state j at $t+1$ during subinterval y (week). This transition probability holds for $[t_y, t_y + \Delta y]$, where t_y is defined as the first time step in sub-interval y with length Δy. $P_{ij}(m)$ denotes the transition probability from state i at time t to state j at $t+1$ during interval m (month).

This transition probability holds for $[t_m, t_m + \Delta m]$, where t_m is defined as the first time step in sub-interval m with length Δm. The maximum likelihood estimates of the transition probabilities during subinterval y or interval m are calculated as follows (where int denotes y or m):

$$\hat{P}_{ij}(int) = \frac{N_{ij}(int)}{\sum_{j \in S} N_{ij}(int)}, \quad \forall i, j \in S \tag{6.4}$$

The number of transitions from state i at time t to state j at time $t+1$ in the (sub)interval is denoted with $N_{ij}(int)$. The Chi-square test[2] (or χ^2 test) is used to test the null-hypothesis. It is defined as follows [4]:

$$\chi_i^2 = \sum_{y=1}^{Y} \sum_{j \in S} \frac{N_{ij}(y)(\hat{P}_{ij}(y) - P_{ij}(m))^2}{P_{ij}(m)}, \quad \forall i, j \in S \tag{6.5}$$

The limiting χ_i^2 distribution has $(n_s^u - 1) \cdot Y$ degrees of freedom (u is the order of the chain). Summing over all χ_i^2, the total test statistic χ_i^2 has a limiting χ_i^2 distribution with $(n_s^u - 1) \cdot Y \cdot n_s^u$ degrees of freedom. A small number (10^{-10}) is added to the number of transitions for smoothing to avoid $\hat{P}_{ij} = 0$. If the null-hypothesis is true, the hindcast data is considered to be piece-wise time homogeneous. Alternatively, the non-time homogeneity is assigned to the DMM-model.

Order-test [4] The transition probabilities for a Markov chain order u and a Markov chain order $u+1$ should be more or less the same, if the assumption of a Markov chain order u is correct. In other words, the last state before the u states should not have an influence on the transition probabilities.

- H_0 : The Markov chain order is of order u, implying that $P_{ij...k} = P_{j...kl}, \forall i \in S$ (the workability sequence $ij...k$ covers the last $u+1$ states and the workability sequence $j...k$ covers the last u states, l is the next state)
- H_1 : The Markov chain is not order u, hence $P_{ij...kl} \neq P_{j...kl}$

A χ^2-test is used to test the null hypothesis. Higher order chains are only applicable for piece-wise stationarity, therefore this test will only be performed if the homogeneity test proved that the hindcast data is piece-wise time homogeneous. Furthermore, in [45] it is concluded that after order 6, not much more knowledge is gained and using an even higher order chain would lead to an exact replica of the original data. Therefore, the order test is limited to the 6th-order. The maximum likelihood estimate of $P_{ij...kl}$ for a stationary chain is defined as:

$$\hat{P}_{ij...kl} = \frac{N_{ij...kl}}{N^*_{ij...k}}, \quad \forall i, j, ..., k, l \in S \tag{6.6}$$

[2] A chi-square test compares two variables in order to determine if they are related.

With:

$$N^*_{ij...k} = \sum_{l \in S} N_{ij...kl}, \quad \forall i, j, k \in S \tag{6.7}$$

The χ^2 statistic for the null hypothesis is defined as:

$$\chi^2_{j...k} = \sum_{i \in S} \sum_{l \in S} \frac{N^*_{ij...k}(\hat{P}_{ij...kl} - \hat{P}_{j...kl})^2}{\hat{P}_{j...kl}}, \quad \forall i, j, ..., k \in S \tag{6.8}$$

With:

$$\hat{P}_{j...kl} = \frac{\sum_{i \in S} N_{ij...kl}}{\sum_{i \in S} N^*_{ij...kl}}, \quad \forall i, j, ..., k \in S \tag{6.9}$$

The limiting χ^2 distribution has $(n_s - 1)^2$ degrees of freedom. Summing over all χ^2, the total test statistic χ^2 has a limiting χ^2 distribution with $(n_s - 1)^2 \cdot n_s^u$ degrees of freedom (where u is the chain order). A small number (10^{-10}) is added to the number of transitions for smoothing to avoid $\hat{P}_{ij} = 0$. If the null-hypothesis is true, then the workability sequence has a Markov chain order u.

For comparison purposes, another test statistic is analyzed; the log likelihood ratio test statistic [52], which is given by:

$$-2ln(\Delta) = -2 \sum_{i \in S, j \in S} N_{ij...kl}(ln(\hat{P}_{ij...kl}) - ln(\hat{P}_{j...kl})), \quad \forall i, j, ..., k, l \in S \tag{6.10}$$

This test statistic has χ^2 distribution with $(n_s^{u+1} - n_s^u) \cdot (n_s - 1)$ degrees of freedom.

Conclusion In Appendix E.2 the results of the hypothesis-tests are presented and summarized in Tables 6.1 and 6.2. A project simulation in the DMM-model is ran only in the homogeneous mode or only in the non-homogeneous mode. To run it in the homogeneous mode, all of the homogeneity hypothesis tests must be fulfilled (for all operations for all months). In the results it can be noticed that only one operation ($H_s \leq 2.5$ m) in the Tasman Sea can be considered piece-wise time homogeneous (PWTH) and all of the other operations are non-time homogeneous (NTH). A (large) marine project could consist of 25 different operations. Therefore, it will be unlikely the homogeneity tests result in the piece-wise time homogeneous mode for larger projects. However, for smaller projects consisting of only a few operations, there is a chance that the operation(s) is/are piece-wise homogeneous. In that case the order test has to be performed as well, since the DMM-model is able to simulate 2nd-order Markov chain with the homogeneous mode. A handful of order-tests resulted in an accepted hypothesis, which means even higher order are needed in case the hypothesis was rejected. The rejected tests are denoted with a - in Table 6.2. All of the order-tests have to be fulfilled to run the DMM-model with a 2nd-order Markov chain. In other words, it is not valid to run Operation A with a 2nd-order and Operation B with a 1st-order. It can be concluded for the used operations and datasets, that the DMM-model will always be more accurate with a 2nd-order than a 1st-order Markov chain.

Table 6.1: Summarized results of the seasonality (chi-squared) hypothesis tests, where NTH means non-time homogeneous and PWTH means piece-wise time homogeneous.

	$H_s \leq 1m$	$H_s \leq 2m$	$H_s \leq 2.5m$	$U \leq 10m/s$	$T_p \leq 7s$	$H_s \leq 2m; U \leq 10m/s$	$H_s \leq 2m; T_p \leq 7s$
Gulf of Guinea	NTH	NTH	NTH	NTH	NTH	NTH	NTH
North sea	NTH	NTH	NTH	NTH	NTH	NTH	NTH
Tasman sea	NTH	NTH	PWTH	NTH	NTH	NTH	NTH

Table 6.2: Summarized results of the order hypothesis tests, where the lowest order is reported in case the test was not rejected. The - denotes that all tests were rejected for orders 1 to 6.

	$H_s \leq 1m$	$H_s \leq 2m$	$H_s \leq 2.5m$	$U \leq 10m/s$	$T_p \leq 7s$	$H_s \leq 2m; U \leq 10m/s$	$H_s \leq 2m; T_p \leq 7s$
Chi-squared test							
Gulf of Guinea	-	-	5	2	-	-	-
North sea	-	-	-	-	-	-	-
Tasman sea	2	4	6	-	2	-	2
Log likelihood ratio test							
Gulf of Guinea	-	6	5	2	3	6	3
North sea	-	-	-	-	-	-	-
Tasman sea	2	4	3	-	2	-	2

It is expected that most of the future projects will be performed with non-time homogeneity and first-order based on the hypothesis tests, certainly the complex projects consisting of multiple operations. In case the seasonality test results is accepted, it is expected that the order-test will almost always result in a higher Markov chain order. Furthermore, it is recommended to study the possibility to run a project simulation with each operation assigned to its best test results. In this thesis, a project simulation will be run with a predetermined Markov chain order and predetermined homogeneity.

The likelihood ratio test statistic resulted in a better description of the workability sequences with a higher order chain for more operations. This is due to the use of the natural logarithm instead of squaring the differences. The likelihood ratio test statistic is preferred for the order test, because the differences in $\hat{P}_{j\ldots kl}$ and $\hat{P}_{ij\ldots kl}$ are too significant to square them.

Remarks In this thesis solely the chi-squared and the log likelihood ratio test statistics are used. It is recommended to study the influence of different test statistics, considering the differences in the two used statistics. Alternative test statistics are the Akaike information criterion (AIC) [54], the Bayesian information criterion (BIC) [25], the exact test [42] and the ϕ-divergence test statistic [33]. Furthermore, in this thesis add-one smoothing is applied, where one-count is added to each N_{ij} before calculating $\hat{P}_{ij}$ [38]. The reason for that is that in the metocean hindcast data some transitions might not have been observed, while they could occur in reality. This is called the zero-count problem or the sparse data problem. There are alternative smoothing techniques: back off smoothing, Bayesian smoothing [38] or Good-Turing smoothing [30]. In this thesis only the transition probabilities are used for both hypothesis tests, while the limiting probabilities can also be used.

6.2.3 Module C: Linked Markov chains

Module C will be validated with the operations given in Table 6.3.

Table 6.3: The operations used for the white-box validation of the influence period and the cross-transition probability (Module C).

Operation No:	Limit:
1	$H_s \leq 1$ m
2	$H_s \leq 2$ m
3	$H_s \leq 2.5$ m
4	$U \leq 10$ m/s
5	$T_p \leq 7$ s
6	$H_s \leq 2$ m; $U \leq 10$ m/s
7	$H_s \leq 2$ m; $T_p \leq 7$ s

Influence period In the verification (Section 5.1.3) it is concluded the concept of the influence period is not correctly implemented. This conclusion is disregarded for the white-box validation. The white-box validation focuses solely on the obtained exceedance curves. In Section 5.2.3 it was concluded the MATLAB code is written correctly for that purpose. The yearly exceedance curve of D for the North sea dataset is validated in Appendix E.4. The obtained figures show the expected results. The closer two operational limits (p and q) are to each other, the shorter the influence period $D(p, q)$ gets. In case operational limit q is stricter than operational limit p, there is no influence period. From the figures it can be noted, that some exceedance curves do not start at a probability of 1. This happens when operational limits p and q are assigned to different parameters (e.g. $D(H_s \leq 2.5$ m, $U \leq 10$ m/s)). Hence, the DMM-model creates correctly the exceedance probability curves, but the implementation of the influence period goes wrong. In Section 7.1.1 the influence period will be rectified.

Cross-transition probability In the verification (Section 5.2.3) it was concluded the MATLAB code of the cross-transition probabilities contains an error. In Appendix E.5 the cross-transition probability P_{01}^{pq} (i.e. from a non-workable state in operation p at time step t to a workable state in operation q in time step $t+1$) is presented throughout the year with monthly stationarity. In the North sea (Figure E.6) this probability is larger during the summer months, because of calmer weather conditions (seasonality). The cross-transition probability P_{01}^{pq} in the Gulf of Guinea is significantly larger (Figure E.7), than the North sea. This can be explained by its swell region which is calmer than the wind-waves of the North sea. Besides, the seasonal phenomena are less present considering the location is approximately at the equator. Also, the cross-transition probability P_{01}^{pq} in the Tasman sea (Figure E.6) is large, due to calm weather conditions.

Furthermore, it can be noticed that the cross-transition probabilities decrease in case the limits of operations p and q are close to each other. This can be explained by the following example: if operation p with operational limit $H_s \leq 1$ m is *non-workable* at t, the

cross-transition probability will be larger if we move to a workable state of operation q at $t+1$ with operation limit of $H_s \leq 2$ m, instead of moving to a workable state of an operation with an operational limit of $H_s \leq 1.5$ m. Note that in this example the operational limit of the same parameter is less strict, which will not happen in the current DMM-model with the cross-transition probability because of the influence period. However, the logic remains the same when two parameters are considered which differ from each other.

It is concluded that the cross-transition probability is well modelled in the DMM-model. And, the error found in the verification phase is of small significance that it is unnoticeable in the results.

6.2.4 Module D: Coupled operations

In the verification it was concluded that multiple sequentially coupled operations could not be simulated. Nor can coupled operations be simulated in the non-time homogeneous method. Therefore, it is validated in this Section what the influence is of these findings. Several hypothetical projects will be simulated in order to find the limitations (Table 6.4). First, a project is simulated *without* a coupled operation 1st-order and piece-wise time homogeneous) to find out whether the DMM-model simulates the set operations correctly. Subsequently, the same operations with non-time homogeneity *with* a coupled operation is simulated, because in the verification (Section 5.2.4) it was concluded this was not possible. After confirming this conclusion, only piece-wise time homogeneous projects will be simulated with each a different module adjustment. The modules are adjusted by changing the parametric values of the operational limits. It will be validated what the effect is on the coupled operations by varying the influence period (No. 3), cross-transition probability (No. 4), 2nd-order Markov chain (No. 5) and multiple coupled operations (No. 6). Table 6.4 indicates which scenarios succeeded during this validation.

Table 6.4: The simulation of 6 small hypothetical projects, wherein the other modules are adapted. Abbreviations: O = Order, PWTH = Piece-Wise Time Homogeneous, NTH = Non-Time Homogeneous, * = Coupled operation

No.	Settings:	Operations:	Succeeded:
1.	No coupled; 1^{st} O; PWTH	(1) $H_s \leq 1.5$ m, (2) $T_p \leq 7$ s, (3) $U \leq 9$ m/s	✓
2.	1 coupled; 1^{st} O; NTH	(1*) $H_s \leq 1.5$ m, (2) $T_p \leq 7$ s, (3) $U \leq 9$ m/s	×
3.	1 coupled; 1^{st} O; PWTH	(1*) $H_s \leq 1.5$ m, (2) $H_s \leq 2$ m, (3) $U \leq 9$ m/s	×
4.	1 coupled; 1^{st} O; PWTH	(1*) $H_s \leq 1.5$ m, (2) $T_p \leq 7$ s, (3) $U \leq 9$ m/s	×
5.	1 coupled; 2^{nd} O; PWTH	(1*) $H_s \leq 1.5$ m, (2) $T_p \leq 7$ s, (3) $U \leq 9$ m/s	×
6.	2 coupled; 1^{st} O; PWTH	(1*) $H_s \leq 1.5$ m, (2*) $T_p \leq 7$ s, (3) $H_s \leq 1$ m/s	×

From the 6 performed tests only the first one succeeded, where no coupled operation was included. The other tests included a coupled operation with different settings of the Modules A, B and C. These resulted in a crash or computational errors were observed in the simulation. The observations are explained below:

No. 1 Without coupled operations the DMM-model works correctly.

No. 2 It is observed that the non-time homogeneous probabilities cannot be determined for more than 2 states. Coupled operations have 4 states ($S = 1, 2, 3, 4$), because the coupled operation and the succeeding operation are bundled, as explained in Section 2.7.

No. 3 The project may not encounter downtime between operation 1 (coupled) and operation 2. The simulation, however, continues when operation 2 is finished regardless what operation 1 has done.

No. 4 Same error as in No. 3. In some tests the DMM-model did not recognize two sequentially workable net durations which were generated.

No. 5 The initial state cannot be generated, hence the simulation crashes. A 2nd-order Markov chain with piece-wise time-homogeneity and a coupled operation will always result in a crash (it does not matter if there is influence period or cross transition probability in the project).

No. 6 Same error is made as in No. 3 for the 1^{st} operation. Furthermore, the DMM-model should generate 8 states ($S = 1, 2, .., 8$) when there are 2 sequentially coupled operations. The DMM-model can create 4 states maximum, hence a second error is observed at the start of operation 3.

Based on the preceding observations it can concluded this module does not work at all.

6.3 Data validation

The metocean data ('hindcast' data) near project locations used for the DMM-model and HADDOCK is obtained from the in-house global offshore database. These datasets are already validated to ensure the data is clean, correct and useful. The measured metocean parameters are not validated in this thesis. Nor are the net durations and operational limits. These are deterministic, while in practice this does not necessarily have to be true. An operation can be executed longer or shorter than the predefined net duration. Also, a vessel captain can decide with his own judgment or experience whether the operation will be executed or not. Therefore, the focus of this Section is addressed to the quantity of the data. Questions arise like 'How much input data is needed? How many years are needed to generate?'. The answering of these questions are closely related to uncertainty assessment, as Section 2.9 describes that the simulation uncertainty decreases by increasing the sample size n (number of generated years). In this data validation the focus is put on the number of output years, because the number of input years is fixed. Two datasets (North sea and Gulf of Guinea) from Section 6.1 and four different operational limits ($H_s \leq 1$ m, $H_s \leq 2.5$ m, $T_p \leq 6$ s and $U \leq 5$ m/s) are considered. From the datasets and the operational limits, the workability sequences are obtained. Both datasets consist of 23 years of hindcast data, which are augmented to 1000 years. The first state is determined with the limiting probability (Equation 2.9) and all of the other states are determined with the transition probabilities (Equation 2.3). The workability percentage and the persistency are assessed in the following.

Workability percentage From the 1000 generated years the workability percentage is determined. Subsequently, the generated 1000 years are divided into bins of 1, 10, 15, 20, 25 and 100 years. From these bins the workability percentages are determined (Equation 1.1). In Figure 6.5 one of the results is presented as an example, and in Appendix E.6 the other box plots are shown of the results.

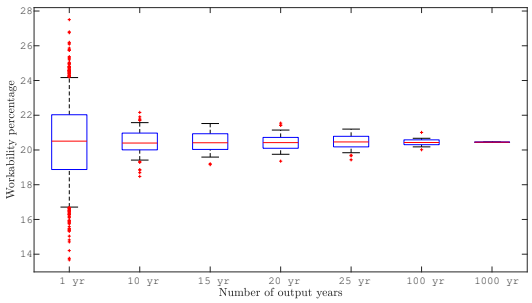

Figure 6.5: The workability percentage of the North sea dataset subject to an operational limit $H_s \leq 1$ m for non-time homogeneity and 1st-order measured for different bins of years. The whiskers of the box plot indicate the 95th percentiles and the red cross are its outliers.

The smaller the bin size, the more variation in the workability percentage, however the variation decreases quickly with a larger bin size. The χ^2-test is used to analyze the variation

around the mean. Considering the small differences between piece-wise time homogeneous and non-time homogeneous methods, only the piece-wise time homogeneous method is used in the following. The following hypotheses can be defined:

- H_0: $T_i^*(b) = T_i^* \quad \forall i \in S, b = 1, ..., B$
- H_1: $T_i^*(b) \neq T_i^* \quad \forall i \in S, b = 1, ..., B$

Where $T_i^*(b)$ is the number of observed time steps with state i in generated bin b, and T_i^* is expected number of time steps with state i. The expected number of time steps is obtained by multiplying the workability percentage of the original dataset by the total number of time steps in bin b. The χ^2 statistic to test the hypothesis H_0 is defined as follows:

$$\chi^2 = \sum_{b=1}^{B} \sum_{i \in S} \frac{(T_i^*(b) - T_i^*)^2}{T_i^*}, \quad \forall i \in S \tag{6.11}$$

In case the null-hypothesis is true, a limiting χ^2 distribution can be obtained with $(n_s - 1)n_t$ degrees of freedom. Where n_s and n_t denotes the number of states and the number of time steps respectively. From this test it can be concluded whether the number of generated years is enough to preserve the workability percentage of the original dataset. If the null-hypothesis is rejected, it can concluded more years need to be generated. The results of the χ^2-test are presented in Table 6.5, and conclusions are drawn in the conclusion Section.

Additionally, the root mean square error (RMSE) is used to analyze the variation around the mean, which is defined as follows:

$$RMSE_i = \sqrt{\frac{\sum_{b=1}^{B} (\hat{W}_{b,i} - \bar{W}_i)^2}{B}} \tag{6.12}$$

Where, $\hat{W}_{b,i}$ indicates the workability percentage per bin and $\bar{W}_i$ indicates the mean of the workability percentages of the bins. The 1 year bin (i) has 1000 bins (B) in the 1000 generated years. $\hat{W}_{b,i}$ indicates the workability percentage for every 1 year and $\bar{W}_i$ indicates the mean of these workability percentages. The results of the RMSE are presented in Table 6.6.

Table 6.5: The results of the χ^2 statistic test for the North sea dataset, with the homogeneous method and 1st Markov chain order. α-value of 0.05 is used for the test.

	Dataset: North sea						
Operation	1 year	10 years	15 years	20 years	25 years	100 years	1000 years
$H_s \leq 1$ m	$p \leq \alpha$	$p > \alpha$	$p > \alpha$	$p > \alpha$	$p > \alpha$	$p > \alpha$	$p > \alpha$
$H_s \leq 2.5$ m	$p \leq \alpha$	$p > \alpha$	$p > \alpha$	$p > \alpha$	$p > \alpha$	$p > \alpha$	$p > \alpha$
$T_p \leq 6$ s	$p \leq \alpha$	$p > \alpha$	$p > \alpha$	$p > \alpha$	$p > \alpha$	$p > \alpha$	$p > \alpha$

Persistency $L_1, ..., L_n$ are the lengths of consecutive 1s in the workability sequence and the ECDF of persistency is computed as Equation 2.14 by replacing X_i with L_i. The

Table 6.6: The results of RMSE for the workability of North sea and Gulf of Guinea datasets are given. Solely the homogeneous methods are regarded, with 1st-order Markov chain.

Dataset: North sea						
Operation	1 year	10 years	15 years	20 years	25 years	100 years
$H_s \leq 1$ m	0.0214	0.0070	0.0054	0.0050	0.0043	0.0020
$H_s \leq 2.5$ m	0.0260	0.0074	0.0060	0.0048	0.0043	0.0015
$T_p \leq 6$ s	0.0230	0.0070	0.0054	0.0051	0.0043	0.0025
Dataset: Gulf of Guinea						
Operation	1 year	10 years	15 years	20 years	25 years	100 years
$H_s \leq 1$ m	0.0118	0.0038	0.0028	0.0025	0.0017	0.0011
$U \leq 5$ m/s	0.0160	0.0047	0.0042	0.0037	0.0034	0.0015

corresponding confidence bands are computed as Equation 2.16. In Appendix E.6 the graphs of the cumulative probability functions are presented of the results. The confidence bands are significantly larger of the original dataset compared to the generated datasets. A larger dataset means more workability windows, and therefore a larger sample size n is obtained which reduces the confidence bands (Equation 2.16). For quantification purposes, the two-sample Kolmogorov-Smirnov test is used to analyze the differences between two cumulative distribution functions, which is defined as follows:

$$D_{n,m} = \sup_x |F_{1,n}(x) - F_{2,m}(x)|, \tag{6.13}$$

Where $F_{1,n}$ and $F_{2,m}$ are the cumulative distribution functions of both samples. The smaller the distance $D_{n,m}$, the better the persistency is preserved. To test whether the two samples are drawn from the same distribution (null-hypothesis), the following formula is defined [43]:

$$P(D_{n,m} > \alpha) = Q_{KS}\left(\left[\sqrt{\frac{nm}{n+m}} + 012 + \frac{0.11}{\sqrt{\frac{nm}{n+m}}}\right] D_{n,m}\right) \tag{6.14}$$

Where,

$$Q_{KS}(\lambda) = 2\sum_{j=1}^{\infty}(-1)^{j-1}e^{-2j^2\lambda^2} \tag{6.15}$$

With limiting values,

$$Q_{KS}(0) = 1 \quad Q_{KS}(\infty) = 0 \tag{6.16}$$

Figure 6.6 presents the persistency curves of the original hindcast (HADDOCK) dataset, the 1000 years generated piece-wise time homogeneously and the 1000 years generated non-time homogeneously with the DMM-model. The persistency curves for the other operations are given in Figures E.13 - E.15 in Appendix E.6. The confidence bands are disregarded. In Table 6.7 the distances between the three datasets and the results of the test statistics are

given. The big difference between HADDOCK and the DMM model in the figure below can be explained by the low workability percentage (20%) with this operational limit ($H_s \leq 1$ m). The result of a low workability percentage is that a low number of persistency samples (blocks of consecutive 1s in the workability sequence) is obtained. Hence, an increase in probability is easy obtained when certain persistency blocks are more frequently observed.

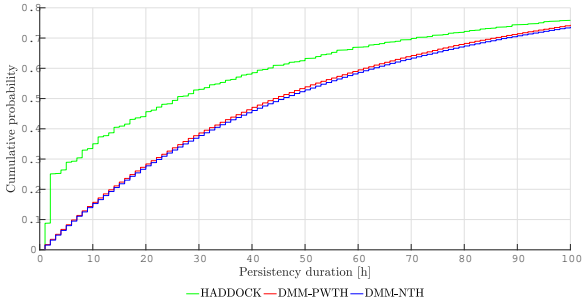

Figure 6.6: The cumulative distribution of persistency for the North sea subject to an operational limit of $H_s \leq 1$ m and 1st-order and both homogeneity.

To conclude how many years are needed based on persistency purposes, the two-sample Kolmogorov-Smirnov test is used on multiple different output years (10, 20, 50, 100, 1000 years). The generated ECDFs and the lower band are used in Equation 6.13 to determine the maximum distances. This maximum distance should be sufficiently small enough (approximately 0.05 based on Figure 2.7), to conclude how many years are needed based on persistency. It is not expected to have large differences between piece-wise time homogeneous and non-time homogeneous methods, therefore the non-time homogeneous method is analyzed only and just 1 with the homogeneous mode. In Table 6.8 the test results of are presented, where the * denotes the homogeneous method. Conclusions from this study are drawn in the conclusion Section.

Table 6.7: Statistic test results of the two-sample Kolmogorov-Smirnov test, with the datasets of the North sea and the Gulf of Guinea for several operational limits. 1st Markov chain order is used for all operations. The significance level is set on 5%. Abbreviations: PWTH = Piece-Wise Time Homogeneous, NTH = Non-Time Homogeneous, O = Original

		Dataset: North sea			Dataset: Gulf of Guinea	
n, m		$H_s \leq 1$ m	$H_s \leq 2.5$ m	$T_p \leq 6$ s	$H_s \leq 1$ m	$U \leq 5$ m/s
PWTH, NTH	$D_{n,m}$	0.0107	0.0082	0.0070	0.0101	0.0031
	p-value	$p \leq \alpha$	$p \leq \alpha$	$p \leq \alpha$	$p \leq \alpha$	$p > \alpha$
O, NTH	$D_{n,m}$	0.7754	0.0293	0.0887	0.7020	0.0570
	p-value	$p \leq \alpha$	$p \leq \alpha$	$p \leq \alpha$	$p \leq \alpha$	$p \leq \alpha$
O, PWTH	$D_{n,m}$	0.7728	0.0232	0.0830	0.7062	0.0590
	p-value	$p \leq \alpha$	$p > \alpha$	$p \leq \alpha$	$p \leq \alpha$	$p \leq \alpha$

Table 6.8: The maximum distances of the two-sample Kolmogorov-Smirnov statistic test, with the datasets of the North sea and the Gulf of Guinea for several operational limits. Non-time homogeneity and 1st Markov chain order is used for all operations, * indicates homogeneous.

	Dataset: North sea			Dataset: Gulf of Guinea		
	$H_s \leq 1$ m	$H_s \leq 2.5$ m	$T_p \leq 6$ s	$H_s \leq 1$ m	$H_s^* \leq 1$ m	$U \leq 5$ m/s
10 yrs	0.0469	0.0470	0.0355	0.0348	0.0351	0.0248
20 yrs	0.0332	0.0334	0.0252	0.0246	0.0249	0.0175
50 yrs	0.0213	0.0210	0.0159	0.0157	0.0157	0.0110
100 yrs	0.0152	0.0149	0.0113	0.0111	0.0111	0.0078
1000 yrs	0.0048	0.0047	0.0036	0.0035	0.0035	0.0025

Conclusion *Workability percentage*: It is noticed that the differences between piece-wise time homogeneous and non-time homogeneous are small, meaning that the workability percentage is presented well for both methods. Furthermore, it is remarkable that there are more outliers below the median for the North sea dataset than above the median, and for the Gulf of Guinea dataset vice versa. The North sea tends more to stormy weather, causing lower workability percentage. While, in the Gulf of Guinea a calmer weather is more likely to be expected, hence higher outliers in the workability percentages are observed. Based on the χ^2-test and the RMSE it can be concluded that 10 years is enough to preserve the workability percentage of the original dataset.

Persistency: The differences between piece-wise time homogeneous and non-time homogeneous methods are very small. However, the differences between the original and the generated datasets is remarkable, specifically when the workability percentage is low (less persistency samples are present). The hypotheses tests are rejected, meaning that the distributions are different. The generated datasets overestimate the persistency compared to the original dataset till a cumulative probability of approximately 0.8. An overestimation of persistency would lead to less downtime of the project consisting of longer net durations. However, this is partly compensated by the same overestimation of persistency of non-workable hours, leading to longer downtime durations. The same cumulative distributions are obtained for the different output years (10, 20, 50, 100, 1000 years), which means that generating 10 years is enough already (keep in mind that more years would make it more accurate). However, the DMM-model is not able to generate the same persistency distribution as observed in the hindcast data, resulting in rejections of the hypothesis tests. The influence of it in terms of downtime is studied in Section 6.4.

6.4 Black-box validation

In the white-box validation (Section 6.2) it is observed that the coupled operations are not working correctly, therefore Module D is disregarded in the black-box validation and thus only Modules A, B and C will be used. Different geographical locations, different projects and different data are regarded in the following Sections to validate the DMM-model.

6.4.1 Different geographical locations

In this Section the same project as analyzed in Rip [45], will be validated on other geographical locations in order to study the influence of different hindcast datasets.

Project The project is called West of Duddon Sands (WoDS). The project is delimited to the foundation installation of the monopiles (MPs) and the transition pieces (TPs) with the Pacific Orca (PO) only. The planned cycle of operations with the corresponding operational limits are given in Table 6.9. This cycle was repeated 17 times to install 78 monopiles and transition pieces, mostly 5 sets per trip (cycle) were installed. Operation 4*a* used to be a coupled operation, but in this project it is considered uncoupled as it is proved not to work correctly in Section 6.2.4. Warranty windows shorter than the net durations are not considered in the DMM-model, because this crashes the DMM-model and simulating without them does not affect the results. Operation 3*b* and operation 5 are not considered, because operation 3*b* has no operational limit and operation 5 requires the water depth which is not measured.

The net durations vary per cycle in the executed project, as they are not deterministic in reality. This is due to difference in number of MPs/TPs to be installed, a learning curve, and other random variations. Table 6.9 shows the average net duration of each operation of the 4 considered cycles.

Table 6.9: Planned installation cycle and operational limits on Pacific Orca with the warranty windows, extracted from Rip [45].

No.	Description	Operational limit	Warranty window	Net duration
1	Load up to 5 MPs and TPs from the quay wall onto installation vessel	$U \leq 12$ m/s	-	19 h
2	Sail to project site & jack-up Installation (2-5 × per cycle)	$H_s \leq 2.5$ m/s $U \leq 13$ m/s	12 h	19 h
3*a*	Handle MP and place in gripper frame	$H_s \leq 1$ m $U \leq 13$ m/s	6 h	4 h
3*b*	Pile MP & remove hammer	-	-	4 h
4*a*	Place TP	$H_s \leq 1.5$ m $U \leq 13$ m/s	-	4 h
4*b*	Grout TP	$H_s \leq 2$ m	24 h	3 h
5	On-site relocation & jack-up	10 m keel clearance	-	6 h
6	Sail back to port	$H_s \leq 2.5$ m $U \leq 13$ m/s	12h	17 h

Settings

- Locations: The North sea, Gulf of Guinea and Tasman sea (datasets in Section 6.1).
- Seasonality: non-time homogeneity
- 1st-order
- 1000 years to be generated
- Start date: January 1

Results The downtime distributions of the 1000 generated years (DMM-model) and the original dataset (HADDOCK) are compared with each other for each location. In Figures 6.8 - 6.10 the cumulative probability curves are presented and the confidence bands are based on Equation 2.16. It is observed that the downtime distribution for the DMM-model deviates significant from the HADDOCK simulation in the Gulf of Guinea (Figure 6.8). The longest downtime duration of HADDOCK is even longer than all downtime durations of the DMM-model, which is statistically unlikely. Downtime in the Gulf of Guinea is almost only due to operation 3a ($H_s \leq 1$ m, $U \leq 13$ m/s). In the data validation it is observed that the persistency of this operational limit deviated between both models significant as well (Figure 6.7). It is concluded in Section 6.3 that this deviation is due to the low workability percentage of the specific operation, which results in a low number of persistency samples. Thus, deviations in persistency are more likely to occur. This persistency deviation explains the downtime deviation between HADDOCK and the DMM-model. The other two locations (North sea and Tasman sea in Figures 6.9 and 6.10 respectively) show that the downtime distribution of the DMM-model follows the downtime distribution of HADDOCK reasonably well. In the data validation it is observed that the persistency distribution for these locations were better preserved (as these operations have a higher workability percentage). Therefore, the downtime distribution is more trustworthy for locations where the persistency distribution is more preserved. Furthermore, the downtime distributions of the DMM-model are above the downtime distributions from HADDOCK. In Section 5.1.3 it is concluded that the influence period is incorrectly implemented; the approach is too optimistic, resulting in less downtime.

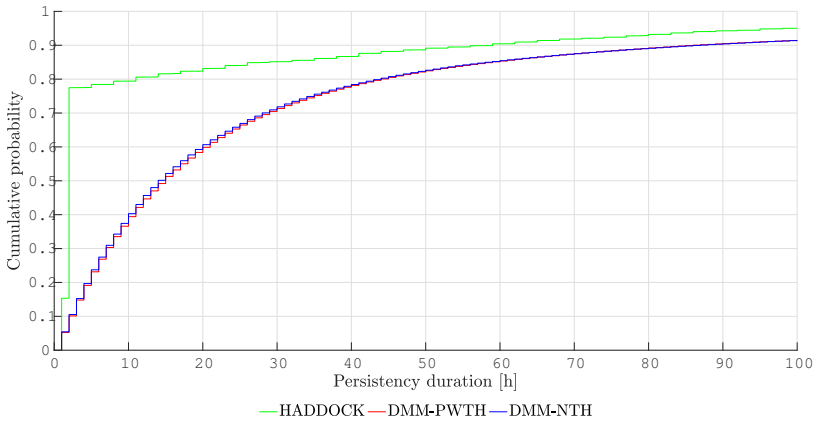

Figure 6.7: The cumulative distribution of persistency for the Gulf of Guinea subject to a set operational limit: $H_s \leq 1$ m with 1st-order and both homogeneities.

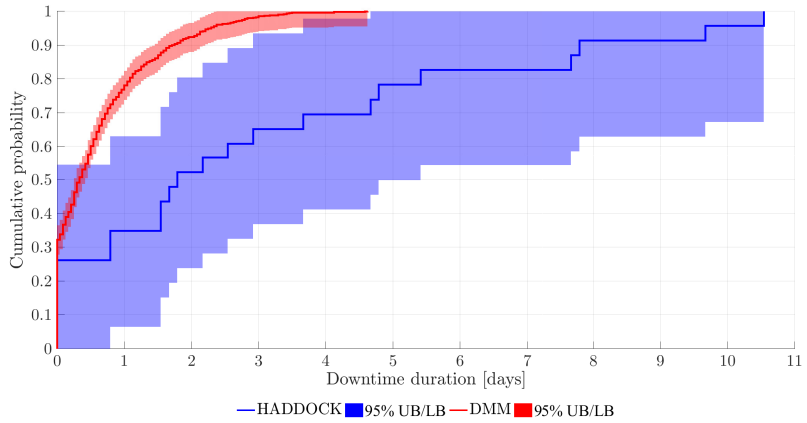

Figure 6.8: The cumulative probability distributions of the downtime on the Gulf of Guinea dataset with start date January 1. The duration is computed with HADDOCK and with the DMM-model simulated 1000 years.

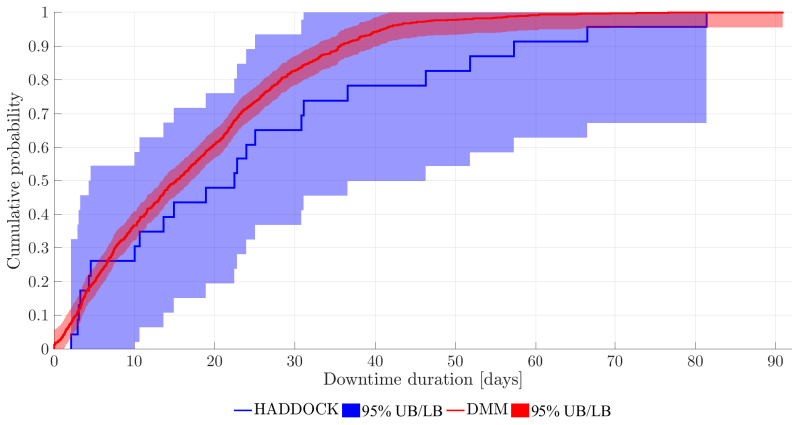

Figure 6.9: The cumulative probability distributions of the downtime on the North sea dataset with start date January 1. The duration is computed with HADDOCK and with the DMM-model simulated 1000 years.

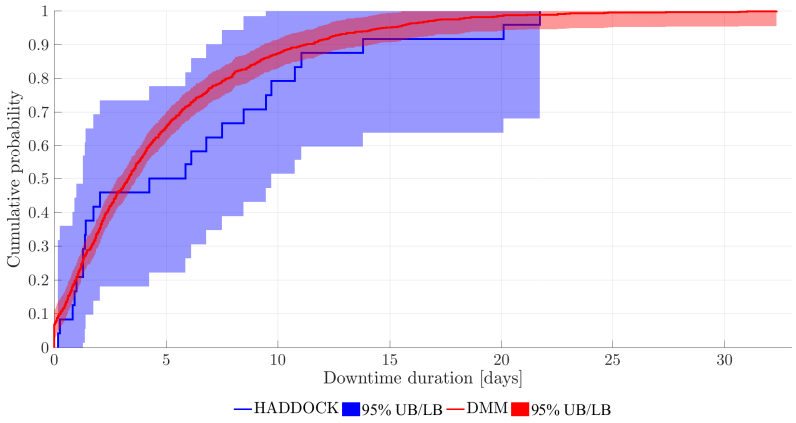

Figure 6.10: The cumulative probability distributions of the downtime on the Tasman sea dataset with start date January 1. The duration is computed with HADDOCK and with the DMM-model simulated 1000 years.

6.4.2 Different project

Project So far only the H_s and U have been modelled with the DMM-model. This Section validates whether other metocean parameters are correctly simulated. For that purpose the hypothetical project in Table 6.10 is created. It is the installation of MPs and TPs, but instead of a gripper frame, a seabed template is used for the installation. Besides the H_s and U, there have also been set limits to T_p and v (which indicate the peak wave period and the surface current velocity respectively). In some cases combinations of H_s,T_p are set, like operation 3 is limited to ($H_s \leq 2$ m, $T_p \leq 7$ s), ($H_s \leq 1.5$ m, $T_p \leq 9$ s). This is visualized in Figure 6.11 with a red line, where every point between this line and the axes is workable.

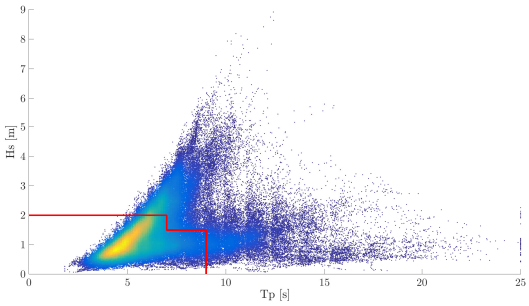

Figure 6.11: H_s, T_p-scatter of a dataset that has been collected at the North sea ($53.91°N, 2.15°E$). The red line indicates a combination of operational limits: ($H_s \leq 2$ m, $T_p \leq 7$ s), ($H_s \leq 1.5$ m, $T_p \leq 9$ s).

Table 6.10: Planned installation cycle and operational limits of a hypothetical project.

No.	Description	Operational limit	Warranty window	Net duration
1	Sailing to site	$H_s \leq 3$ m	-	17 h
2	Boom up and prepare lifting template	$H_s \leq 2$ m, $U \leq 12$ m/s, $v = 1$ m/s m	-	1 h
3	Connect template + lifting + position on seabed	($H_s \leq 2$m, $T_p \leq 7$ s), ($H_s \leq 1.5$ m, $T_p \leq 9$ s), $U \leq 12$ m/s, $v = 1$ m/s	-	1 h
4	Connect upending-lifting tool to MP + upending MP + place on seabed	$H_s \leq 2m$, $T_p \leq 7$ s, $U \leq 12$ m/s, $v = 1$ m/s	8 h	2 h
5	Place hammer on MP, piling, place hammer on deck	$H_s \leq 1.5$ m, $T_p \leq 9$ s, $v = 1$ m/s	-	4 h
6	Lift and install anode cage	$H_s \leq 1.5$ m	3 h	2 h
7	Lift TP on MP + change rigging (spreader bar) + final bolting	$U \leq 10$ m/s, $v = 1$ m/s	4 h	2 h
8	Retrieving template	($H_s \leq 2$ m, $T_p \leq 7$ s), ($H_s \leq 1.5$ m, $T_p \leq 9$ s), $U \leq 12$ m/s	-	1 h
9	Sailing back to port	$H_s \leq 3$ m	-	17 h

Settings

- Location: Another North sea dataset collected at ($53.91°N, 2.15°E$), consisting of 23 years (from 1992 till 2015) sampled with an interval of 3 hours.
- Seasonality: non-time homogeneity
- 1st-order
- 1000 years to be generated

- Start date: January 1

Results The downtime distributions of the 1000 generated years (DMM-model) and the original dataset (HADDOCK) are compared with each other for the North sea location. In Figure 6.12 the cumulative probability curves are presented and the confidence bands are based on Equation 2.16. The transition probabilities are determined similarly as H_s and U and the simulation with these transition probabilities occurs correctly. It is remarkable that the DMM-model curve is again above the HADDOCK curve. The optimistic influence period (as explained in Section 5.1.3) and the overestimation of the persistency (see Figure E.19) would be a logical explanation for this. Longer persistency durations are more likely to occur in the DMM-model, than they occurred in reality (HADDOCK). Both explanations lead to less downtime in the project simulation.

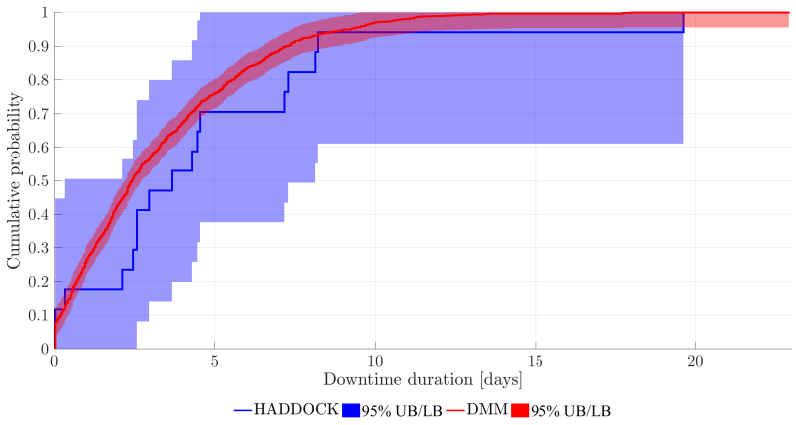

Figure 6.12: The cumulative probability distributions of the downtime on the given North sea dataset with start date January 1. The duration is computed with HADDOCK (original) and with the DMM-model simulated 1000 years.

6.4.3 Different data

This Section focuses on the input of different data, as a harmonic sinusoidal motion and 1000 output years of the DMM-model are used as input data in the DMM-model.

Harmonic sinusoidal motion A harmonic sinusoidal motion has been created representing the wave height (H_s) and three different operational limits have been set: $H_s \leq 1.5$ m, $H_s \leq 2$ m and $H_s \leq 2.5$ m. This is schematized in Figure 6.13 for only 24 hours of the 23 years (January 1, 1992 - December 31, 2014) with a mean at $H_s = 2$ m. With a 2-hourly time step, the workability sequences per operational limit are shown in Figure 6.14.

It can be noticed that the less strict the operational limit, the more workable time steps are obtained in the workability sequence and hence a longer workable persistency period is achieved. The harmonic sinusoidal motion is constant throughout all the 23 years, hence the workability percentage and persistency are constant. The workability percentage and the persistency of the hindcast dataset are presented in Table 6.11. From a harmonic sinusoidal motion it can be predicted how it will propagate, because it will remain constant and continuous.

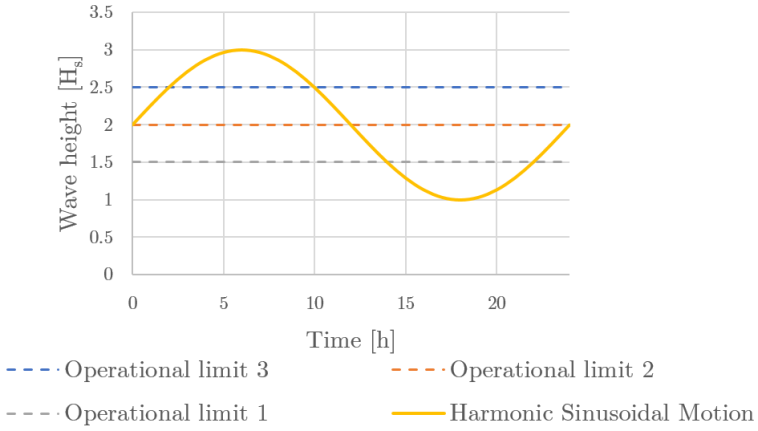

Figure 6.13: Wave height modelled as a sinusoidal harmonic motion with three operational limits schematized for 1 day.

However, the DMM-model introduces randomness, since DMM-model is based on a Markov chain Monte Carlo (MCMC) procedure. This causes the persistency to change. The hindcast dataset subject to the 3 operations is augmented to a 1000 years. From these 1000 years the workability percentage and persistency values are obtained, which are presented in Table 6.11 and Figures 6.15 and E.20a - E.21.

hours	0	2	4	6	8	10	12	14	16	18	20	22	0
Operational limit 1	0	0	0	0	0	0	0	1	1	1	1	0	0
Operational limit 2	1	0	0	0	0	0	1	1	1	1	1	1	1
Operational limit 3	1	1	0	0	0	1	1	1	1	1	1	1	1

Figure 6.14: 2-Hourly measured workability sequences per operational limit presented for 24 hours corresponding to Figure 6.13.

It can be concluded that the workability percentage is well preserved by the DMM-model, however from Figure E.22 it can be noticed that the variation is still significant when smaller bins are generated. Furthermore, it can be concluded that the persistency is completely

changed. The 1000 years are generated with a 1st-order Markov chain, which results in the transition probabilities of Equation 6.17 of Operation 1 of the harmonic sinusoidal motion. Hence, shorter and longer (non)-workability windows can be created (i.e. a persistency distribution is obtained). By increasing the Markov chain order it is expected that the persistency distribution is more like the original one. For instance, if the 13th-order Markov chain for Operation 2 of the harmonic sinusoidal motion is considered, then the DMM-model would create exact copies of the hindcast data. Hence, the new persistency distribution will be the exact same as the hindcast persistency distribution.

$$P_{ij}^{1} = \begin{bmatrix} 0.9413 & 0.0587 \\ 0.1429 & 0.8571 \end{bmatrix} \tag{6.17}$$

Table 6.11: The workability percentage and the persistency presented of the harmonic sinusoidal motion subject to the three operations of the hindcast data (HADDOCK) and only the workability percentage of the 1000 years generated with the DMM-model.

	HADDOCK		DMM-model
	Workability percentage	Persistency [h]	Workability percentage
Operation 1: $H_s \leq 1.5$ m	29.17%	7	29.08%
Operation 2: $H_s \leq 2$ m	54.17%	13	54.27%
Operation 3: $H_s \leq 2.5$ m	70.83%	17	70.94%

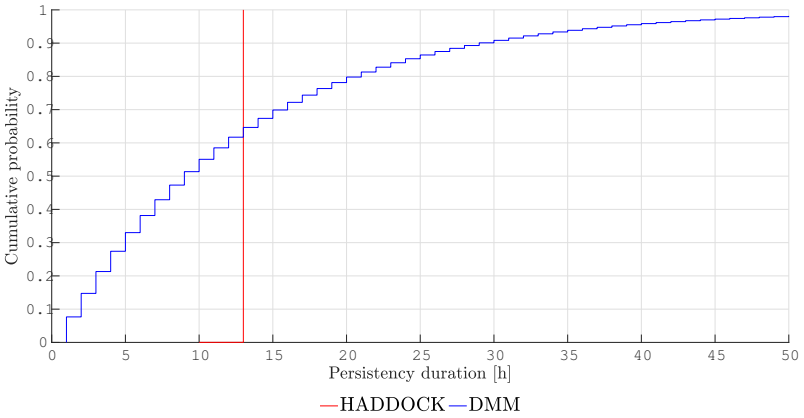

Figure 6.15: The persistency duration distribution of the original (hindcast) and DMM-model generated 1000 years datasets are presented for operation 2 (limit of $H_s \leq 2$ m).

1000 years So far all of the persistency distributions have deviated from the hindcast persistency distribution, some less distinct than other. In this Section 1000 years generated by the DMM-model will be used as input for the DMM-model. From these 1000 years the

transition probabilities will be determined and DMM-model will regenerate 1000 years based on these probabilities. The following 1000 generated years will be input for the DMM-model:

- $H_s \leq 1$ m subject to the Gulf of Guinea dataset (as Figure E.13a)
- $H_s \leq 1$ m subject to the North sea dataset (as Figure E.14a)

The regeneration will be done with 1st-order Markov chain for piece-wise time homogeneity. The results of the cumulative distribution functions (CDF) are depicted in Figure 6.16. The operations with the biggest deviation are used in validation (operational limit $H_s \leq 1$ m in the North sea and Gulf of Guinea). The green line is based on the hindcast dataset (23 years). The CDF of the 1000 years generated based on the probabilities of the hindcast data deviated significantly (input red line). However, the CDF of the regenerated 1000 years (output, blue line) closely follows CDF of the 1000 years input curve (red). Hence, with the obtained transition probabilities (1st-order) the persistency is preserved. The significant change in persistency between the original and the 1000 years will be improved in Chapter 7. From the harmonic sinusoidal motion it can be concluded that the time-dependency has an influence on the persistency and it is kept in mind that lower workability percentages can result in stronger persistency deviations (as the data validation concluded).

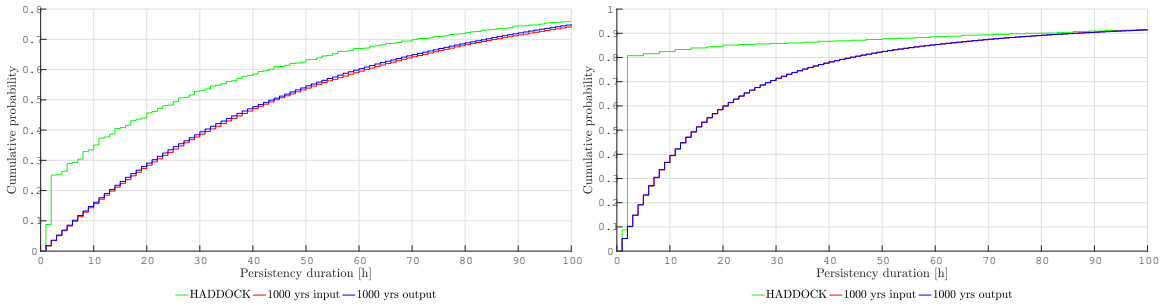

(a) North sea **(b)** Gulf of Guinea

Figure 6.16: The cumulative distribution of persistency for both 1000 years datasets with operational limit: $H_s \leq 1$ m. The 1000 years output is the regenerated workability sequence.

6.5 Conclusion

In this Chapter a software validation study is conducted, which is divided into a white-box validation, a data validation and a black-box validation. In the beginning of this Chapter the research question No. 3a: '*Do the DMM-model and its individual modules perform sufficiently accurate?*' was asked. It can be unfolded into two aspects, whether the total DMM-model performs sufficiently accurate and whether the modules perform sufficiently accurate. In the verification phase errors have been found for each of the modules. With 'sufficiently accurate' is meant, whether these errors influence the output of the modules/model in such a way that they become unreliable. Based on the white-box validation it can be concluded that only Module A works sufficiently accurate. The downtime distributions produced by the DMM-model are too optimistic, which is a result of the inaccuracies of the other modules. Additionally, a data validation is conducted which validated that 10 years are needed to simulate to preserve the workability percentage and the persistency. Table 6.12 summarizes per validation the most important observations.

Table 6.12: Summarized conclusions of the validation process

	Comment:
White-box:	• Module A: The seasonality is presented properly, despite the found errors in the verification. Therefore, these found errors are ascribed to low priority for fixing and the module performs sufficiently accurate to simulate projects. • Module B: Due to the found errors in the verification phase, this module had to be rewritten in order to execute the hypotheses tests. From these tests is concluded that futuristic project are most accurately performed with non-time homogeneity and with a higher order. • Module C: The small error of the cross-transition probability found in the verification is not noticeable. However, the influence period is incorrectly implemented as noticed in the verification phase. • Module D: Based on several tests it is concluded that, this module does not work at all. Rectifying this module has high priority.
Data:	• Based on workability, 10 years is enough to preserve the workability percentage of the original dataset with sufficient accuracy. • Based on persistency (with 95% confidence bounds), 10 years is enough, as the cumulative distribution curves result in the same distribution. However, the generated persistency distribution curves deviate from the original dataset.
Black-box:	• Similarly as concluded in the data validation, the cumulative distribution function of persistency changes when 1000 years are generated with the DMM-model from the hindcast data. This affects the downtime duration and therefore it has to be improved. • The influence period is too optimistic, in which results less downtime. • The persistency is overestimated, which results in less downtime. In Chapter 7 it is studied whether a higher order could solve this deviation.

7 Extensions & Improvement

This chapter aims to answer the research question No. 4a: '*How can the current DMM-model be improved/extended?*'. The findings of the verification and the validation already answer the question '*Can the current DMM-model be improved/extend?*', but the answer does not incorporate the '*how*'. At the end of the software-testing process, the findings of the verification and validation are rectified. In this thesis only the most important findings will be rectified, for that matter a prioritization is made in Section 7.1. In Section 7.2 new coding methods are introduced, which are based on an image compression technique of a DNA-sequence. This method has the potential to solve the problems that were established with coupled operations.

7.1 Rectifications

In Appendix B the found errors, limitations and inconsistencies during the Verification and Validation process are listed, some of which have already been rectified. The errors in the influence period, persistency and the coupled operations are considered to have the highest priority. These will be elaborated in the following Sections (7.1.1 - 7.1.3). The other improving points are not reviewed any further in this thesis, but it is recommended to rectify them too.

7.1.1 Influence period

The influence period is bounded by the 1/0 crossing of operation p (left boundary) and the 1/0 crossing of operation q (right boundary) (see Figure 2.4). In Section 5.1.3 it is concluded that it is not correctly implemented, because in the implementation the left boundary is given by the net duration of operation p and the right boundary is a workable time step instead of a non-workable time step of operation q. This problem can be solved in two ways by recoding the existing module.

Method 1: The *'reasonably' smallest* influence period is implemented, instead of taking a random influence period from the exceedance probability curve. The smallest influence period is the minimum number of time steps observed in hindcast data that operation q has to be workable after operation p crosses its 1/0 boundary. This is where the exceedance probability of the influence period is equal to 1 (see Figure 7.1). To avoid data collection

mistakes, the 'reasonably' smallest influence period is chosen, which is defined as the influence period corresponding to an exceedance probability of 0.98 (the red marker in figure). It is assumed that no more than 2% in the data contains errors, hence the 0.98 probability. The DMM-model does not generate states for operation p after it is completed, therefore it is not known whether the next state of operation p is workable or not. However, it is known that operation q has to be workable for a minimum amount of time steps. After implementation of the reasonably smallest influence period the regular transition probabilities P_{ij}^{q} can continue. It might be possible that the reasonably smallest influence period is zero (where the exceedance probability is equal to 0.98). In that case, the DMM-model should generate the next time step based on the cross-transition probability.

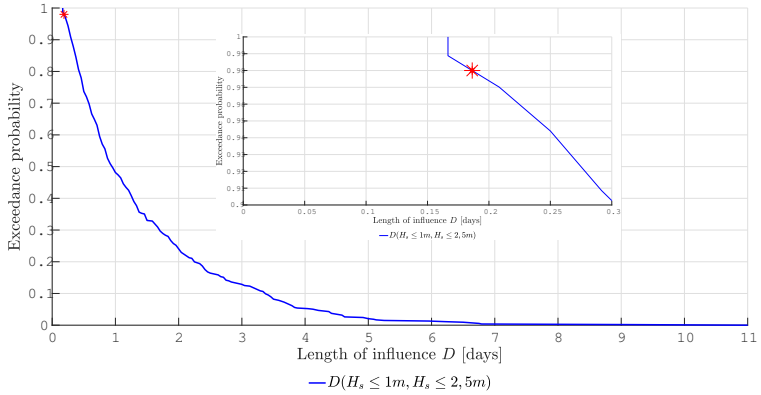

Figure 7.1: Exceedance probability of the influence period $D(H_s \leq 1$ m, $H_s \leq 2.5$ m) with a zoom in at the reasonably smallest influence period (approximately 5 hours) at an exceedance probability of 0.98.

Method 2: Just like the original method, a random influence period will be taken from the exceedance probability curve. However, a non-workable state is followed at the end of the influence period. The non-workable state is the right boundary of the influence period, as shown in Figure 2.4, and therefore it should be generated as well. In case the randomly chosen influence period is zero, a non-workable state is generated. This adaption ensures that the cross-transition probability can be dropped, because the influence period will be used at all times for the transition between two Markov chains. In the current model the cross-transition probability is only used when there is no influence period scheduled, which is no longer the case.

Furthermore, seasonality is taken into account for both methods of the influence periods (which was not yet incorporated in the model). The yearly exceedance curves are considered to be too conservative, hence monthly exceedance curves are made. Figure 7.2 presents how these 2 methods are implemented.

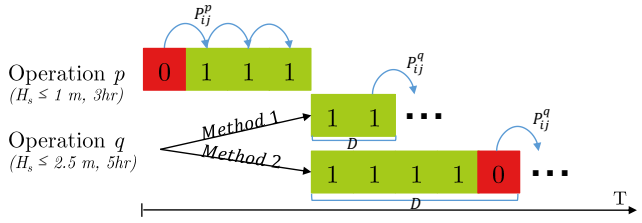

Figure 7.2: A hypothetical project simulation with 2 operations (p and q), where operation q encounters the influence period. Method 1 denotes the reasonably smallest and method 2 denotes a randomly chosen influence period from the exceedance curve.

Additionally, the influence periods and the cross-transition probabilities are determined in advance of generating years (as recommended in Section 5.2.3), because they are based on hindcast data. This rectification assures that the influence periods and cross-transition probabilities are being called just once instead of a 1000 times (if 1000 years are generated), which makes the simulation more efficient. It is recommended to study more thoroughly the influence periods and the cross-transition probabilities, since no literature was found for these concepts.

Conclusion Method 1 will be more appropriate for the current DMM-model because the current DMM-model stops generating states for operation p after it is finished, and hence it is unknown in which state operation p will be. Therefore, implementing the reasonably smallest number of time steps is a logical choice. Method 2 implements after the influence period of operation q an additional non-workable state as the right boundary. This influence period actually happened after the crossing of a 1/0 boundary of operation p, and not after finishing operation p. For that reason method 2 is not applicable for the DMM-model, however it can be used for the new coding method, which will be explained in Section 7.2.

7.1.2 Persistency calibration

In Chapter 6 it is observed that the persistency is not preserved when simulating with the DMM-model, therefore the persistency will be *calibrated* by varying the Markov chain order. Calibration is fitting the model to the observed data by adjusting the parameters (the Markov chain order in this case) [27]. In Section 6.4.3 it is proposed that a higher Markov chain order will lead to a higher accuracy of the persistency. Moreover, for the harmonic sinusoidal motion it is expected the DMM-model will generate the exact persistency of the harmonic sinusoidal motion from a specific Markov chain order. In order to study the effect of the Markov chain order on the DMM-model, the harmonic sinusoidal motion and the North sea dataset are augmented to 1000 years with different higher Markov chain orders. For both datasets the operational limit is set to $H_s \leq 2$ m and piece-wise time homogeneity is applied. Such a testing process is called *ad hoc testing* in the software testing world. The DMM-model is treated as a 'black-box' for this purpose. Figures 7.3 - 7.4 present the obtained persistency curves for both datasets.

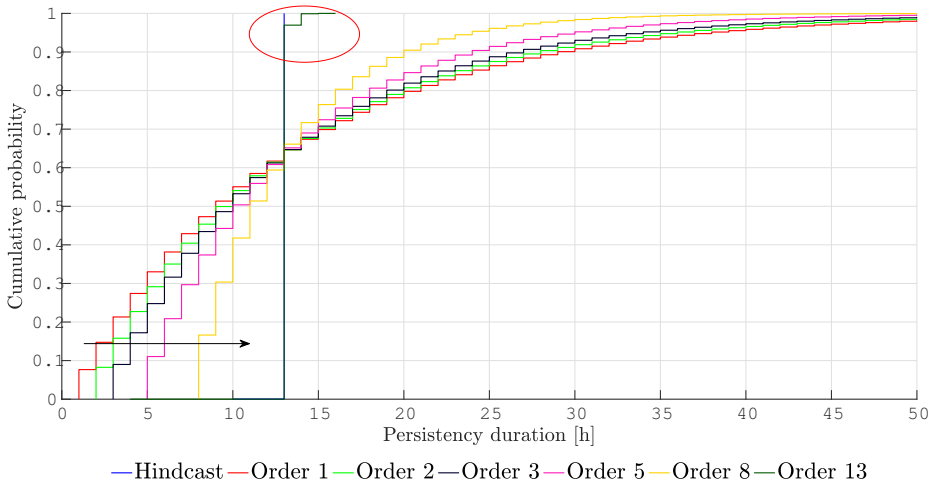

Figure 7.3: Increasing the Markov chain order the cumulative distribution of persistency converges to the hindcast data (persistency of 13 hrs). An operational limit of $H_s \leq 2$ m is used on the harmonic sinusoidal motion.

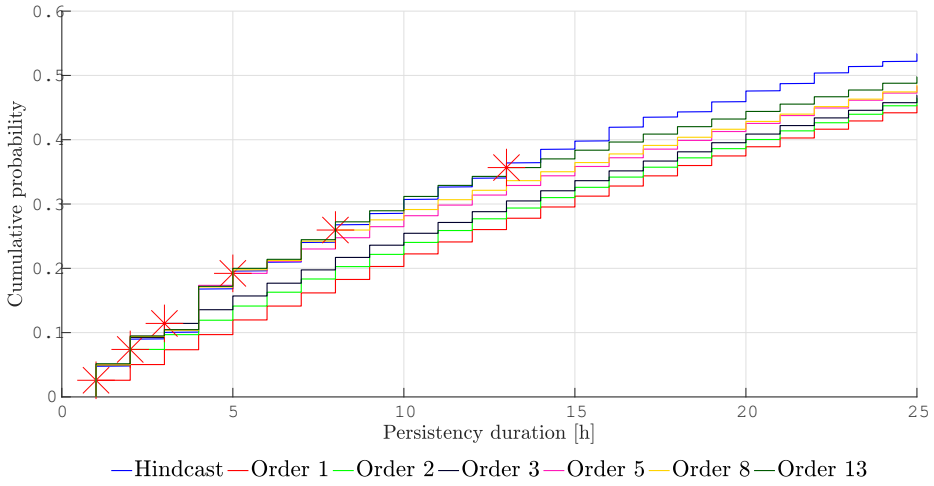

Figure 7.4: Increasing the Markov chain order the cumulative distribution of persistency converges to the hindcast data. An operational limit of $H_s \leq 2$ m is used on the North sea dataset. The red markers indicate the splitting points where the generated dataset splits off the hindcast dataset.

Conclusion The harmonic sinusoidal motion resulted in what was expected: applying a higher chain order resulted in a more accurate persistency preservation. From a 13th-order Markov chain the expectation was that the DMM-model would regenerate the *exact* persistency of the hindcast, because the persistency is 13 hours (see Operation 2 in Table 6.11). However, it can be noticed that there is a slight deviation between a probability of 0.9 - 1 (marked with an ellipse). This deviation can be explained by the error which is made in the determination of the transition probabilities in the piece-wise time homogeneous

function (see Section 5.1.1), which can easily be fixed.

The North sea dataset resulted likewise in a better persistency preservation with a higher Markov chain order, although the 13th-order Markov chain still deviates from the hindcast data. There appears a relation in the duration of the persistency preservation and the Markov order chain. It can be seen in Figure 7.4 that the persistency is preserved until the duration of the persistency (hours) is equal to the Markov chain order. From this point the generated curve seems to release the hindcast data curve. These splitting points are marked with red stars in the figure. In other words, the persistency is preserved for the Nth-order until the Nth-hour.

The rough assumption of monthly stationary transition probabilities in combination with a higher order Markov chain also affects the transition between 2 months, as a *non-existing transition* might occur. This is explained with Figure 7.5 with the 8th-order. The first state of the next month (February) needs to be determined based on the last 8 states of January. It might be possible that this sequence of states is not observed in February in the hindcast data, hence there is no transition probability assigned and no transition is possible. A try-catch block[1] is used in MATLAB to solve this problem. In the simulation of 1000 years with 13th-order Markov chain, there were 79 non-existing transition observations.

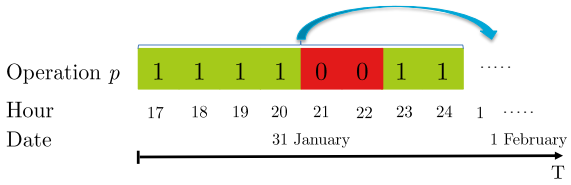

Figure 7.5: A hypothetical non-existing transition possibility, where the first state of the next month (February) is based on the last states of January with 8th-order.

The Markov chain order has to be even higher than order 13 to preserve the persistency more accurate for the North sea. The riskiness in doing this, is that the DMM-model will tend to regenerate the *exact* hindcast data, causing no new information and making the DMM-model worthless. This is visualized in Figure 7.6 where a 14th-order is used and all of the transition probabilities are equal to 1. Therefore, ideally an optimum must be obtained in which the persistency is more or less preserved and the DMM-model is still able to create new data. Currently, the DMM-model simulates every operation from the start date until the operation is completed. To make sure the net duration for each operation has been observed in hindcast data, the DMM-model should use the Nth-order Markov chain with piece-wise time homogeneity, where N denotes the duration of the longest operation. The non-time homogeneity function is only able to simulate 1st-order Markov chain in the current model. This raises the question whether the non-time homogeneous function with 1st-order is more accurate than piece-wise time homogeneous function with the Nth-order. The answer to this question will differ per project per location. A quantification in the

[1] A try-catch block avoids errors and finishes the program in another way.

parametric and model uncertainty could answer this question (as explained in Section 3.2.3).

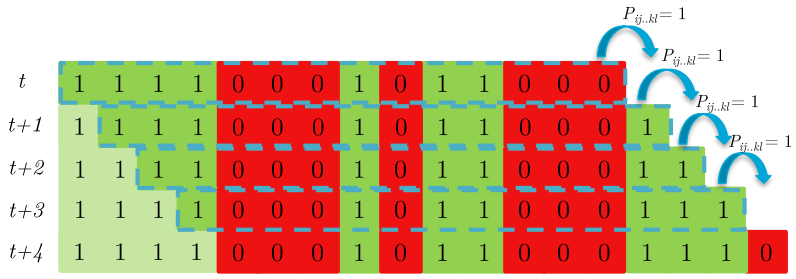

Figure 7.6: A hypothetical workability sequence generation with 14th-order, with the result that every transition probability is equal to 1. Thus, hindcast data is exactly copied.

7.1.3 Sequentially coupled operations

In this Section an idea is given of how the sequentially coupled operations can be solved (it is not yet incorporated in the model). The current DMM-model is not able to simulate sequentially coupled operations. Currently, the DMM-models simulates a coupled operation by generating two parallel workability sequences (the coupled operation and the succeeding operation), which is a small example of a 'Hidden Markov Model' [15]. Two states $i \in \{0, 1\}$ of two operations are converted into four states $i \in \{0, 1, 2, 3\}$ as explained in Section 2.7. This enables the possibility to find the location where the coupled and succeeding operation are finished without downtime in between them. In reality 5 sequentially coupled operations (or even more) are not unthinkable. Prior to the simulation, it is known how many sequentially coupled operations are present in the project. Thus, more states can be created for the sequentially coupled operations and the subsequent operation. For example, if there are 2 sequentially coupled operations eight states $i \in \{0, 1, 2, ..., 7\}$ have to created, as shown in Table 7.1.

Table 7.1: Workability states for 2 sequentially coupled operations (operation A and operation B) and the subsequent operation C.

Op. A	Op. B	Op. C	State
0	0	0	0
0	0	1	1
0	1	0	2
1	0	0	3
0	1	1	4
1	0	0	5
1	0	1	6
1	1	1	7

From the new states the following 1st-order transition probability matrix can be created:

$$P_{ij} = \begin{bmatrix} P_{00} & P_{01} & P_{02} & P_{03} & P_{04} & P_{05} & P_{06} & P_{07} \\ P_{10} & P_{11} & P_{12} & P_{03} & P_{14} & P_{15} & P_{16} & P_{17} \\ P_{20} & P_{21} & P_{22} & P_{23} & P_{24} & P_{25} & P_{26} & P_{27} \\ P_{30} & P_{31} & P_{32} & P_{33} & P_{34} & P_{35} & P_{36} & P_{37} \\ P_{40} & P_{41} & P_{42} & P_{43} & P_{44} & P_{45} & P_{46} & P_{47} \\ P_{50} & P_{51} & P_{52} & P_{53} & P_{54} & P_{55} & P_{56} & P_{57} \\ P_{60} & P_{61} & P_{62} & P_{63} & P_{64} & P_{65} & P_{66} & P_{67} \\ P_{70} & P_{71} & P_{72} & P_{73} & P_{74} & P_{75} & P_{76} & P_{77} \end{bmatrix} \tag{7.1}$$

With the new transition probability matrix the project can be simulated and a window is searched where in between operation A, operation B and operation C no downtime occurs. The disadvantage of multiple sequentially coupled operation is that the number of states increases with $\mathcal{O}(2^{1+n})$, where n denotes the number of sequentially coupled operations. The number of transition probabilities increase as the number of states increase, as explained in Section 5.1.4, and thus the parametric uncertainty increases. Moreover, when a higher-order is used, even more transition probabilities are possible. Having too many sequentially coupled operations in a project and applying a higher chain order could lead to copying the exact hindcast data with the DMM-model.

7.1.4 Result

The current DMM-model is improved by rectifying the influence period and by making it applicable for higher Markov chain order (in the piece-wise time homogeneous function), as is described in Section 7.1.1 and 7.1.2. The theory on improving sequentially coupled operations is given in Section 7.1.3, but this has not been coded yet. In terms of validation the same downtime distributions obtained in Section 6.4.1 are used to indicate the differences with the improved DMM-model. The *settings* in this validation are as follows:

- Location: North Sea, Gulf of Guinea and Tasman sea (datasets in Section 2.3).
- Seasonality: piece-wise time homogeneity
- 6th-order
- 1000 years to be generated
- Start date: January 1

In Figures 7.7 - 7.9 the results of this validation are depicted. It can be noted that the downtime distribution curves are moved to the right in the improved model (as expected), hence more downtime occurs. This is due to less workable states are implemented by the influence period and because the persistency is in a lesser extent overestimated (this will differ per location and per operational limit).

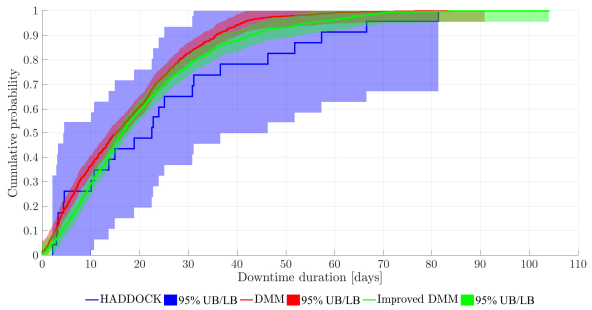

Figure 7.7: The cumulative probability distribution of the downtime on the North Sea dataset computed with HADDOCK, DMM-model and the improved DMM-model.

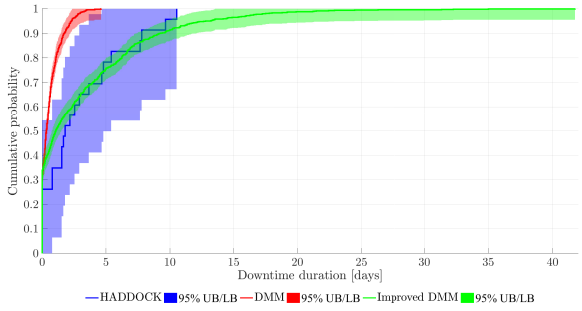

Figure 7.8: The cumulative probability distribution of the downtime on the Gulf of Guinea dataset computed with HADDOCK, DMM-model and the improved DMM-model.

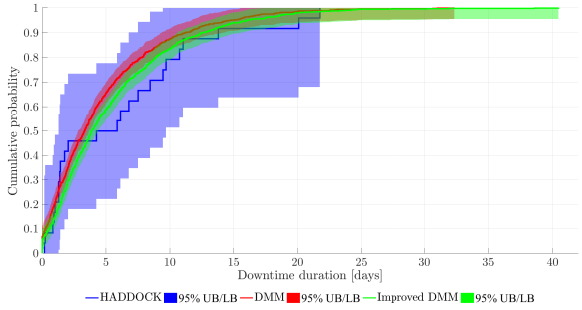

Figure 7.9: The cumulative probability distribution of the downtime on the Tasman Sea dataset computed with HADDOCK, DMM-model and the improved DMM-model.

7.2 New coding methods

In this Section new coding methods are introduced. These methods are based on a compression technique, which decreases the simulation time significantly. And, the problem of sequentially coupled operations is solved. In Appendix A the algorithm block schemes are presented for the new methods, which visualize the following steps clearer.

7.2.1 Initializing

Before generating time-series the model initializes by loading the hindcast data and the project with its operations. Subsequently, the 'workability-array' is created similarly as in the DMM-model (Section 2.3). From the workability-array the (1) probabilities, (2) influence periods and the (3) undoubted periods can be determined as follows:

1. Not any different from the current DMM-model, the limiting probabilities π_i and the transition probabilities $\hat{P}_{ij}$ are determined from the hindcast data with a predetermined Markov chain order. For simplicity reasons, only the piece-wise time homogeneity is applied.

2. The influence periods are determined according to Method 2, as suggested in Section 7.1.1. Additionally, this module is extended by including the non-workable influence period, as suggested in Section 5.1.3. The symbol of the influence period is changed to $D^1(p,q)$ for the regular (workable) influence period and $D^0(p,q)$ for the non-workable influence period.

3. The '**undoubted periods**', $U(p,q)$, is a new module, which indicates states that are *never* visited at specific time steps t. For example, if operation A has an operational limit of $H_s \leq 1$ m and operation B has an operational limit of $H_s \leq 2$ m, it can be concluded that state $\{B_t = 0\}$ can never be visited if state $\{A_t = 1\}$ at time step t. From the workability-array is determined which operations will induce undoubted periods for succeeding operations. The following equation are established for the undoubted periods:

$$U(p,q) = \begin{cases} 0, & if \quad p(t) = q(t) = 0 \quad \forall t : p = 0 \\ 1, & if \quad p(t) = q(t) = 1 \quad \forall t : p = 1 \\ 2, & if \quad p(t) = q(t) \quad \forall t : p = i \in S \end{cases} \tag{7.2}$$

   A '0' is assigned to the undoubted periods when operation p has a less strict operational limit than operation q. Similarly, a '1' is assigned to the undoubted periods when operation p has a stricter operational limit than operation q. When the workability sequence of operation p is *exactly* the same as the workability sequence of operation q, the undoubted period is assigned with a '2'. This could happen when both operations have the same operational limit.

7.2.2 Generating time-series

Two methods are developed in order to generate time-series for the operations within a project: the 'Updated Conditional Markov Probabilities' and the 'Markov Dependency'. The explanation of these new methods are further elaborated in Section 7.2.3. The process of both methods are the same for steps 1 to 3. Given the initializations, the generation of time-series can be started by the following steps:

1. The first symbol(s) of each operation is determined by its limiting probability π_i.
2. The workability chain for the first operation will be generated with the transition probabilities $\hat{P}_{ij...k}$, where k denotes the next state dependable of the Markov chain order.
3. Implement the undoubted periods $U(p, q)$ for the succeeding operations. After this step the workability-array will look like Figure 7.10.

The 'Updated Conditional Markov Probabilities' continues as follows:

4. Implement the influence periods for the succeeding operations ($D^0(p, q)$ and $D^1(p, q)$).
5. Move to the next operation and update the transition probabilities according to the propositions in Section 7.2.3. With the (new) transition probabilities the workability chain can be generated.
6. Repeat step 3 to 5, until the complete workability-array is filled.

The 'Markov Dependency' continues as follows:

4. Determine the new transition probabilities with the Markov Dependency according to the principles explained in Section 7.2.3. With the new transition probabilities the workability chain can be generated.
5. Repeat step 3 to 4, until the complete workability-array is filled.

The algorithm block scheme are provided in Appendix A to visualize the different processes of the different methods.

7.2.3 Missing data imputation

Missing data refers to the absence of some part of a familiar data structure. These can appear for example in the hindcast data at a time step which was not measured by the buoy. Survey or research data are prone to missing data, because observations might be missed due to human/computational errors. Research in this field has risen over the last few decades, because errors like these are made in daily life. Imputation theories focus on the estimation of the parameter of interest in the missing data situation [17]. As well as the

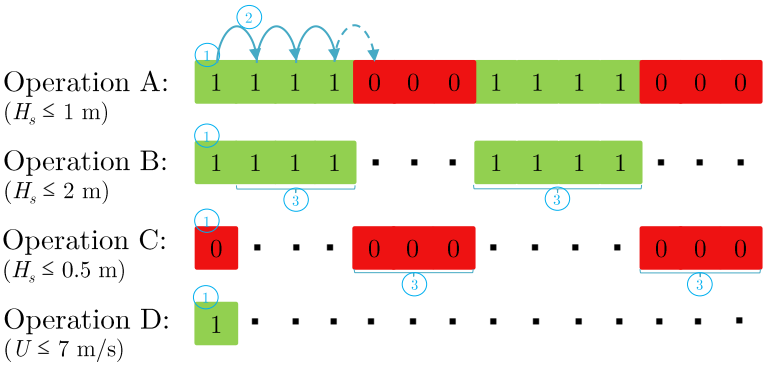

Figure 7.10: A hypothetical schematization of the project generation in the new coding method after step 3.

situation in the new coding method presented in Figure 7.10, there are time steps missing data and hence an imputation theory needs to be applied. For certain operations undoubted periods and/or influence periods are inserted without the use of the Markov theory. Filling up the time steps missing data with the current Markov transition probabilities would be wrong, because the implemented states 'should' be generated with the current transition probabilities. In doing so, too many workable time steps will be generated for operations having implemented workable periods (like operation B in Figure 7.10), or too many non-workable time steps in operation C. As a result, the workability percentage will deviate for those operations. Therefore another process is required which solves these problems. This is where the 'Updated Conditional Markov probabilities' and the 'Markov Dependency' come in, which will be explained below.

Updated Conditional Markov Probabilities This process recalculates the limiting probabilities and the transition probabilities, given that a preceding operation has inserted states by means of the undoubted or influence period for the current operation. The gaps are filled by the updated transition probabilities. This Section explains how the limiting and the transition probabilities are updated, but before doing so the following principles need to be determined:

$$\tilde{T} = T - N_i^{\mathbf{C}} - N_j^{\mathbf{C}}, \qquad \forall i, j \in S \tag{7.3}$$

Where $\tilde{T}$ denotes the total time steps that need to be generated for the operation that misses data and T denotes the total time steps to be generated per operation, which is predetermined by the user. $N_i^{\mathbf{C}}$ and $N_j^{\mathbf{C}}$ denote the number of implemented time steps for states i and j by the undoubted and influence periods.

In Section 2.1.5 is concluded that the 1st-order limiting probability is equal to the workability, hence it can be computed according to Equation 5.1. Where $N_i + N_j$ is equal to the total time steps of the hindcast data. The number of expected states $N_i^{\mathbf{E}}$ in the to be

generated workability sequence can be calculated as:

$$N_i^{\mathbf{E}} = \pi_i \cdot T, \qquad \forall i \in S \tag{7.4}$$

Finally, the number of time steps of state i that are expected to be placed $N_i^{\mathbf{P}}$ can be obtained by:

$$N_i^{\mathbf{P}} = \begin{cases} N_i^{\mathbf{E}} - N_i^{\mathbf{C}}, & if \quad N_i^{\mathbf{E}} \geq N_i^{\mathbf{C}} \\ 0, & otherwise \end{cases} \tag{7.5}$$

With the preceding principles the following proposition can be defined:

Proposition 7.1. *The updated limiting probability for the unfilled time steps for the operation missing data is given by:*

$$\tilde{\pi}_i = \frac{N_i^{\mathbf{P}}}{\tilde{T}}, \qquad \forall i \in S \tag{7.6}$$

Proof. For state $i = 1$ Equation 7.5 can be rewritten as:

$$N_1^{\mathbf{P}} = \begin{cases} N_1^{\mathbf{E}} - N_1^{\mathbf{C}}, & if \quad N_1^{\mathbf{E}} \geq N_1^{\mathbf{C}} \\ 0, & otherwise \end{cases} \tag{7.7}$$

For state $i = 0$ Equation 7.5 can be rewritten as:

$$N_0^{\mathbf{P}} = \begin{cases} N_0^{\mathbf{E}} - N_0^{\mathbf{C}}, & if \quad N_0^{\mathbf{E}} \geq N_0^{\mathbf{C}} \\ 0, & otherwise \end{cases} \tag{7.8}$$

By combining Equation 7.7, Equation 7.8 and Equation 5.1, it will result in:

$$\tilde{\pi}_1 = \frac{N_1^{\mathbf{P}}}{N_1^{\mathbf{P}} + N_0^{\mathbf{P}}} \tag{7.9}$$

Equation 7.3 is equal to the denominator of Equation 7.9, therefore holds:

$$\tilde{\pi}_1 = \frac{N_1^{\mathbf{P}}}{\tilde{T}} \tag{7.10}$$

Analogously, $\tilde{\pi}_0$ can be derived. □

The number of gaps (indicated with dots in Figure 7.10) are defined as N_{n0}, N_{nn}, N_{0n}, which mean the transitions from a gap to a non-workable state ($n \to 0$), from a gap to a gap ($n \to n$), from a non-workable state to a gap ($0 \to n$) respectively. Similarly, N_{n1} and N_{1n} can be defined in case an operation has workable states and gaps (as operation B in Figure 7.10). Analogously as Equation 7.4 and Equation 7.5, the number of expected transitions (1st-order) and the number of to be placed transitions can be derived.

$$N_{ij}^{\mathbf{E}} = P_{ij} \cdot \pi_i \cdot (T-1), \qquad \forall i \in S \tag{7.11}$$

$$N_{ij}^{\mathbf{P}} = \begin{cases} N_{ij}^{\mathbf{E}} - N_{ij}^{\mathbf{C}}, & if \quad N_{ij}^{\mathbf{E}} \geq N_{ij}^{\mathbf{C}} \\ 0, & otherwise \end{cases} \tag{7.12}$$

Furthermore it is concluded that the Markov reversibility condition holds, which is defined as [2]:

$$\pi_i P_{ij} = \pi_j P_{ji} \quad \forall i, j \in S \tag{7.13}$$

Proposition 7.2. *The updated transition probabilities for the unfilled time steps for the operation missing data are given by:*

$$\begin{aligned} \tilde{P}_{00} &= \frac{N_{00}^{\mathbf{P}}}{N_{0n} + N_{n0} + \tilde{\pi}_0 \cdot N_{nn}} \\ \tilde{P}_{01} &= 1 - \tilde{P}_{00} \\ \tilde{P}_{11} &= \frac{N_{11}^{\mathbf{P}}}{N_{1n} + N_{n1} + \tilde{\pi}_1 \cdot N_{nn}} \\ \tilde{P}_{10} &= 1 - \tilde{P}_{11} \end{aligned} \tag{7.14}$$

Proof. Analogously as Equation 7.4, the following can be defined:

$$N_{ij}^{\mathbf{E}} = \hat{P}_{ij} \cdot \pi_i \cdot (T-1) \tag{7.15}$$

Analogously as Equation 7.5, the following can be defined:

$$N_{ij}^{\mathbf{P}} = \begin{cases} N_{ij}^{\mathbf{E}} - N_{ij}^{\mathbf{C}}, & if \quad N_{ij}^{\mathbf{E}} \geq N_{ij}^{\mathbf{C}} \\ 0, & otherwise \end{cases} \tag{7.16}$$

$N_{0n} = N_{n0}$ because of the Markov reversibility condition (Equation 7.13) holds. $\tilde{P}_{00}$ can be determined with the gaps and Equation 7.16.

$$\begin{aligned} \tilde{P}_{00} &= \frac{N_{00}^{\mathbf{P}}}{N_{0n} + N_{n0} + \tilde{\pi}_0 \cdot N_{nn}} \\ \tilde{P}_{01} &= 1 - \tilde{P}_{00} \end{aligned} \tag{7.17}$$

Similarly, $\tilde{P}_{11}$ and $\tilde{P}_{10}$ are determined. Note that transitions of N_{11} are only possible at the gaps N_{nn}, N_{1n} and N_{n1}.

$$\begin{aligned} \tilde{P}_{11} &= \frac{N_{11}^{\mathbf{P}}}{N_{1n} + N_{n1} + \tilde{\pi}_1 \cdot N_{nn}} \\ \tilde{P}_{10} &= 1 - \tilde{P}_{11} \end{aligned} \tag{7.18}$$

□

The disadvantage of the updated conditional Markov probabilities is that it is limited to a 1st-order Markov chain, which has proven to wrongly reproduce the persistency. However, it is partly compensated by the implemented states. Another disadvantages appears in case an operation has a limited number of implemented states. In that case, there is hardly a link between this operation and any other operation, which is unrealistic. The *Markov Dependency* aims to capture this missing link.

Markov Dependency Since metocean parameters are correlated with each other, it is striven to capture these dependencies. This Section proposes a new method for that purpose. No literature was found, but there is some resemblance with 'Hidden Markov Models'.

The first operation in the new coding method will be generated with regular Markov transition probabilities $\hat{P}_{ij...k}$, and then the undoubted states are implemented (as explained in Section 7.2.2). This marks the start of step 4, where the project generation could look like Figure 7.10. The second and succeeding operations q will be dependable of its preceding operation p. Equation 7.19 presents how the new transition probability matrix Q is created for a 1st-order Markov chain of the succeeding operation q with a dependency to its preceding operation p. $T^p_{ij...k}$ denotes the number of time steps of the observed transition $ij...k$ in hindcast data of the preceding operation p. For each of these observed transitions a new transition probability matrix is created for operation q with order u. In other words, a new matrix is created for operation q, with its probabilities based on operation q at the same time steps transition $ij...k$ is observed in operation p. This means that a 1st-order Markov chain results in 16 transition probabilities instead of 4. Analogously can be seen in Equation 7.20, which represents the dependency matrix for a 2nd-order Markov chain, that 64 transition probabilities are possible. The number of transition probabilities grows by $\mathcal{O}(2^{2u+2})$, where u denotes the order. It indicates that the parametric uncertainty (as explained in Section 3.2) grows as well, because more parameters need to be estimated. The given two examples have a 1st- and 2nd-order Markov chain, yet any order is possible in the MATLAB function.

$$Q_{ij} = \begin{bmatrix} T^p_{00}: \begin{bmatrix} Q_{00} & Q_{01} \\ Q_{10} & Q_{11} \end{bmatrix} & T^p_{01}: \begin{bmatrix} Q_{00} & Q_{01} \\ Q_{10} & Q_{11} \end{bmatrix} \\ T^p_{10}: \begin{bmatrix} Q_{00} & Q_{01} \\ Q_{10} & Q_{11} \end{bmatrix} & T^p_{11}: \begin{bmatrix} Q_{00} & Q_{01} \\ Q_{10} & Q_{11} \end{bmatrix} \end{bmatrix} \tag{7.19}$$

$$Q_{ijk} = \begin{bmatrix} T^p_{000}: \begin{bmatrix} Q_{000} & Q_{001} \\ Q_{010} & Q_{011} \\ Q_{100} & Q_{101} \\ Q_{110} & Q_{111} \end{bmatrix} & T^p_{001}: \begin{bmatrix} Q_{000} & Q_{001} \\ Q_{010} & Q_{011} \\ Q_{100} & Q_{101} \\ Q_{110} & Q_{111} \end{bmatrix} \\ T^p_{010}: \begin{bmatrix} Q_{000} & Q_{001} \\ Q_{010} & Q_{011} \\ Q_{100} & Q_{101} \\ Q_{110} & Q_{111} \end{bmatrix} & T^p_{011}: \begin{bmatrix} Q_{000} & Q_{001} \\ Q_{010} & Q_{011} \\ Q_{100} & Q_{101} \\ Q_{110} & Q_{111} \end{bmatrix} \\ T^p_{100}: \begin{bmatrix} Q_{000} & Q_{001} \\ Q_{010} & Q_{011} \\ Q_{100} & Q_{101} \\ Q_{110} & Q_{111} \end{bmatrix} & T^p_{101}: \begin{bmatrix} Q_{000} & Q_{001} \\ Q_{010} & Q_{011} \\ Q_{100} & Q_{101} \\ Q_{110} & Q_{111} \end{bmatrix} \\ T^p_{110}: \begin{bmatrix} Q_{000} & Q_{001} \\ Q_{010} & Q_{011} \\ Q_{100} & Q_{101} \\ Q_{110} & Q_{111} \end{bmatrix} & T^p_{111}: \begin{bmatrix} Q_{000} & Q_{001} \\ Q_{010} & Q_{011} \\ Q_{100} & Q_{101} \\ Q_{110} & Q_{111} \end{bmatrix} \end{bmatrix} \tag{7.20}$$

Figure 7.11 is a simple example to clarify the aforementioned theory with 1st-order Markov chain. The transitions $1 \rightarrow 1$ for operation p are indicated with arrows. At these time steps the transitions are counted for operation q: $N^q_{00} = 0$, $N^q_{01} = 2$, $N^q_{10} = 2$, $N^q_{11} = 1$. From these counted transitions the transition probabilities can be computed with Equation 2.2. These probabilities correspond with transition probability matrix $T^p_{11} : Q_{ij}$ in Equation 7.19. This can be done analogously for the other transitions observed in operation p.

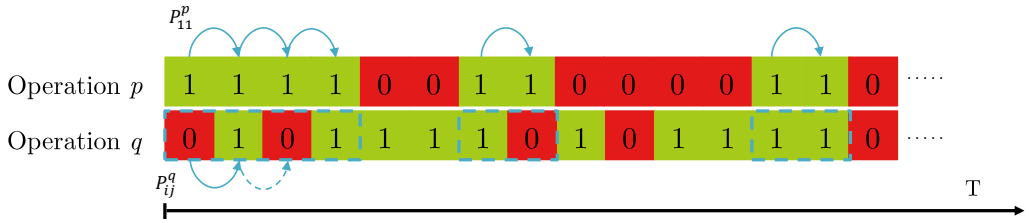

Figure 7.11: An hypothetical workability sequence for 2 operations to clarify the Markov dependency, where the transitions $1 \rightarrow 1$ are indicated with arrows. At these time steps the transition probabilities are determined for operation q.

As explained, the number of transition probabilities grows quickly using a higher order, which increases the parametric uncertainty. To restrain this uncertainty within narrower limits, the order can be reduced for one of the operations. In the 2nd-order example from above (Equation 7.20), a 2nd-order is used for both operations p and q. In theory, it is possible to use different order for different operations. For example, a 1st-order for operation q and a 2nd-order for operation p will result in Equation 7.21. Vice versa, a 2nd-order for operation q and 1st-order for operation p will result in Equation 7.22. This is possible for any order u, and the number of transition probabilities grows by $\mathcal{O}(2^{u_p+u_q+2})$, where u_p and u_q denote the order of operation p and q respectively.

$$Q_{ij} = \begin{bmatrix} T^p_{000} : \begin{bmatrix} Q_{00} & Q_{01} \\ Q_{10} & Q_{11} \end{bmatrix} & T^p_{001} : \begin{bmatrix} Q_{00} & Q_{01} \\ Q_{10} & Q_{11} \end{bmatrix} \\ T^p_{010} : \begin{bmatrix} Q_{00} & Q_{01} \\ Q_{10} & Q_{11} \end{bmatrix} & T^p_{011} : \begin{bmatrix} Q_{00} & Q_{01} \\ Q_{10} & Q_{11} \end{bmatrix} \\ T^p_{100} : \begin{bmatrix} Q_{00} & Q_{01} \\ Q_{10} & Q_{11} \end{bmatrix} & T^p_{101} : \begin{bmatrix} Q_{00} & Q_{01} \\ Q_{10} & Q_{11} \end{bmatrix} \\ T^p_{110} : \begin{bmatrix} Q_{00} & Q_{01} \\ Q_{10} & Q_{11} \end{bmatrix} & T^p_{111} : \begin{bmatrix} Q_{00} & Q_{01} \\ Q_{10} & Q_{11} \end{bmatrix} \end{bmatrix} \tag{7.21}$$

$$Q_{ijk} = \begin{bmatrix} T^p_{00} : \begin{bmatrix} Q_{000} & Q_{001} \\ Q_{010} & Q_{011} \\ Q_{100} & Q_{101} \\ Q_{110} & Q_{111} \end{bmatrix} & T^p_{01} : \begin{bmatrix} Q_{000} & Q_{001} \\ Q_{010} & Q_{011} \\ Q_{100} & Q_{101} \\ Q_{110} & Q_{111} \end{bmatrix} \\ T^p_{10} : \begin{bmatrix} Q_{000} & Q_{001} \\ Q_{010} & Q_{011} \\ Q_{100} & Q_{101} \\ Q_{110} & Q_{111} \end{bmatrix} & T^p_{11} : \begin{bmatrix} Q_{000} & Q_{001} \\ Q_{010} & Q_{011} \\ Q_{100} & Q_{101} \\ Q_{110} & Q_{111} \end{bmatrix} \end{bmatrix} \tag{7.22}$$

Additionally, **time-shifting** can be applied to the Markov Dependency, which means other time steps of operation p can be used to determine the dependency probabilities for operation q. The previous theory uses the same time steps of operation p to generate states for operation q, hence no time shift is applied. This can be seen in Figure 7.11. Another possibility would be to use *earlier* time steps of operation p to determine the transition probabilities of operation q, which is called *backward* time shifting. Vice versa, *forward* time shifting is also possible, where *further* time steps are used of operation p to determine the transition probabilities of operation q. Figure 7.12 clarifies how time shifting works with a 2nd-order for both operations. The black bracket indicates the current time step of operation q. In case of backward time shifting the blue bracket of operation p is used, and similarly the red bracket is applied for no time shift, and the green bracket for forward time shifting.

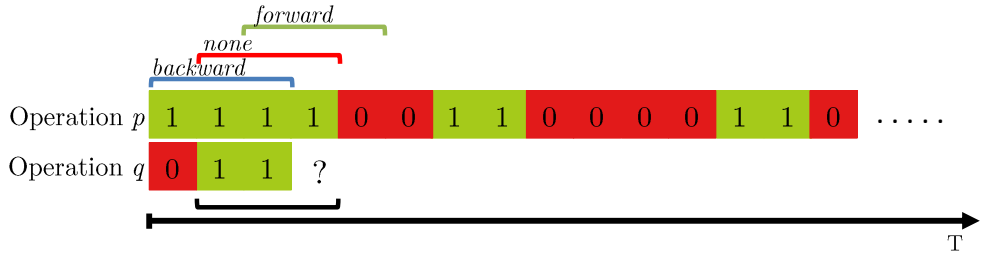

Figure 7.12: Time-shifting visualized for the Markov Dependency method, where backward-, no- and forward-shifting are indicated with blue, red and green brackets respectively.

The pitfall of the Markov Dependency is that some transition probabilities might not have been assigned to a value, since these were not observed in hindcast data. This is probable with operations with a limited number of transitions from $1 \rightarrow 0$ and $0 \rightarrow 1$, especially when a higher order is assigned to the operation. For example, if a 2nd-order is assigned to such an operation p with limited number of transitions; it can be imagined that not all of the possible transition variations of operation q have been observed at the time steps of operation p transitions as $1 \rightarrow 0 \rightarrow 1$. Hence, it will be expected some Q_{ijk} probabilities are not assigned to any value in the matrix of T^{p}_{101} in Equation 7.20. This problem is solved with a try-catch block, which ensures that the model will only create transitions which did occur in hindcast data.

Remarks The proposed dependency is only dependent on the preceding operation. The paradox is that a state can be generated for operation C depending on operation B, while the combination of states $S = \{X_A, X_B, X_C\}$ might never been observed in hindcast data. Another remark is that, in case two operations do not have a distinct correlation (i.e. temperature and wave period), the added value of the Markov Dependency is questionable. It can be improved by calculating a correlation coefficient (CC) on the raw hindcast data and applying the Markov Dependency with the operation having the highest CC-value. These remarks are recommended for further study, in which [39] and [62] can be used to determine correlations between multivariate ocean parameters.

7.2.4 Data compression

The generated dichotomous workability-array Z consists of T rows $\times$ O columns, where T is equal to 8766 $\times$ years and O is equal to the number of operations. In case the user wants to generate 1000 years, the workability-array will enlarge to $8.766 \cdot 10^6$ rows. Simulating projects through this dataset will take tremendously long, and thus a data compression technique is used. Data compression reduces the storage space and processing costs, along with speeding up data transmission [21], which happens for example by compressing a raw image to a JPEG file. A simple example of data compression (the so-called 'run-length encoding method') works as follows:

Dataset: $A \quad A \quad A \quad A \quad B \quad B \quad B \quad A \quad A \quad A \quad A \quad A \quad A \quad A \quad C \quad B \quad B \quad B \quad C \quad C$
Compressed dataset: $4A \quad 3B \quad 7A \quad 1C \quad 3B \quad 2C$

The compressed dataset can be interpreted as a sequence of four As, three Bs, seven As, one C, three Bs and two Cs. The original dataset consists of 20 characters, where the compressed dataset consists only of 12 characters. This example is a lossless compression, meaning that the original dataset can be perfectly reconstructed by reversing the compression, which happens for example in ZIP file formats. Contrary to the JPEG file example is a lossy compression, which partially discards the original data and therefore an inexact original dataset is obtained by reversing the compression.

The same methodology as the example above is applied in the generated dataset by the new coding method. The generated binary dataset is reconstructed into persistency blocks (consecutive workable time steps and consecutive non-workable time steps), by finding the

transitions where a workable moves to a non-workable state $1 \rightarrow 0$ and vice versa $0 \rightarrow 1$. From these blocks the initial time step, final time step and the block length are saved. Note that for small persistency blocks (i.e. blocks consisting of only 1 to 3 time steps) more data is created instead of reduced. The net durations of all operations are given at the beginning of the simulation. These can be compared with the workable persistency block lengths. In case the net duration is longer than the persistency block length, the persistency block length plus the following non-workable persistency block length is downtime. This process continues until a workable persistency block length is found, in which the net duration fits. At this point the model continues with the next operation at the specific time step, and the preceding process repeats itself. Unless, the operation is coupled, which means the next operation has to start immediately after completing the current operation. In that case, it is checked whether the persistency block of the next operation is a workable persistency block and whether it is longer than the net duration of the next operation. If so, the project simulation can continue. If not, the model will look for a new sufficient persistency block for the coupled operation and thereafter check whether the persistency block of the next operation is workable and longer that the net duration. This methodology allows projects to be generated efficiently, because the simulation time is reduced significantly. A data compression module is already incorporated in HADDOCK and can be used for this process as well. An additional advantage is that the workability-array (for all years for all operations) is generated, which allows the model-user to take any start date he pleases.

In the article of Schouhamer Immink [50] more compression methods are described, in which for example the blocks lengths can be coded alphabetically where the Z denotes 26. In [21] a survey is conducted to capture existing compression approaches in the field of DNA sequences, biological data and file formatting, which could be used for further study into metocean data compression techniques.

7.2.5 Small validation

A small scale validation is conducted for the two proposed methods: Updated Conditional Markov Probabilities (UCMP) & Markov Dependency (MD). The workability percentage and the persistency are compared with the hindcast data and with the results of the improved DMM-model. Furthermore, the downtime of a hypothetical project (Table 7.2) is analyzed for the different models. Note in Table 7.2, the last three columns indicate whether the operation has a workable influence period $D^1(p,q)$, a non-workable influence period $D^0(p,q)$ or undoubted periods $U(p,q)$. The undoubted periods are applied in the UCMP method and MD method, and the influence periods are only applied in the UCMP method.

Settings For all the methods there are several general settings, such as the North sea dataset given in Section 6.1 is used as location. Furthermore, 1000 years will be generated with a project start date on May-1. In the DMM-model the 1st-order is used and for the new methods operation A corresponds with a 7th-order, because the longest net duration is 7 hours (this was suggested in Section 7.1.2) and the other operations correspond with a 1st-order.

Table 7.2: A hypothetical project to validate the new coding method.

No.	Description	Operational limit	Warranty window	Net duration	$D^1(p,q)$	$D^0(p,q)$	$U(p,q)$
1	Operation A	$U \leq 10$ m/s	-	6 h	-	-	-
2	Operation B	$H_s \leq 2.5$ m	10 h	7 h	-	Yes	-
3	Operation C	$H_s \leq 1$ m $U \leq 10$ m/s	8 h	5 h	Yes	Yes	Yes
4	Operation D	$H_s \leq 2$ m	-	4 h	Yes	Yes	Yes
5	Operation E	$T_p \leq 7$ s	-	5 h	Yes	Yes	-

Table 7.3: The settings belong to the hypothetical project from Table 7.2 to validate the new coding method.

	DMM-model	Conditional Updated Markov Probabilities	Markov Dependency
Seasonality:	PWTH	PWTH	PWTH
Order:	1st-order	Operation A: 7th-order Other operations: 1st-order	Operation A: 7th-order Other operations: 1st- and 2nd-order

Workability percentage The workability percentage of the hindcast data extracted from HADDOCK is assumed to be representative for the truth, since it has enough samples. The generated datasets should preserve this percentage with a certain accuracy and the results are presented in Table 7.4. It is calculated with Equation 1.1.

Table 7.4: The workability percentage per operation of the new coding method with the Updated Conditional Markov Probabilities (UCMP) and with the Markov Dependency (MD) compared with the hindcast data (HADDOCK).

Operation No.	HADDOCK	DMM	UCMP	MD 1st-order	MD 2nd-order
Operation A	71.73%	71.77%	71.64%	71.75%	71.85%
Operation B	73.10%	73.13%	70.20%	71.37%	72.97%
Operation C	20.52%	20.45%	15.44%	12.86%	14.75%
Operation D	58.88%	58.83%	56.64%	42.69%	44.32%
Operation E	46.79%	46.79%	78.46%	40.27%	40.44%

It can be seen that the DMM-model preserves the workability percentage very well, just as operation A for all other methods. The modelling of operation A is very similar as the DMM-model. The only difference is that this operation is generated with a 7th-order Markov chain with the other methods (UCMP and MDs). Operation B implements only the non-workable influence periods $D^0(p,q)$ for the UCMP (see Table 7.2). The updated probabilities are not much affected when a limited number of states are implemented. It can be concluded that the workability percentage is well preserved for all methods. Operation C has both influence periods ($D^1(p,q)$ and $D^0(p,q)$) and undoubted periods. The latter can be explained because if operation B cannot be workable, operation C cannot be workable

either. Due to the many implemented states the workability percentage changes significantly, resulting in a too low percentage for all new methods. Operation D has both influence periods and both undoubted states, hence many states are implemented for the UCMP method resulting in a slightly too low workability percentage. The MD methods produced a too low workability percentage for operation C, hence succeeding operations are dependent on this operation, causing a low workability percentage as well. In other words, in the MD method operation E is dependent on operation D, which is in turn dependent on operation C, and so forth. When Operation C experiences a too low workability percentage, it automatically influences the succeeding operations in the MD method. The result of the UCMP method turns out exceptionally high for operation E, namely 78.46%, where the others are between 40-47%. In the UCMP method a specific operation is influenced by all its preceding operations, hence the workability percentage of operation E is not trustworthy anymore.

Persistency The persistency of the hindcast data extracted from HADDOCK is assumed to be representative for the truth, since it has enough samples. The generated datasets should preserve this persistency with a certain accuracy. The cumulative distribution curves of Operation A and Operation C are presented below in Figure 7.13, and for the other operations consult Appendix F.1.

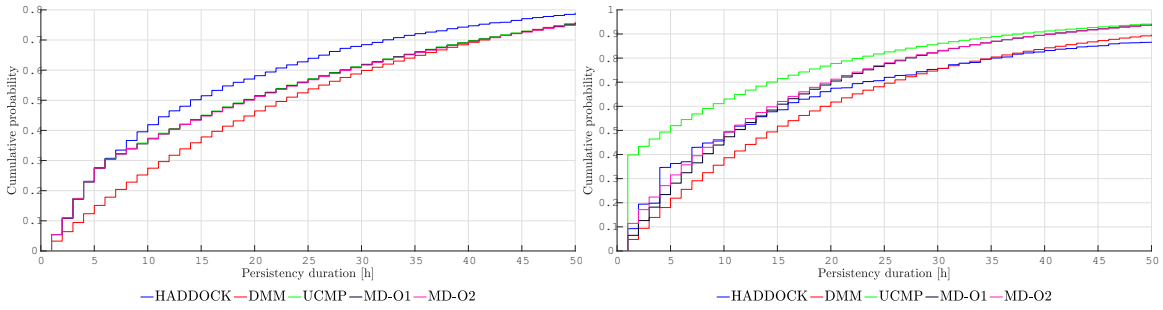

(a) Operation A **(b)** Operation C

Figure 7.13: The cumulative distribution of persistency for the North sea subject to a set operational limit of $U \leq 10$ m/s (left) and $H_s \leq 2.5$ m (right)

Operation A clearly shows the difference between a 1st-order (DMM) and a 7th-order Markov chain (UCMP and both MD methods). From a persistency of 7 hours the UCMP and MD curves start to release the HADDOCK curve and start to converge to the DMM-model curve. In the graph of operation C can be observed that the hindcast persistency is well kept with the MD methods, to a persistency duration of approximately 15 hours. The UCMP method gives a too high probability for a 1 hour persistency, that can be explained by the overlapping influence periods of the preceding operations. This phenomenon repeats itself for the other operations as well. It can be concluded based on all operations that the UCMP method is not trustworthy and that the MD methods preserve the persistency more accurate than the DMM-model and the UCMP method. The difference between the 1st-

and 2nd-order of the MD method is not so much. Based on these operations it is concluded that the 2nd-order is slightly more accurate, but more research is recommended for this method since only 5 operations are regarded on 1 location.

Downtime The downtime of the original dataset, as produced by HADDOCK, is not assumed to be representative for the truth, since it only has 23 samples. However, it gives an idea of how the downtime distribution is going to look like. The cumulative probability distributions are given in Figure 7.14 for all the used models with their confidence bounds (α-value of 0.05).

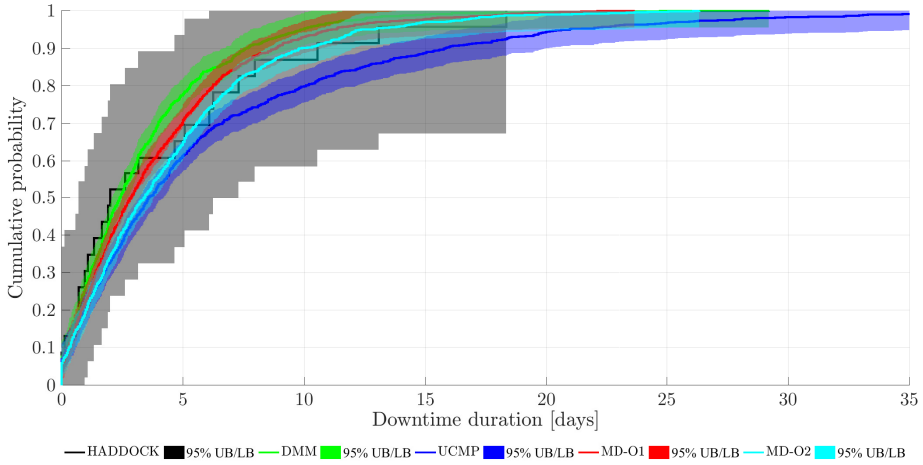

Figure 7.14: The cumulative probability distribution of the downtime, based on the project in Table 7.2 and the North sea dataset with start date 1-May. The durations are computed with HADDOCK, DMM, UCMP, MD-O1 and MD-O2 models.

The confidence bands are much wider of the HADDOCK simulation (black), due to the smaller sample size. The DMM-model is used with the rectified influence period (method 1: implementing the reasonably smallest number of time steps). The distributions of the DMM-model and the MD methods are somewhat similar to each other, where downtime for the DMM-model is to a lesser extend than the MD methods for this hypothetical project. The downtime of the UCMP-method is overestimated, because the probability of the 1 hour persistency is too high which causes more downtime. Furthermore, the workability percentage did not correspond with the hindcast data. As a result, the downtime distribution cannot be considered reliable of the UCMP method.

The workability is better preserved for the DMM-model, but the persistency is better preserved for the MD methods. Therefore, it is difficult to say which method is better. Both methods need further development, where for the DMM-model the persistency needs to be improved and for the MD methods the workability percentage needs to be improved. The UCMP-method did not show any promising results, it is therefore not recommended

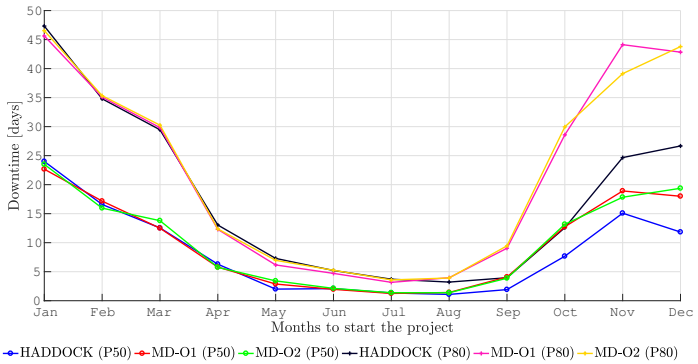

Figure 7.15: Comparison between HADDOCK, MD-O1 and MD-O2 methods with the P50 and the P80 values, based on the hypothetical project in Table 7.2 and the North sea dataset.

to further study this approach. The MD methods open up new perspectives since multiple sequentially coupled operations are possible.

An additional advantage of the MD method is that any start date can be chosen, hence it can be studied which date is most reliable to start your project. This is also possible for the UCMP method, but this method is not considered any further since it brought many repercussions regarding to the workability percentage and persistency. The effect of different start dates of HADDOCK and the MD methods are shown in Figure 7.15. The P50 and P80 values are plotted throughout the year and the seasonality effects are clearly present in the graph. The curves of MD methods follow the HADDOCK curves similarly till the months August and September. The differences in these months can be explained by analyzing the cumulative probability distribution curves of these months. Figure 7.16 represents the cumulative probability curve with 1-December as start date. It can be noted that the differences between the different methods is large at the values of P50 and P80 (green markers in figure). It is believed that the percentile values of the hindcast data is too inaccurate due to the large confidence bands. The P80 value of hindcast data could be according to Figure 7.16 between 12.2 and 98.9 days, which is a significant bandwidth. The lower workability percentage of the MD methods (Table 7.4) is not considered to be the reason for the deviation, because in that case the first months of the year should deviate as well. But it must be kept in mind that the lower achieved workability percentage can result in more downtime.

Increasing Markov chain order It is concluded in Section 7.1.2 that a higher Markov chain order results in a better persistency preservation. It is therefore validated in this paragraph how this affects the downtime. The same operations from Table 7.2 and the same North sea location from Section 6.1 is used. The 1st-order for the improved DMM-model resulted in Figure 7.14. Since a higher order Markov chain is still not possible in the non-time homogeneous function, the piece-wise time homogeneous function is used. Figure 7.17 presents the cumulative downtime distribution curve for this project without the confidence bands (1000 projects are generated for all different Markov chain orders). It can be seen

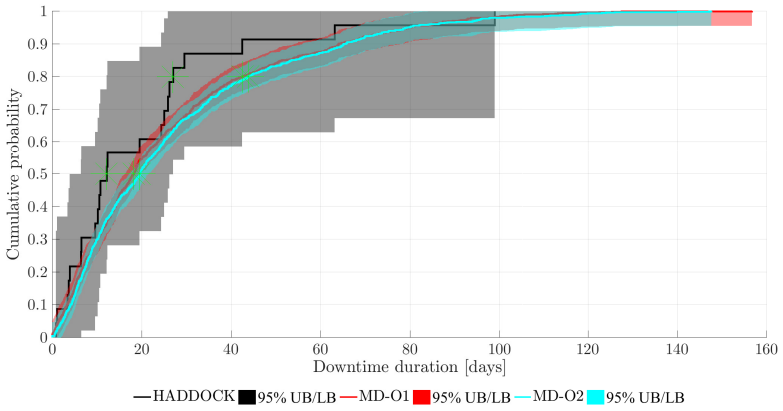

Figure 7.16: The cumulative probability distribution of the downtime, based on the project in Table 7.2 and the North sea dataset with start date 1-December. The durations are computed with HADDOCK, MD-O1 and MD-O2 models. The P50 and P80 values indicated with green markers.

that the 1st- and 2nd-order result in less downtime, than the other higher orders. The other higher orders result in more or less the same distribution curve.

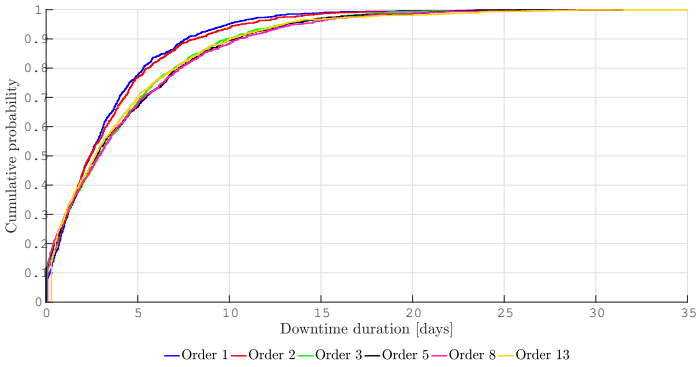

Figure 7.17: The cumulative probability distribution of the downtime based on the project in Table 7.2 and the North sea dataset with start date 1-May.

For the 1000 generated projects the total encountered downtime per operation is given in the bar chart of Figure 7.18. It can be seen that Operation C and Operation D are most vulnerable to downtime. In Operation C it can also be seen that the higher orders resulted in more downtime, which explains the observation in Figure 7.17. Therefore, the persistency distribution curve for Operation C is provided in Figure 7.19, which reveals that the lower Markov chain orders overestimate the persistency and hence result in less downtime. The other persistency curves are provided in Appendix F.3.

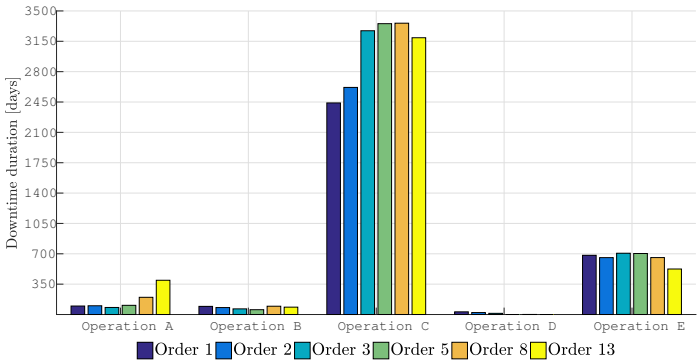

Figure 7.18: The bar chart per operation with the total downtime encountered of all the 1000 generated projects.

Figure 7.19: The cumulative probability distribution of the persistency based on Operation C in Table 7.2 with the North sea dataset and start date 1-May.

7.3 Conclusion

'Yes' is the answer whether the DMM-model can be improved, and in Appendix B an overview is structured on which points each module can be further developed. The most important considered rectifications are the influence period, persistency preservation and the coupled operations. Research question No. 4a addresses to '*How can the current DMM-model be improved/extended?*'. This question is answered in threefold by using the most important considered rectifications. The influence period is improved by applying *method 1* for the DMM-model as explained in Section 7.1, where the 'reasonably' minimum number of workable time steps are implemented instead of an arbitrarily period from the exceedance probability curve. The persistency preservation is improved by increasing the Markov chain order. The DMM-model was only limited to 1st-order for non-time homogeneity method and 2nd-order for piece-wise time homogeneity method. The piece-wise time homogeneity function is now applicable for higher orders, but the non-time homogeneity method is still limited to a 1st-order Markov chain. It is therefore recommended to further develop

the non-time homogeneity method, as this method yielded in promising results in Section 6.2.1. The DMM-model cannot simulate coupled operations, let alone sequentially coupled operations. The error causing the failure for coupled operations is indicated and needs to be solved. Sequentially coupled operations can be improved in the model by incorporating the suggested theories of Section 7.1.3. Also, the Markov Dependency method (as introduced in Section 7.2) is able to model sequentially coupled operations, and it shows potentials in terms of persistency preservation. However, this method needs more validation before it can be used.

8 Synthesis

The purpose of this study was to develop the 'Downtime Modular Markov' model (DMM-model). A software-testing process is used in order to achieve this. Such a process consists of a verification phase followed by a validation phase and finished with an improvement phase. In this chapter the conclusions derived from the conducted work of this thesis are presented, and answers are given to the research questions. Additionally, recommendations are given for Boskalis and for further research. The chapter closes with a discussion, in which the study is brought into a broader perspective and where the DMM-model will be evaluated.

8.1 Conclusions

Thesis goals The first goal of this thesis was to analyze the DMM-model and summarize the work methods. It has been compared with other stochastic simulation models of metocean parameters in terms of downtime of complex projects. The main goal of this thesis was to thoroughly develop the DMM-model. A total list of all findings for improvement can be found in Appendix B. From the development study it is concluded that the DMM-model cannot be used practically yet, as it still contains several important (some fatal) errors and limitations. The crucial findings to make the DMM-model practicable are: the influence period, coupled operations, higher-order Markov chains. These are further elaborated in the next paragraph. It is concluded that the DMM-model has an additional value regarding the uncertainty quantification of weather conditions, as the simulation uncertainty is significantly reduced.

Main findings The main findings of this thesis are summarized below, with the first 3 concerning the DMM-model and the last concerning the new methods:

- In the verification phase it is concluded that the influence period (Module C) is incorrectly interpreted. It is solved by implementing the influence period corresponding with a probability of 0.98 of the exceedance curve, instead of implementing an arbitrary chosen influence period of the exceedance curve.
- In the validation phase it is concluded that the simulation of projects consisting of coupled operations (Module D) does not work at all; even some test scenarios resulted in a fatal error. This module has to be recoded correctly and extended to make it work for multiple sequentially coupled operations.

- The DMM-model is limited to a 2nd-order Markov chain (Module B). It is observed that the workability percentage is well preserved, but the persistency deviates significantly. The DMM-model is calibrated by using higher Markov chain order, which resulted in a better persistency preservation.

- In the improvement phase two new methods are developed, the so-called 'Updated Conditional Markov Probability' (UCMP) method and the 'Markov Dependency' (MD) method. In these methods the problems regarding the coupled operations are solved. Alas, the results of the UCMP-method did not preserve the statistics of the hindcast data accurately enough, hence no further study is recommended for this method. The MD-method showed good results in terms of persistency, but it needs further improvement regarding workability percentage. Therefore, more research is recommended for this MD-method.

With the required rectifications the DMM-model can be practically implemented. The most important rectifications are to make it workable for (sequentially) coupled operation(s) and applicable for higher-order Markov chains in both seasonality methods. Additionally, smaller errors, limitations, inconsistencies are provided which ought to be rectified as well.

Added value The added value of the DMM-model regarding downtime analysis in general, is that there was no stochastic model in current literature to simulate complex marine projects. Secondly, it provides a mathematical approach to quantify the simulation uncertainty. The added value of the DMM-model in comparison to HADDOCK (Boskalis' current method to estimate downtime) can be expressed in assessing the uncertainties related to the models. The uncertainty in the hindcast data related to observational errors, is the same for both models and hence no assessing is needed. Nor the code uncertainty is considered, as it is believed that code errors should rather be rectified instead of quantified. Thus, only the simulation, parametric and model uncertainties are considered to influence the downtime estimation. The DMM-model reduces the simulation uncertainty at the expense of the parametric and model uncertainty. In the list below a summarized overview of the causes that determine the uncertainties in HADDOCK and the DMM-model is given.

- Simulation uncertainty:
  - HADDOCK: available hindcast datasets of approximately 10-25 years
  - DMM-model: number of project realizations as required (1000 years is suggested)

- Parametric uncertainty:
  - HADDOCK: interpolation
  - DMM-model: interpolation (same) + estimation of input parameters

- Model uncertainty:
  - HADDOCK: basis
  - DMM-model: basis (same) + statistical deviations

Research questions For this research the questions below were stated. The answers to these questions are already provided in the course of this thesis. In this paragraph summarized answers are described, and for a more detailed answer it is recommended to address the corresponding chapters.

- *How can downtime be analyzed with the current DMM-model?* The DMM-model abstract actual metocean conditions by stochastically producing binary 'workability sequences' for each operation within a project. Additional modules are incorporated to include effects such as seasonality, time-dependency, coupled operations. From every project simulation the downtime duration is estimated. Sections 2.3 to 2.11 explain more comprehensively the work methods of the DMM-model. For an even more thorough explanation consult the thesis of Rip [45].

- *Which methods for metocean parameter generators can be found in literature?* Gaussian based models such as the 'Box-Jenkins method' and 'Translated Gaussian Process'; re-sampling models such as 'Block re-sampling' and 'Markov chain re-sampling'; Parametric models such as 'Finite state space Markov chain', 'Copula method', 'Multivariate distribution method' and 'Nonlinear autoregressive models' are found in literature. See Section 3.1 in Chapter 3.

- *Is it possible to quantify uncertainties concerning the DMM-model?* In terms of simulation uncertainty 'yes', however the quantification of the other uncertainties is not that straightforward. Hence, more research is required for that purpose. Consult Section 3.3 for a more detailed answer (Chapter 3).

- *Is the concept and the model code of the current DMM-model correct, consistent and complete?* Only the concept of the influence period is incorrect, the other theoretical concepts are correct, consistent and complete. In terms of the model code, the DMM-model is incorrect, inconsistent and incomplete. See Table 5.3 in Chapter 5 for the full assessment.

- *Do the DMM-model and its individual modules perform sufficiently accurate?* Based on the white-box validation it can be concluded only Module A performs sufficiently accurate. As a result of this, the DMM-model performs inaccurate as well. A more comprehensive answer is given in Section 6.5 of Chapter 6, where Table 6.12 summarizes the findings of the validation.

- *How can the current DMM-model be improved/extended?* The most important points to improve are: applicability of higher-order Markov chains (Module B), the correct influence period (Module C), workable coupled operations (Module D). The influence period and the applicability of higher-order Markov chains is already improved, and the theory on how to rectify the coupled operations is provided. Consult Appendix B for all the improving points regarding the DMM-model. See Section 7.3 for a more detailed answer (Chapter 7).

8.2 Recommendations

In terms of recommendations a distinction has been made between recommendations to Boskalis and recommendations for further research.

Boskalis The *short-term* recommendation for Boskalis is to submit to the improving points of Appendix B. These should be rectified in order to make the DMM-model practically workable. It is still believed that the gained lower simulation uncertainty, at the expense of increase in parametric and model uncertainty, is of added value compared to the current methodology to determine downtime (with HADDOCK). Besides, the parametric and model uncertainties can be controlled by choosing a different seasonality method or Markov chain order. The conducted hypotheses tests indicated that futuristic projects should be simulated with non-time homogeneity. However, with coupled operations in the project the number of transition probabilities grows very quickly (see Table 5.1). In that case a piece-wise time homogeneous approach could be suitable. It is therefore recommended to further assess and quantify the parametric and model uncertainty.

The *long-term* recommendation to Boskalis is to develop a model that segregates the stochastically generation of metocean parameters and the simulation of projects, where the DMM-model performs this simultaneously. This gives the advantage that any start date can be chosen and sequentially coupled operations can be simulated without the increased model and parametric uncertainty. For this purpose, a model such as the Markov Dependency method should be developed.

Further research Throughout this thesis several recommendations are made already for further research. This paragraph lists recommendations considered to be the most important. In Rip [45] additional recommendations can be found regarding the DMM-model and downtime simulation analysis in general.

- The main recommendation is to further study and quantify the model and the parametric uncertainties; Section 3.2.3 creates a basis for this purpose. The model uncertainty decreases as more parameters are estimated (e.g. a higher Markov chain order), but at the same time the parametric uncertainty increases. An optimum study should be performed where the sum of both uncertainties is minimized. Consider also other estimators for the transition probabilities (as the most likelihood estimator is used in this thesis).
- Formalize mathematically the (improved) influence period $D(p, q)$ and the cross-transition probability P_{ij}^{pq}, as these concepts were not found in literature but in only Rip [45].
- Formalize mathematically the Markov Dependency as introduced in Chapter 7; investigate whether it can be written as a theorem. Furthermore, extensive validation is required for this method.
- Recode Modules A and B (seasonality and time-dependency) of the DMM-model in such a way that any Markov chain order can be used for both homogeneities.

- Recode Module D (coupled operations) of the DMM-model to make it workable for multiple sequentially coupled operations: e.g. a 'Hidden Markov Model' can be used for this purpose.
- A persistency preservation study: e.g. find the highest possible Markov chain order to preserve the persistency accurately, but still new information can be obtained with the specific order.
- It is recommended to further study the Updated Conditional Markov Probability method despite the results. Such a method could open new doors in the field of data imputation (replacing missing data).

8.3 Discussion

This thesis provides a framework for the use of software-testing. Many companies use a variety of models as black-boxes without knowing exactly what happens inside the box. Many users assume their models work *correctly*, where the provided framework initially assumes a model works *incorrectly* until evidence indicates otherwise. In this manner the DMM-model is tested and more confidence has been built to obtain reliable results. It should be kept in mind that there are still other unquantified uncertainties besides the simulation uncertainty while using the DMM-model. Altogether, it is still believed that the DMM-model can make more accurate downtime estimations than HADDOCK based on metocean conditions. This especially holds for big cyclic projects, since more variations of project progressions are realizable than they are for smaller projects. Big cyclic project mostly consist of coupled operations which increases other uncertainties. Ideally, the simulation of the DMM-model should be segregated into stochastic generation of metocean parameters and the project simulation. This would reduce the model uncertainty and speed up the simulation time. It can be concluded that models, such as the DMM-model, can help tender teams in making their decisions based on project duration, giving them a competitive advantage. However, it should be kept in mind that the hindcast data used as input for the downtime estimation is assumed to be representative for the truth, which is not certain. If in the hindcast data a 1000-year storm occurred, then the model will treat it as it happens every 20 years (if the dataset is recorded for 20 years). This is obviously not true.

A Algorithm block schemes

A.1 Improved DMM-model scheme

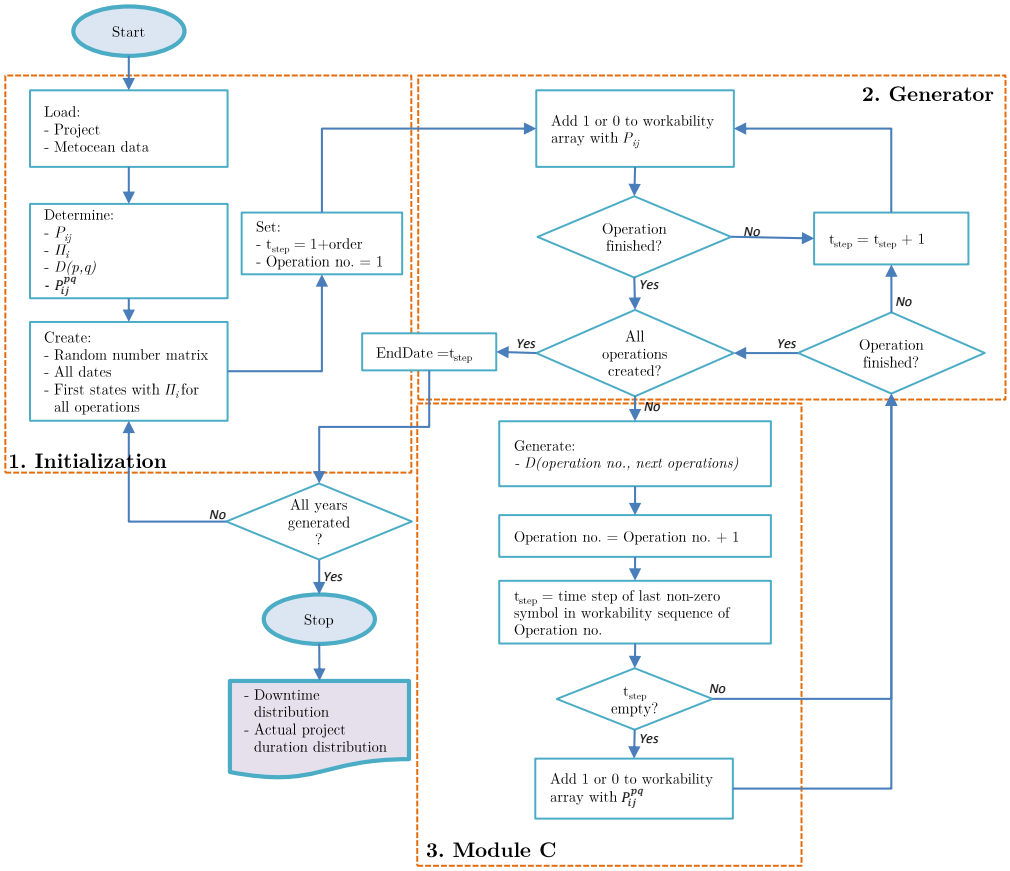

Figure A.1: A schematization of the algorithm for constructing workability sequences of marine projects with the improved 'Downtime Modular Markov' model.

A.2 Updated Conditional Markov probabilities scheme

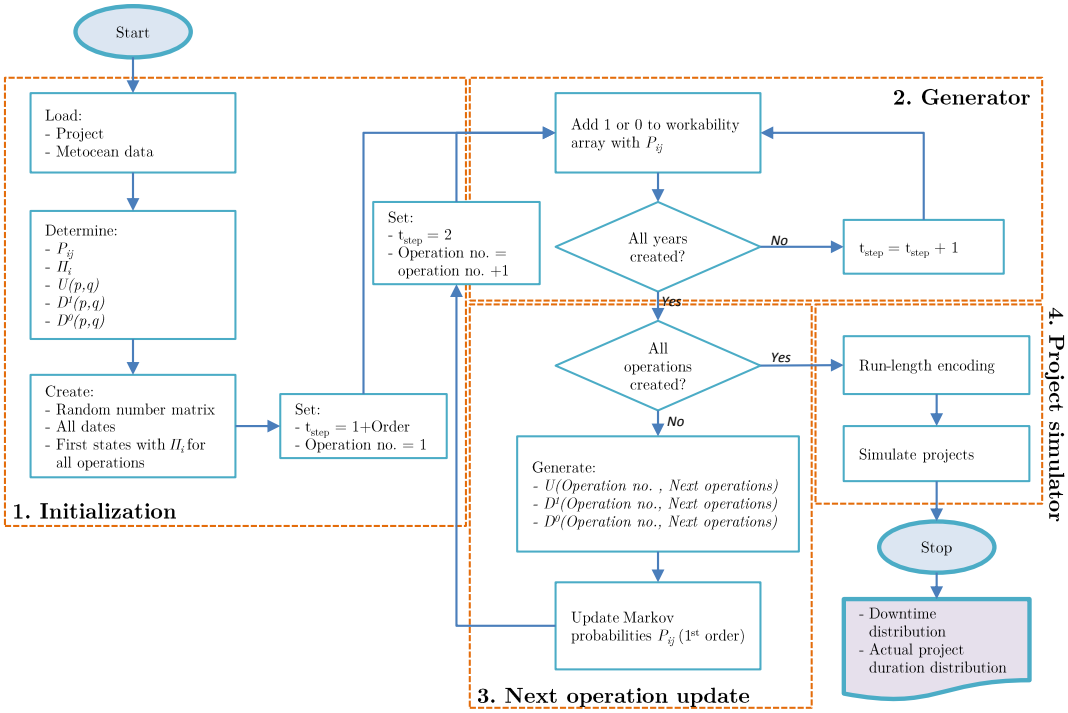

Figure A.2: A schematization of the algorithm for constructing workability sequences of marine projects with the 'Updated Conditional Markov probabilities' method.

A.3 Markov Dependency scheme

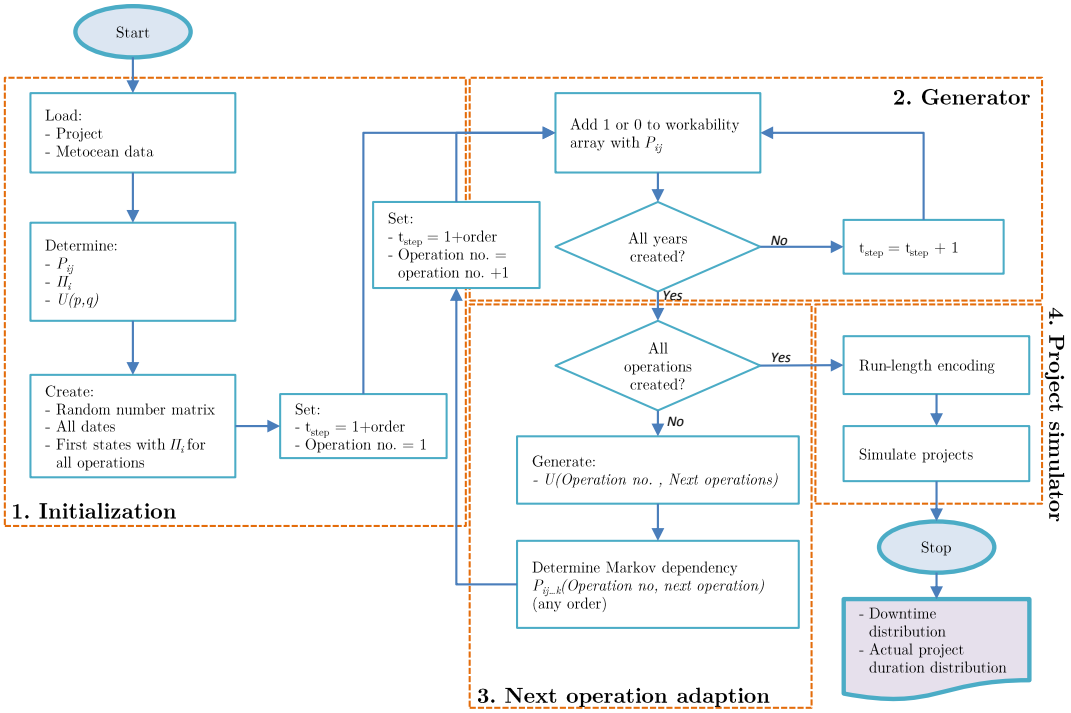

Figure A.3: A schematization of the algorithm for constructing workability sequences of marine projects with the 'Markov Dependency' method.

B Improving points

During the verification and validation process several errors/ limitations/ inconsistencies have been found, which are sorted below per module (and some have already been reported). Furthermore, the priority is assigned alphabetically, with (a) being the highest priority, (b) being next, etc. The following numbers have been solved already: 5d, 5e, 3e, 5c.

1. Module A: Seasonality
   (a) Miscalculation in the daily transition probabilities, due to leap years in hindcast data (Section 5.2.1).
   (b) The least squared cross validation (LSCV) is not defined when $P_{01,init} = \hat{P}_{01,-t_i}$. Additive smoothing can solve this problem.
   (c) The transition probabilities are limited to daily/monthly probabilities. For the sake of completeness, weekly/seasonally/yearly transition probabilities should be created.
   (d) The limiting probabilities π_i are based on monthly stationarity. For the sake of completeness and consistency, the limiting probabilities should be made daily/weekly/seasonally/yearly.
   (e) Error in the derivation of $\hat{P}_{ij}(m)$, as explained in Section 5.1.1.
2. Module B: Time-dependency
   (a) The piece-wise time homogeneous function is limited to 1st and 2nd order Markov chain. Higher orders should be made possible (Section 5.1.2).
   (b) A higher order Markov chain should be possible for the non-time homogeneous function. applicable for piece-wise time homogeneity (Section 5.1.2).
   (c) The hypothesis-tests should be redefined; Listing 5.1 represents the idea of how it should be coded. If the homogeneity hypothesis-test is rejected for any operation, take the inhomogenous mode with 1st order. If the homogeneity test is confirmed (for all operations), perform the order hypothesis-test. If the order hypothesis-test is rejected for any operation, take 1st-order. If the order test is confirmed (for all operations) take the 2nd-order. Also, the degrees of freedom are differently defined in this thesis.

3. Module C: Linked Markov chains
   (a) The exceedance curves of the influence period are yearly based, while seasonally/monthly based should be possible too.
   (b) The influence period can also work the other way around. When a non-workable state is observed in operation p the next state(s) have to be non-workable in operation q in case it has a stricter operational limit.
   (c) The DMM-model crashes when: Operation A has an influence period for the next 2 operations (C, D) & the influence period length of operation D is longer than the influence period length of operation C & the net duration of operation C is shorter than the influence period length of operation C.
   (d) The cross-transition probability is monthly stationary. For the sake of completeness and consistency, the cross-transition probabilities should be made daily/weekly/seasonally/yearly.
   (e) The influence period can be coded more efficient.
   (f) The cross-transition probability can be coded more efficient.
4. Module D: Coupled operations
   (a) This module does not work at all, when non-time homogeneity is applied (Section 5.2.4).
   (b) The DMM-model is limited to one sequentially coupled operation, while in practice more sequentially coupled operations take place as well (Section 5.2.4).
5. Miscellaneous
   (a) Without a warranty window in the project, the DMM-model is unable to create binary workability sequences.
   (b) Warranty windows shorter than the net durations, results in an incorrect project schematization. The duration of the warranty window is considered as the net duration of the operation.
   (c) The DMM-model will crash in case a project consist of cycles, due to incorrectness programming of certain variables.
   (d) The DMM-model is unable to run a project consisting of operations without a determined operational limit in the inhomogeneous mode. There are no `'columnStates'` defined, resulting in a crash. Nor the defining of the `'columnStates'` is done correctly in the inhomogeneous mode for multiple operations with the same operational limits.
   (e) Dvoretzky-Kiefer-Wolfowitz inequality results in the following confidence bands: $\hat{F}_n(x) \pm \sqrt{\frac{1}{2n} ln(\frac{2}{\alpha})}$ (differs slightly from Equation (4.3) in Rip [45]).
   (f) The persistency is not preserved simulating with the DMM-model.

C Relation between P_{ij}^{pq} and π_j^q

This chapter gives a mathematical derivation of the relation between $\hat{P}_{ij}^{pq}$ and π_j^q. It is partly adopted from Rip [45] and extended. The cross-transition probability $\hat{P}_{ij}^{pq}$ is defined as follows:

$$\hat{P}_{ij}^{pq} = \frac{N_{ij}^{pq}}{N_i^p} \tag{C.1}$$

Where N_i^p denotes the number of observed transitions that start from $i \in 0, 1$ in the workability sequence of operation p. N_{ij}^{pq} denotes the number of observed transitions that start from the same state i, as assigned in N_i^p, to state $j \in 0.1$ in the workability sequence of operation q. An example of the derivation of N_{11}^{pq} is presented in Figure C.1. Table C.1 presents the values of N_i^p,N_i^q and N_{ij}^{pq} for the sequence of Figure C.1.

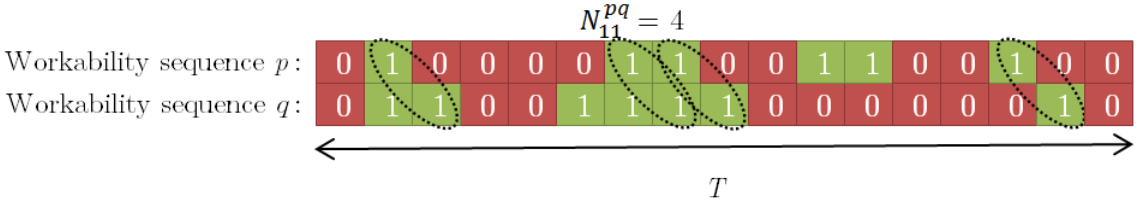

Figure C.1: Example of the derivation of N_{11}^{pq}

Table C.1: The values of N_i^p,N_i^q and N_{ij}^{pq} for the sequence of Figure C.1

$N_{00}^{pq} = 7$	$N_{01}^{pq} = 3$	$N_0^p = 11$
$N_{10}^{pq} = 2$	$N_{11}^{pq} = 4$	$N_1^p = 6$
$N_1^p = 6$	$N_1^p = 6$	$T = 17$

The limiting probability for state i of operation q is defined as:

$$\pi_i^q = \frac{N_i^q}{T} \tag{C.2}$$

Where T denotes the length of the workability sequence and is defined as:

$$T = N_1^p + N_0^p = N_1^q + N_0^q \tag{C.3}$$

N_1^q, N_1^p, N_0^q and N_0^p can be rewritten in terms of N_{ij}^{pq}:

$$N_1^q = \begin{cases} N_{11}^{pq} + N_{01}^{pq}, & \text{if the first symbol of the workability sequence } q = 0 \\ N_{11}^{pq} + N_{01}^{pq} + 1 & \text{if the first symbol of the workability sequence } q = 1 \end{cases} \tag{C.4}$$

Hence:

$$N_1^q \geq N_{11}^{pq} + N_{01}^{pq} \tag{C.5}$$

Analogously,

$$N_1^p = \begin{cases} N_{11}^{pq} + N_{10}^{pq}, & \text{if the first symbol of the workability sequence } p = 0 \\ N_{11}^{pq} + N_{10}^{pq} + 1 & \text{if the first symbol of the workability sequence } p = 1 \end{cases} \tag{C.6}$$

Hence:

$$N_1^p \geq N_{11}^{pq} + N_{10}^{pq} \tag{C.7}$$

$$N_0^q = \begin{cases} N_{10}^{pq} + N_{00}^{pq}, & \text{if the first symbol of the workability sequence } q = 1 \\ N_{10}^{pq} + N_{00}^{pq} + 1 & \text{if the first symbol of the workability sequence } q = 0 \end{cases} \tag{C.8}$$

Hence:

$$N_0^q \geq N_{10}^{pq} + N_{00}^{pq} \tag{C.9}$$

Analogously,

$$N_0^p = \begin{cases} N_{01}^{pq} + N_{00}^{pq}, & \text{if the first symbol of the workability sequence } p = 1 \\ N_{01}^{pq} + N_{00}^{pq} + 1 & \text{if the first symbol of the workability sequence } p = 0 \end{cases} \tag{C.10}$$

Hence:

$$N_0^p \geq N_{10}^{pq} + N_{00}^{pq} \tag{C.11}$$

The '**boundary states**', BS^{qp}, are defined as the states of the first time step in the workability sequence of operation q and the last time step in the workability sequence of operation p. Four different combinations of boundary states can be established, defined as follows:

$$BS^{qp} : BS^{00}, BS^{01}, BS^{10}, BS^{11} \tag{C.12}$$

From these four boundary states, the following four propositions can be determined:

Proposition C.1. *The relation between the cross-transition probability $\hat{P}_{ij}^{pq}$ and the limiting probability π_i^q of state i in operational q with BS^{00} is given by:*

$$\hat{P}_{00}^{pq}\begin{cases} > \pi_0^q & if \quad \frac{N_1^p+1}{N_0^p-1} > \frac{N_{10}^{pq}+1}{N_{00}^{pq}} \\ = \pi_0^q & if \quad \frac{N_1^p+1}{N_0^p-1} = \frac{N_{10}^{pq}+1}{N_{00}^{pq}} \\ < \pi_0^q & if \quad \frac{N_1^p+1}{N_0^p-1} < \frac{N_{10}^{pq}+1}{N_{00}^{pq}} \end{cases} \qquad \hat{P}_{01}^{pq}\begin{cases} > \pi_1^q & if \quad \frac{N_1^p+1}{N_0^p-1} > \frac{N_{11}^{pq}}{N_{01}^{pq}} \\ = \pi_1^q & if \quad \frac{N_1^p+1}{N_0^p-1} = \frac{N_{11}^{pq}}{N_{01}^{pq}} \\ < \pi_1^q & if \quad \frac{N_1^p+1}{N_0^p-1} < \frac{N_{11}^{pq}}{N_{01}^{pq}} \end{cases}$$

$$\hat{P}_{10}^{pq}\begin{cases} > \pi_0^q & if \quad \frac{N_0^p}{N_1^p} > \frac{N_{00}^{pq}+1}{N_{10}^{pq}} \\ = \pi_0^q & if \quad \frac{N_0^p}{N_1^p} = \frac{N_{00}^{pq}+1}{N_{10}^{pq}} \\ < \pi_0^q & if \quad \frac{N_0^p}{N_1^p} < \frac{N_{00}^{pq}+1}{N_{10}^{pq}} \end{cases} \qquad \hat{P}_{11}^{pq}\begin{cases} > \pi_1^q & if \quad \frac{N_0^p}{N_1^p} > \frac{N_{01}^{pq}}{N_{11}^{pq}} \\ = \pi_1^q & if \quad \frac{N_0^p}{N_1^p} = \frac{N_{01}^{pq}}{N_{11}^{pq}} \\ < \pi_1^q & if \quad \frac{N_0^p}{N_1^p} < \frac{N_{01}^{pq}}{N_{11}^{pq}} \end{cases} \tag{C.13}$$

Proof. Equation C.1 can be rewritten as:

$$P_{11}^{pq} = \frac{N_{11}^{pq}}{N_1^p} \tag{C.14}$$

And with Equation C.3 and Equation C.4, Equation C.2 can be rewritten as:

$$\pi_1^q = \frac{N_{11}^{pq} + N_{01}^{pq}}{N_1^p + N_0^p} \tag{C.15}$$

Comparing Equation C.14 and Equation C.15 results in:

$$\hat{P}_{11}^{pq}\begin{cases} > \pi_1^q & if \quad \frac{N_0^p}{N_1^p} > \frac{N_{01}^{pq}}{N_{11}^{pq}} \\ = \pi_1^q & if \quad \frac{N_0^p}{N_1^p} = \frac{N_{01}^{pq}}{N_{11}^{pq}} \\ < \pi_1^q & if \quad \frac{N_0^p}{N_1^p} < \frac{N_{01}^{pq}}{N_{11}^{pq}} \end{cases} \tag{C.16}$$

Analogously, the relations between P_{10}^{pq}, P_{01}^{pq}, P_{00}^{pq} and π_1^q, π_0^q can be obtained □

Cautionary note If the workability percentage of p = 100%, i.e. the workability sequence of p only contains workable states, 1s, thus $N_{01}^{pq} = N_{00}^{pq} = 0$ and $N_1^p = T$. Hence: $\pi_1^q = \frac{N_{11}^{pq}}{N_1^p}$ and $P_{11}^{pq} = \frac{N_{11}^{pq}}{N_1^p - 1}$, due to BS^{q1}, resulting in $\pi_1^q \approx P_{11}^{pq}$ if N_{11}^{pq} and $N_1^p \gg 1$.

Lemma C.1.1. *If operation p is less strict than operation q, given that both operations are restricted to the same metocean parameter and the time interval is sufficiently small, which results in $D(p,q) = 0$ and $N_{01}^{pq} = 0$, the following relations can be determined for BS^{00}:*

$$\begin{aligned} \hat{P}_{00}^{pq} &= 1 \quad \hat{P}_{01}^{pq} = 0 \\ \hat{P}_{10}^{pq} &\leq \pi_0^q \quad \hat{P}_{11}^{pq} \geq \pi_1^q \end{aligned} \tag{C.17}$$

Proof. The workability percentage of operation p has a higher or equal workability percentage of operation q, which implies $\pi_1^p \geq \pi_1^q$. This results in:

$$N_{10}^{pq} \geq N_{01}^{pq} \tag{C.18}$$

Equation C.1 combined with axiom $N_{01}^{pq} = 0$, results in:

$$\hat{P}_{01}^{pq} = 0 \tag{C.19}$$

Combining Equation C.19 with $P_{00}^{pq} = 1 - P_{01}^{pq}$ results in:

$$\hat{P}_{00}^{pq} = 1 \tag{C.20}$$

Equation C.16 combined with the axiom results in:

$$\hat{P}_{11}^{pq} \geq \pi_1^q \tag{C.21}$$

Combining Equation C.21 with $P_{10}^{pq} = 1 - P_{11}^{pq}$ and $\pi_0^q = 1 - \pi_1^q$ results in:

$$\hat{P}_{10}^{pq} \leq \pi_0^q \tag{C.22}$$

□

Equation C.22 is clarified with the following example. In this example workability sequence p has an operational limit of $H_s \leq 3m$ and workability sequence q an operational limit of $H_s \leq 1m$. In Figure C.2 the transitions $N_{01}^{pq} = 0$, hence $P_{00}^{pq} = 1$. For that reason the transitions N_{00}^{pq} are struck through, leaving only workable states in operation p. It follows that $\hat{P}_{11}^{pq} \geq \pi_1^q$, because the number of not-workable states is reduced.

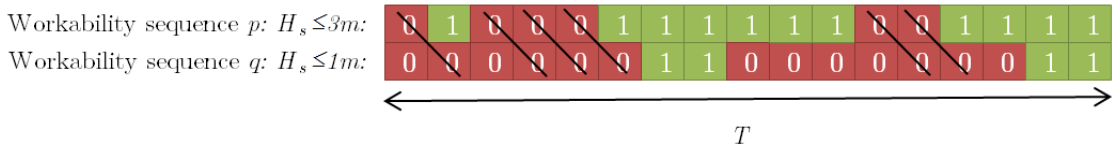

Figure C.2: Clarification for Equation C.22 with an example of operations p and q

Proposition C.2. *The relation between the cross-transition probability $\hat{P}_{ij}^{pq}$ and the limiting probability π_i^q of state i in operational q with BS^{10} is given by:*

$$\hat{P}_{00}^{pq}\begin{cases} > \pi_0^q & if \quad \dfrac{N_1^p+1}{N_0^p-1} > \dfrac{N_{10}^{pq}}{N_{00}^{pq}} \\ = \pi_0^q & if \quad \dfrac{N_1^p+1}{N_0^p-1} = \dfrac{N_{10}^{pq}}{N_{00}^{pq}} \\ < \pi_0^q & if \quad \dfrac{N_1^p+1}{N_0^p-1} < \dfrac{N_{10}^{pq}}{N_{00}^{pq}} \end{cases} \quad \hat{P}_{01}^{pq}\begin{cases} > \pi_1^q & if \quad \dfrac{N_1^p+1}{N_0^p-1} > \dfrac{N_{11}^{pq}+1}{N_{01}^{pq}} \\ = \pi_1^q & if \quad \dfrac{N_1^p+1}{N_0^p-1} = \dfrac{N_{11}^{pq}+1}{N_{01}^{pq}} \\ < \pi_1^q & if \quad \dfrac{N_1^p+1}{N_0^p-1} < \dfrac{N_{11}^{pq}+1}{N_{01}^{pq}} \end{cases}$$

$$\hat{P}_{10}^{pq}\begin{cases} > \pi_0^q & if \quad \dfrac{N_0^p}{N_1^p} > \dfrac{N_{00}^{pq}}{N_{10}^{pq}} \\ = \pi_0^q & if \quad \dfrac{N_0^p}{N_1^p} = \dfrac{N_{00}^{pq}}{N_{10}^{pq}} \\ < \pi_0^q & if \quad \dfrac{N_0^p}{N_1^p} < \dfrac{N_{00}^{pq}}{N_{10}^{pq}} \end{cases} \quad \hat{P}_{11}^{pq}\begin{cases} > \pi_1^q & if \quad \dfrac{N_0^p}{N_1^p} > \dfrac{N_{01+1}^{pq}}{N_{11}^{pq}} \\ = \pi_1^q & if \quad \dfrac{N_0^p}{N_1^p} = \dfrac{N_{01+1}^{pq}}{N_{11}^{pq}} \\ < \pi_1^q & if \quad \dfrac{N_0^p}{N_1^p} < \dfrac{N_{01+1}^{pq}}{N_{11}^{pq}} \end{cases} \tag{C.23}$$

Proof. Equation C.1 can be rewritten as:

$$P_{01}^{pq} = \frac{N_{01}^{pq}}{N_0^p - 1} \tag{C.24}$$

And with Equation C.3 and Equation C.4, Equation C.2 can be rewritten as:

$$\pi_1^q = \frac{N_{11}^{pq} + N_{01}^{pq} + 1}{N_1^p + N_0^p} \tag{C.25}$$

Comparing Equation C.24 and Equation C.25 results in:

$$\hat{P}_{01}^{pq}\begin{cases} > \pi_1^q & if \quad \dfrac{N_1^p+1}{N_0^p-1} > \dfrac{N_{11}^{pq}+1}{N_{01}^{pq}} \\ = \pi_1^q & if \quad \dfrac{N_1^p+1}{N_0^p-1} = \dfrac{N_{11}^{pq}+1}{N_{01}^{pq}} \\ < \pi_1^q & if \quad \dfrac{N_1^p+1}{N_0^p-1} < \dfrac{N_{11}^{pq}+1}{N_{01}^{pq}} \end{cases} \tag{C.26}$$

Analogously, the relations between P_{10}^{pq}, P_{11}^{pq}, P_{00}^{pq} and π_1^q, π_0^q can be obtained □

Proposition C.3. *The relation between the cross-transition probability $\hat{P}_{ij}^{pq}$ and the limiting probability π_i^q of state i in operational q with BS^{01} is given by:*

$$\hat{P}_{00}^{pq}\begin{cases} > \pi_0^q & if \quad \frac{N_1^p}{N_0^p} > \frac{N_{10}^{pq}+1}{N_{00}^{pq}} \\ = \pi_0^q & if \quad \frac{N_1^p}{N_0^p} = \frac{N_{10}^{pq}+1}{N_{00}^{pq}} \\ < \pi_0^q & if \quad \frac{N_1^p}{N_0^p} < \frac{N_{10}^{pq}+1}{N_{00}^{pq}} \end{cases} \qquad \hat{P}_{01}^{pq}\begin{cases} > \pi_1^q & if \quad \frac{N_1^p}{N_0^p} > \frac{N_{11}^{pq}}{N_{01}^{pq}} \\ = \pi_1^q & if \quad \frac{N_1^p}{N_0^p} = \frac{N_{11}^{pq}}{N_{01}^{pq}} \\ < \pi_1^q & if \quad \frac{N_1^p}{N_0^p} < \frac{N_{11}^{pq}}{N_{01}^{pq}} \end{cases}$$

$$\hat{P}_{10}^{pq}\begin{cases} > \pi_0^q & if \quad \frac{N_0^p+1}{N_1^p-1} > \frac{N_{00}^{pq}+1}{N_{10}^{pq}} \\ = \pi_0^q & if \quad \frac{N_0^p+1}{N_1^p-1} = \frac{N_{00}^{pq}+1}{N_{10}^{pq}} \\ < \pi_0^q & if \quad \frac{N_0^p+1}{N_1^p-1} < \frac{N_{00}^{pq}+1}{N_{10}^{pq}} \end{cases} \qquad \hat{P}_{11}^{pq}\begin{cases} > \pi_1^q & if \quad \frac{N_0^p+1}{N_1^p-1} > \frac{N_{01}^{pq}}{N_{11}^{pq}} \\ = \pi_1^q & if \quad \frac{N_0^p+1}{N_1^p-1} = \frac{N_{01}^{pq}}{N_{11}^{pq}} \\ < \pi_1^q & if \quad \frac{N_0^p+1}{N_1^p-1} < \frac{N_{01}^{pq}}{N_{11}^{pq}} \end{cases} \tag{C.27}$$

Proof. Equation C.1 can be rewritten as:

$$P_{00}^{pq} = \frac{N_{00}^{pq}}{N_0^p} \tag{C.28}$$

And with Equation C.3 and Equation C.8, Equation C.2 can be rewritten as:

$$\pi_0^q = \frac{N_{10}^{pq} + N_{00}^{pq} + 1}{N_1^p + N_0^p} \tag{C.29}$$

Comparing Equation C.28 and Equation C.29 results in:

$$\hat{P}_{00}^{pq}\begin{cases} > \pi_0^q & if \quad \frac{N_1^p}{N_0^p} > \frac{N_{10}^{pq}+1}{N_{00}^{pq}} \\ = \pi_0^q & if \quad \frac{N_1^p}{N_0^p} = \frac{N_{10}^{pq}+1}{N_{00}^{pq}} \\ < \pi_0^q & if \quad \frac{N_1^p}{N_0^p} < \frac{N_{10}^{pq}+1}{N_{00}^{pq}} \end{cases} \tag{C.30}$$

Analogously, the relations between P_{10}^{pq}, P_{11}^{pq}, P_{01}^{pq} and π_1^q, π_0^q can be obtained □

Proposition C.4. *The relation between the cross-transition probability $\hat{P}_{ij}^{pq}$ and the limiting probability π_i^q of state i in operational q with BS^{11} is given by:*

$$\hat{P}_{00}^{pq}\begin{cases} > \pi_0^q & if \quad \frac{N_1^p}{N_0^p} > \frac{N_{10}^{pq}}{N_{00}^{pq}} \\ = \pi_0^q & if \quad \frac{N_1^p}{N_0^p} = \frac{N_{10}^{pq}}{N_{00}^{pq}} \\ < \pi_0^q & if \quad \frac{N_1^p}{N_0^p} < \frac{N_{10}^{pq}}{N_{00}^{pq}} \end{cases} \qquad \hat{P}_{01}^{pq}\begin{cases} > \pi_1^q & if \quad \frac{N_1^p}{N_0^p} > \frac{N_{11}^{pq}+1}{N_{01}^{pq}} \\ = \pi_1^q & if \quad \frac{N_1^p}{N_0^p} = \frac{N_{11}^{pq}+1}{N_{01}^{pq}} \\ < \pi_1^q & if \quad \frac{N_1^p}{N_0^p} < \frac{N_{11}^{pq}+1}{N_{01}^{pq}} \end{cases}$$

$$\hat{P}_{10}^{pq}\begin{cases} > \pi_0^q & if \quad \frac{N_0^p+1}{N_1^p-1} > \frac{N_{00}^{pq}}{N_{10}^{pq}} \\ = \pi_0^q & if \quad \frac{N_0^p+1}{N_1^p-1} = \frac{N_{00}^{pq}}{N_{10}^{pq}} \\ < \pi_0^q & if \quad \frac{N_0^p+1}{N_1^p-1} < \frac{N_{00}^{pq}}{N_{10}^{pq}} \end{cases} \qquad \hat{P}_{11}^{pq}\begin{cases} > \pi_1^q & if \quad \frac{N_0^p+1}{N_1^p-1} > \frac{N_{01}^{pq}+1}{N_{11}^{pq}} \\ = \pi_1^q & if \quad \frac{N_0^p+1}{N_1^p-1} = \frac{N_{01}^{pq}+1}{N_{11}^{pq}} \\ < \pi_1^q & if \quad \frac{N_0^p+1}{N_1^p-1} < \frac{N_{01}^{pq}+1}{N_{11}^{pq}} \end{cases} \tag{C.31}$$

Proof. Equation C.1 can be rewritten as:

$$P_{10}^{pq} = \frac{N_{10}^{pq}}{N_1^p - 1} \tag{C.32}$$

And with Equation C.3 and Equation C.8, Equation C.2 can be rewritten as:

$$\pi_0^q = \frac{N_{10}^{pq} + N_{00}^{pq}}{N_1^p + N_0^p} \tag{C.33}$$

Comparing Equation C.32 and Equation C.33 results in:

$$\hat{P}_{10}^{pq}\begin{cases} > \pi_0^q & if \quad \frac{N_0^p+1}{N_1^p-1} > \frac{N_{00}^{pq}}{N_{10}^{pq}} \\ = \pi_0^q & if \quad \frac{N_0^p+1}{N_1^p-1} = \frac{N_{00}^{pq}}{N_{10}^{pq}} \\ < \pi_0^q & if \quad \frac{N_0^p+1}{N_1^p-1} < \frac{N_{00}^{pq}}{N_{10}^{pq}} \end{cases} \tag{C.34}$$

Analogously, the relations between P_{00}^{pq}, P_{11}^{pq}, P_{01}^{pq} and π_1^q, π_0^q can be obtained □

D Hypothesis testing

Hypothesis testing concerns statistical testing in order to determine whether there is enough 'evidence' to conclude a condition (the hypothesis) is true. It consists of the following steps (based on Wikipedia):

1. State the Null Hypothesis (H_0) and the Alternative Hypothesis (H_1).
2. State the appropriate test statistic T.
3. Derive the sampling distribution under the null-hypothesis of the test statistic T.
4. Select a significance value α, in this thesis $\alpha = 0.05$ is used.
5. The distribution of the test statistic under the null hypothesis partitions the possible values of T into those for which the null hypothesis is rejected (the so-called critical region), and those for which it is not. The probability of the critical region is α.
6. Compute from the observations the observed value t_{obs} of the test statistic T.
7. Compute the p-value (probability) of the test statistic. $p = P(T \geq t_{obs})$
8. Conclude, based on a comparison of the computed value of the test statistic and the significal value α, whether to accept or reject the null hypothesis.

Reject the null-hypothesis, if the p-value is less than the significance value α. If the p-value is not less than the significance level α, then the test has no result. "The probability of rejecting the null hypothesis is a function of five factors: whether the test is one- or two tailed, the level of significance, the standard deviation, the amount of deviation from the null hypothesis, and the number of observations [7]. A schematization of a 1-sided hypothesis test with a chi-square distribution and the probability is presented in Figure D.1. The used test statistics in this thesis is the Pearson's 'Chi-square test' or χ^2-test and the 'log-likelihood-ratio test', which are defined as follows respectively:

$$\chi^2 = \sum_{i=1}^{n} \frac{(O_i - E_i)^2}{E_i} \tag{D.1}$$

$$-2ln(\Delta) = -2\sum_{i=1}^{n}(ln(O_i) - ln(E_i)) \tag{D.2}$$

Where:

- χ^2 = Pearson's cumulative test statistic, which asymptotically approaches a χ^2 distribution
- $-2ln(\Delta)$ = Log likelihood test statistic, which asymptotically approaches a $-2ln(\Delta)$ distribution
- O_i = The number of observations i
- $E_i = Np_i$ = The expected (theoretical) frequency of type i, asserted by the null hypothesis that the fraction of type i in the observations (the number of observations is N) is p_i

The degrees of freedom (**df**) are the number of values that are free to vary. For purpose of illustration, a sum is set to a fixed 10: $a + b = 10$. The degree of freedom is in this example is 1, since only 1 cell can 'freely' vary. The general principal is:
df = (number of cells) - 1

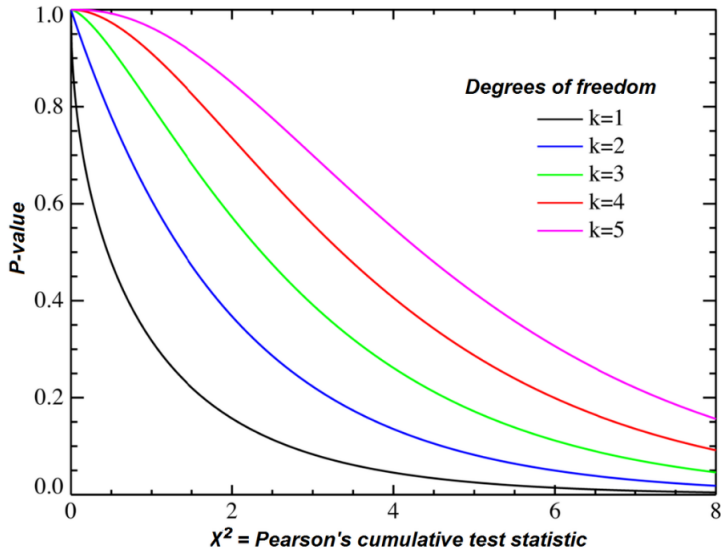

Figure D.1: Chi-squared distribution, with χ^2 on the x-axis and the p-value on the y-axis

E Validation

E.1 Seasonality

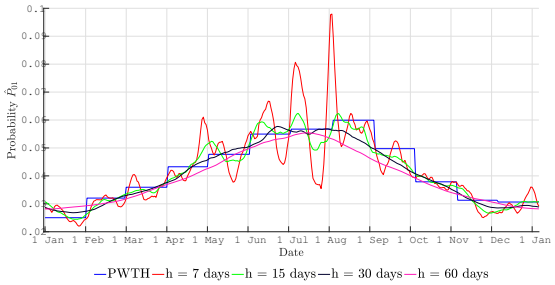

(a) Northern Hemisphere (North sea)

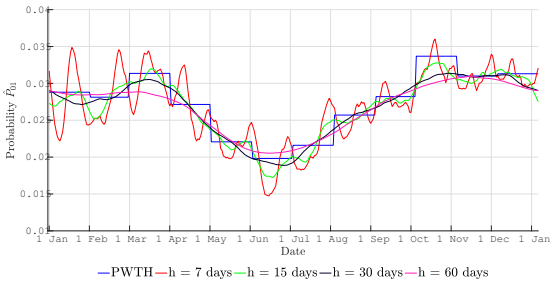

(b) Southern Hemisphere (Tasman Sea)

Figure E.1: Seasonality effects on both hemispheres presented with transition probability P_{01} subject to operational limit $H_s \leq 1.5$ m. Piece-wise time homogeneous method is indicated in blue and the non-time homogeneous method is performed with different kernel bandwidths h.

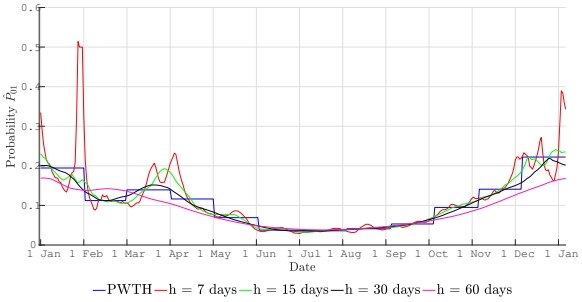

Figure E.2: Seasonality effects in the Gulf of Guinea presented with transition probability P_{01} subject to operational limit $H_s \leq 1.5m$. Piece-wise time homogeneous method is indicated in blue and the non-time homogeneous method is performed with different kernel bandwidths h.

E.2 Results hypothesis tests

E.2.1 Hypothesis chi-square test for monthly piece-wise homogeneity

Table E.1: The results of the hypothesis chi-square test ($\alpha = 0.05$) for 7 different operational limits in the Gulf of Guinea with first-order Markov chain

Location: Gulf of Guinea Markov chain order: 1							
Month:	$H_s \leq 1m$	$H_s \leq 2m$	$H_s \leq 2.5m$	$U \leq 10m/s$	$T_p \leq 7s$	$H_s \leq 2m; U \leq 10m/s$	$H_s \leq 2m; T_p \leq 7s$
Jan	$p > \alpha$	$p > \alpha$	$p > \alpha$	$p \leq \alpha$	$p > \alpha$	$p \leq \alpha$	$p > \alpha$
Feb	$p \leq \alpha$	$p \leq \alpha$	$p > \alpha$	$p > \alpha$	$p > \alpha$	$p \leq \alpha$	$p > \alpha$
Mar	$p \leq \alpha$	$p \leq \alpha$	$p > \alpha$	$p > \alpha$	$p > \alpha$	$p \leq \alpha$	$p > \alpha$
Apr	$p \leq \alpha$	$p \leq \alpha$	$p \leq \alpha$	$p \leq \alpha$	$p > \alpha$	$p \leq \alpha$	$p > \alpha$
May	$p \leq \alpha$	$p \leq \alpha$	$p \leq \alpha$	$p \leq \alpha$	$p \leq \alpha$	$p \leq \alpha$	$p \leq \alpha$
Jun	$p \leq \alpha$	$p \leq \alpha$	$p \leq \alpha$	$p \leq \alpha$	$p > \alpha$	$p \leq \alpha$	$p > \alpha$
Jul	$p \leq \alpha$	$p > \alpha$	$p \leq \alpha$	$p \leq \alpha$	$p > \alpha$	$p > \alpha$	$p > \alpha$
Aug	$p > \alpha$	$p > \alpha$	$p > \alpha$	$p \leq \alpha$	$p > \alpha$	$p > \alpha$	$p \leq \alpha$
Sep	$p \leq \alpha$	$p > \alpha$	$p \leq \alpha$	$p \leq \alpha$	$p > \alpha$	$p > \alpha$	$p > \alpha$
Oct	$p \leq \alpha$	$p \leq \alpha$	$p \leq \alpha$	$p > \alpha$	$p \leq \alpha$	$p \leq \alpha$	$p \leq \alpha$
Nov	$p > \alpha$	$p \leq \alpha$	$p > \alpha$	$p > \alpha$	$p > \alpha$	$p \leq \alpha$	$p > \alpha$
Dec	$p \leq \alpha$	$p > \alpha$	$p > \alpha$	$p > \alpha$	$p > \alpha$	$p > \alpha$	$p > \alpha$

Table E.2: The results of the hypothesis chi-square test ($\alpha = 0.05$) for 7 different operational limits in the North sea with first-order Markov chain

Location: North sea Markov chain order: 1							
Month:	$H_s \leq 1m$	$H_s \leq 2m$	$H_s \leq 2.5m$	$U \leq 10m/s$	$T_p \leq 7s$	$H_s \leq 2m; U \leq 10m/s$	$H_s \leq 2m; T_p \leq 7s$
Jan	$p \leq \alpha$	$p > \alpha$	$p > \alpha$	$p > \alpha$	$p > \alpha$	$p > \alpha$	$p > \alpha$
Feb	$p > \alpha$	$p \leq \alpha$	$p > \alpha$	$p \leq \alpha$	$p > \alpha$	$p \leq \alpha$	$p \leq \alpha$
Mar	$p \leq \alpha$	$p \leq \alpha$	$p \leq \alpha$	$p \leq \alpha$	$p > \alpha$	$p \leq \alpha$	$p \leq \alpha$
Apr	$p > \alpha$	$p \leq \alpha$	$p \leq \alpha$	$p > \alpha$	$p > \alpha$	$p \leq \alpha$	$p > \alpha$
May	$p \leq \alpha$	$p > \alpha$	$p > \alpha$	$p > \alpha$	$p > \alpha$	$p > \alpha$	$p > \alpha$
Jun	$p > \alpha$	$p > \alpha$	$p > \alpha$	$p > \alpha$	$p > \alpha$	$p > \alpha$	$p \leq \alpha$
Jul	$p > \alpha$	$p > \alpha$	$p > \alpha$	$p \leq \alpha$	$p > \alpha$	$p > \alpha$	$p \leq \alpha$
Aug	$p \leq \alpha$	$p \leq \alpha$	$p > \alpha$	$p \leq \alpha$	$p > \alpha$	$p \leq \alpha$	$p \leq \alpha$
Sep	$p > \alpha$	$p \leq \alpha$	$p > \alpha$	$p > \alpha$	$p \leq \alpha$	$p \leq \alpha$	$p \leq \alpha$
Oct	$p \leq \alpha$	$p \leq \alpha$	$p \leq \alpha$	$p > \alpha$	$p \leq \alpha$	$p \leq \alpha$	$p \leq \alpha$
Nov	$p > \alpha$	$p > \alpha$	$p > \alpha$	$p > \alpha$	$p > \alpha$	$p > \alpha$	$p > \alpha$
Dec	$p > \alpha$	$p > \alpha$	$p > \alpha$	$p \leq \alpha$	$p > \alpha$	$p \leq \alpha$	$p \leq \alpha$

Table E.3: The results of the hypothesis chi-square test ($\alpha = 0.05$) for 7 different operational limits in the Tasman sea with first-order Markov chain

Location: Tasman sea Markov chain order: 1							
Month:	$H_s \leq 1m$	$H_s \leq 2m$	$H_s \leq 2.5m$	$U \leq 10m/s$	$T_p \leq 7s$	$H_s \leq 2m;\ U \leq 10m/s$	$H_s \leq 2m;\ T_p \leq 7s$
Jan	$p > \alpha$	$p > \alpha$	$p > \alpha$	$p > \alpha$	$p > \alpha$	$p > \alpha$	$p > \alpha$
Feb	$p > \alpha$	$p > \alpha$	$p > \alpha$	$p > \alpha$	$p > \alpha$	$p > \alpha$	$p > \alpha$
Mar	$p > \alpha$	$p > \alpha$	$p > \alpha$	$p > \alpha$	$p > \alpha$	$p > \alpha$	$p > \alpha$
Apr	$p \leq \alpha$	$p \leq \alpha$	$p > \alpha$	$p \leq \alpha$	$p > \alpha$	$p \leq \alpha$	$p > \alpha$
May	$p > \alpha$	$p > \alpha$	$p > \alpha$	$p \leq \alpha$	$p > \alpha$	$p > \alpha$	$p > \alpha$
Jun	$p \leq \alpha$	$p > \alpha$	$p > \alpha$	$p \leq \alpha$	$p > \alpha$	$p \leq \alpha$	$p \leq \alpha$
Jul	$p > \alpha$	$p \leq \alpha$	$p > \alpha$	$p > \alpha$	$p \leq \alpha$	$p \leq \alpha$	$p \leq \alpha$
Aug	$p > \alpha$	$p > \alpha$	$p > \alpha$	$p \leq \alpha$	$p \leq \alpha$	$p > \alpha$	$p > \alpha$
Sep	$p > \alpha$	$p > \alpha$	$p > \alpha$	$p > \alpha$	$p > \alpha$	$p > \alpha$	$p > \alpha$
Oct	$p \leq \alpha$	$p > \alpha$	$p > \alpha$	$p > \alpha$	$p > \alpha$	$p > \alpha$	$p > \alpha$
Nov	$p \leq \alpha$	$p > \alpha$	$p > \alpha$	$p > \alpha$	$p > \alpha$	$p > \alpha$	$p > \alpha$
Dec	$p > \alpha$	$p > \alpha$	$p > \alpha$	$p > \alpha$	$p > \alpha$	$p > \alpha$	$p > \alpha$

E.3 Hypothesis test for Markov chain order

Table E.4: The results of the hypothesis test ($\alpha = 0.05$) for 7 different operational limits in the Gulf of Guinea

Location: Gulf of Guinea Test statistic: Chi-square test							
Order:	$H_s \leq 1m$	$H_s \leq 2m$	$H_s \leq 2.5m$	$U \leq 10m/s$	$T_p \leq 7s$	$H_s \leq 2m;\ U \leq 10m/s$	$H_s \leq 2m;\ T_p \leq 7s$
1	$p \leq \alpha$	$p \leq \alpha$	$p \leq \alpha$	$p \leq \alpha$	$p \leq \alpha$	$p \leq \alpha$	$p \leq \alpha$
2	$p \leq \alpha$	$p \leq \alpha$	$p \leq \alpha$	$p > \alpha$	$p \leq \alpha$	$p \leq \alpha$	$p \leq \alpha$
3	$p \leq \alpha$	$p \leq \alpha$	$p \leq \alpha$	$p > \alpha$	$p \leq \alpha$	$p \leq \alpha$	$p \leq \alpha$
4	$p \leq \alpha$	$p \leq \alpha$	$p \leq \alpha$	$p > \alpha$	$p \leq \alpha$	$p \leq \alpha$	$p \leq \alpha$
5	$p \leq \alpha$	$p \leq \alpha$	$p > \alpha$	$p > \alpha$	$p \leq \alpha$	$p \leq \alpha$	$p \leq \alpha$
6	$p \leq \alpha$	$p \leq \alpha$	$p > \alpha$	$p > \alpha$	$p \leq \alpha$	$p \leq \alpha$	$p \leq \alpha$

Table E.5: The results of the hypothesis test ($\alpha = 0.05$ for 7 different operational limits in the Gulf of Guinea

Location: Gulf of Guinea Test statistic: Log likelihood ratio test							
Order:	$H_s \leq 1m$	$H_s \leq 2m$	$H_s \leq 2.5m$	$U \leq 10m/s$	$T_p \leq 7s$	$H_s \leq 2m;\ U \leq 10m/s$	$H_s \leq 2m;\ T_p \leq 7s$
1	$p \leq \alpha$	$p \leq \alpha$	$p \leq \alpha$	$p \leq \alpha$	$p \leq \alpha$	$p \leq \alpha$	$p \leq \alpha$
2	$p \leq \alpha$	$p \leq \alpha$	$p \leq \alpha$	$p > \alpha$	$p \leq \alpha$	$p \leq \alpha$	$p \leq \alpha$
3	$p \leq \alpha$	$p \leq \alpha$	$p \leq \alpha$	$p > \alpha$	$p > \alpha$	$p \leq \alpha$	$p > \alpha$
4	$p \leq \alpha$	$p \leq \alpha$	$p \leq \alpha$	$p > \alpha$	$p \leq \alpha$	$p \leq \alpha$	$p \leq \alpha$
5	$p \leq \alpha$	$p \leq \alpha$	$p > \alpha$	$p > \alpha$	$p \leq \alpha$	$p \leq \alpha$	$6p \leq \alpha$
6	$p \leq \alpha$	$p > \alpha$	$p > \alpha$	$p > \alpha$	$p > \alpha$	$p > \alpha$	$p > \alpha$

Table E.6: The results of the hypothesis test ($\alpha 0.05$) for 7 different operational limits in the North sea

Location: North sea Test statistic: Chi-square test							
Order:	$H_s \leq 1m$	$H_s \leq 2m$	$H_s \leq 2.5m$	$U \leq 10m/s$	$T_p \leq 7s$	$H_s \leq 2m; U \leq 10m/s$	$H_s \leq 2m; T_p \leq 7s$
1	$p \leq \alpha$	$p \leq \alpha$	$p \leq \alpha$	$p \leq \alpha$	$p \leq \alpha$	$p \leq \alpha$	$p \leq \alpha$
2	$p \leq \alpha$	$p \leq \alpha$	$p \leq \alpha$	$p \leq \alpha$	$p \leq \alpha$	$p \leq \alpha$	$p \leq \alpha$
3	$p \leq \alpha$	$p \leq \alpha$	$p \leq \alpha$	$p \leq \alpha$	$p \leq \alpha$	$p \leq \alpha$	$p \leq \alpha$
4	$p \leq \alpha$	$p \leq \alpha$	$p \leq \alpha$	$p \leq \alpha$	$p \leq \alpha$	$p \leq \alpha$	$p \leq \alpha$
5	$p \leq \alpha$	$p \leq \alpha$	$p \leq \alpha$	$p \leq \alpha$	$p \leq \alpha$	$p \leq \alpha$	$p \leq \alpha$
6	$p \leq \alpha$	$p \leq \alpha$	$p \leq \alpha$	$p \leq \alpha$	$p \leq \alpha$	$p \leq \alpha$	$p \leq \alpha$

Table E.7: The results of the hypothesis test ($\alpha = 0.05$) for 7 different operational limits in the North sea

Location: North sea Test statistic: Log likelihood ratio test							
Order:	$H_s \leq 1m$	$H_s \leq 2m$	$H_s \leq 2.5m$	$U \leq 10m/s$	$T_p \leq 7s$	$H_s \leq 2m; U \leq 10m/s$	$H_s \leq 2m; T_p \leq 7s$
1	$p \leq \alpha$	$p \leq \alpha$	$p \leq \alpha$	$p \leq \alpha$	$p \leq \alpha$	$p \leq \alpha$	$p \leq \alpha$
2	$p \leq \alpha$	$p \leq \alpha$	$p \leq \alpha$	$p \leq \alpha$	$p \leq \alpha$	$p \leq \alpha$	$p \leq \alpha$
3	$p \leq \alpha$	$p \leq \alpha$	$p \leq \alpha$	$p \leq \alpha$	$p \leq \alpha$	$p \leq \alpha$	$p \leq \alpha$
4	$p \leq \alpha$	$p \leq \alpha$	$p \leq \alpha$	$p \leq \alpha$	$p \leq \alpha$	$p \leq \alpha$	$p \leq \alpha$
5	$p \leq \alpha$	$p \leq \alpha$	$p \leq \alpha$	$p \leq \alpha$	$p \leq \alpha$	$p \leq \alpha$	$p \leq \alpha$
6	$p \leq \alpha$	$p \leq \alpha$	$p \leq \alpha$	$p \leq \alpha$	$p \leq \alpha$	$p \leq \alpha$	$p \leq \alpha$

Table E.8: The results of the hypothesis test ($\alpha = 0.05$) for 7 different operational limits in the Tasman sea

Location: Tasman sea Test statistic: Chi-square test							
Order:	$H_s \leq 1m$	$H_s \leq 2m$	$H_s \leq 2.5m$	$U \leq 10m/s$	$T_p \leq 7s$	$H_s \leq 2m; U \leq 10m/s$	$H_s \leq 2m; T_p \leq 7s$
1	$p \leq \alpha$	$p \leq \alpha$	$p \leq \alpha$	$p \leq \alpha$	$p \leq \alpha$	$p \leq \alpha$	$p \leq \alpha$
2	$p > \alpha$	$p \leq \alpha$	$p \leq \alpha$	$p \leq \alpha$	$p > \alpha$	$p \leq \alpha$	$p > \alpha$
3	$p \leq \alpha$	$p \leq \alpha$	$p \leq \alpha$	$p \leq \alpha$	$p \leq \alpha$	$p \leq \alpha$	$p \leq \alpha$
4	$p \leq \alpha$	$p > \alpha$	$p \leq \alpha$	$p \leq \alpha$	$p \leq \alpha$	$p \leq \alpha$	$p \leq \alpha$
5	$p \leq \alpha$	$p \leq \alpha$	$p \leq \alpha$	$p \leq \alpha$	$p \leq \alpha$	$p \leq \alpha$	$p \leq \alpha$
6	$p \leq \alpha$	$p > \alpha$	$p > \alpha$	$p \leq \alpha$	$p \leq \alpha$	$p \leq \alpha$	$p \leq \alpha$

Table E.9: The resulted p-values of the hypothesis test for 7 different operational limits in the Tasman sea

Location: Tasman sea Test statistic: Log likelihood ratio test							
Order:	$H_s \leq 1m$	$H_s \leq 2m$	$H_s \leq 2.5m$	$U \leq 10m/s$	$T_p \leq 7s$	$H_s \leq 2m;\ U \leq 10m/s$	$H_s \leq 2m;\ T_p \leq 7s$
1	$p \leq \alpha$	$p \leq \alpha$	$p \leq \alpha$	$p \leq \alpha$	$p \leq \alpha$	$p \leq \alpha$	$p \leq \alpha$
2	$p > \alpha$	$p \leq \alpha$	$p \leq \alpha$	$p \leq \alpha$	$p > \alpha$	$p \leq \alpha$	$p > \alpha$
3	$p \leq \alpha$	$p \leq \alpha$	$p > \alpha$	$p \leq \alpha$	$p \leq \alpha$	$p \leq \alpha$	$p \leq \alpha$
4	$p > \alpha$	$p > \alpha$	$p > \alpha$	$p \leq \alpha$	$p \leq \alpha$	$p \leq \alpha$	$p \leq \alpha$
5	$p > \alpha$	$p > \alpha$	$p > \alpha$	$p \leq \alpha$	$p \leq \alpha$	$p \leq \alpha$	$p \leq \alpha$
6	$p > \alpha$	$p > \alpha$	$p > \alpha$	$p \leq \alpha$	$p \leq \alpha$	$p \leq \alpha$	$p \leq \alpha$

E.4 Influence periods

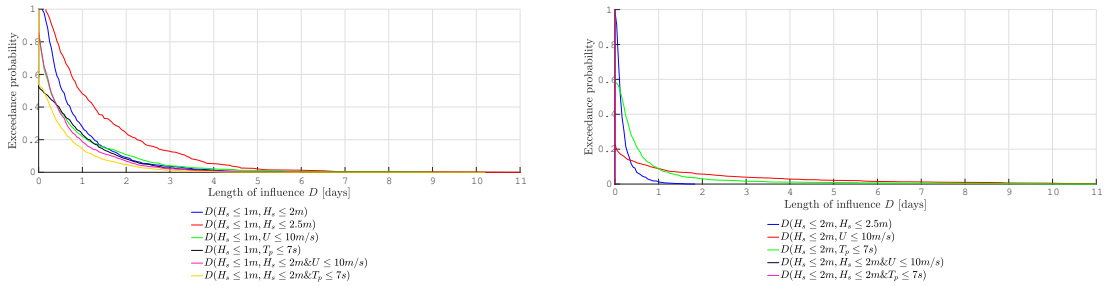

Figure E.3: Exceedance probability of influence periods $D(p, q)$ for operational limit $H_s \leq 1$ m (left) and $H_s \leq 2$ m (right) in the North Sea

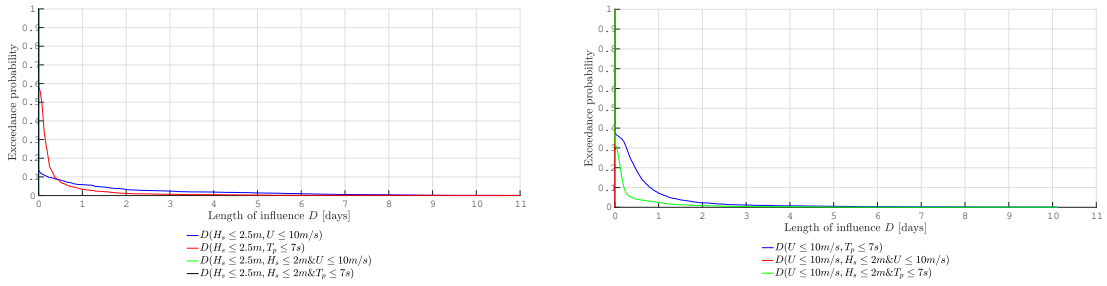

Figure E.4: Exceedance probability of influence periods $D(p, q)$ for operational limits $H_s \leq 2.5$ m (left) and $U \leq 10$ m/s (right) in the North Sea

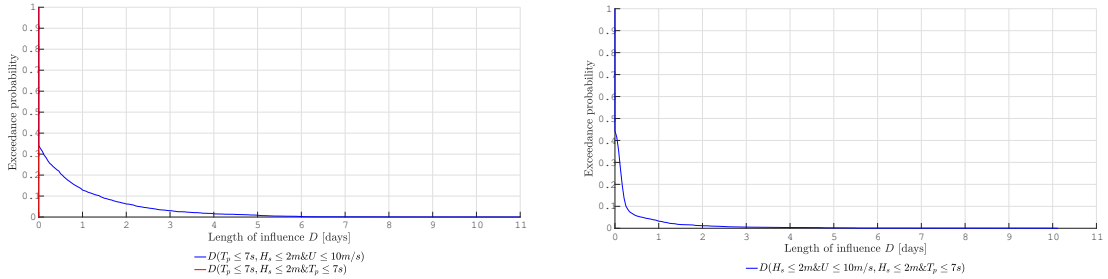

Figure E.5: Exceedance probability of influence periods $D(p, q)$ for operational limit $T_p \leq 7$ s (left) and $H_s \leq 2$ m, $U \leq 10$ m/s (right) in the North Sea

E.5 Cross-transition probabilities

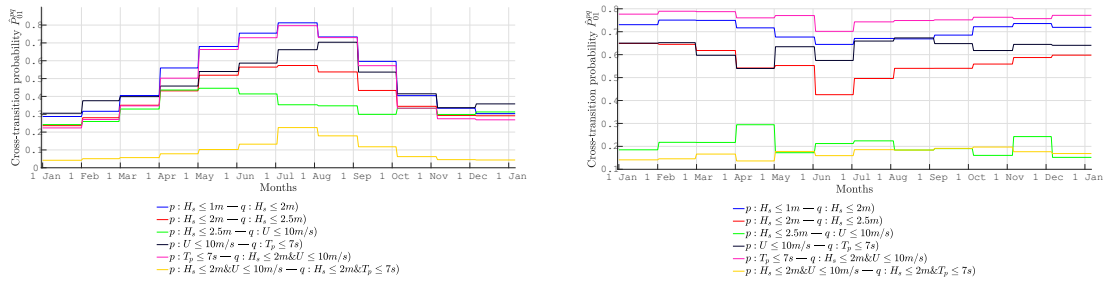

Figure E.6: The cross-transition probability P_{01}^{pq} of the hypothetical project in Table 6.3 presented over the year with monthly stationarity in the North sea (left) and the Tasman sea (right)

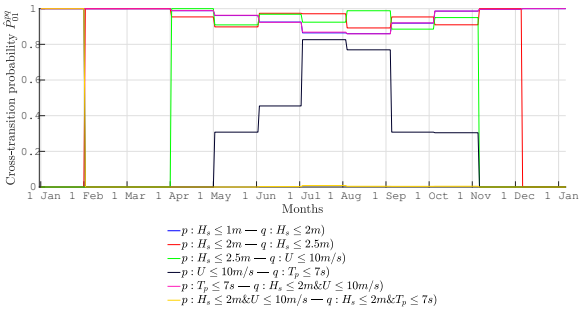

Figure E.7: The cross-transition probability P_{01}^{pq} of the hypothetical project in Table 6.3 presented over the year with monthly stationarity in the Gulf of Guinea

E.6 Data validation

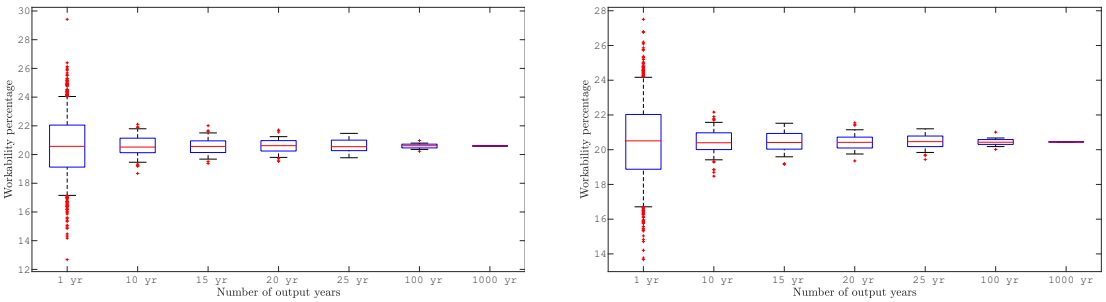

(a) Piece-wise time homogeneity **(b)** Non-time homogeneity

Figure E.8: The workability percentage of the North sea dataset subject to an operational limit $H_s \leq 1$ m for both (in)homogeneities and 1st-order measured for different bins of years. The whiskers of the box plot indicate the 95th percentiles and the red cross are its outliers.

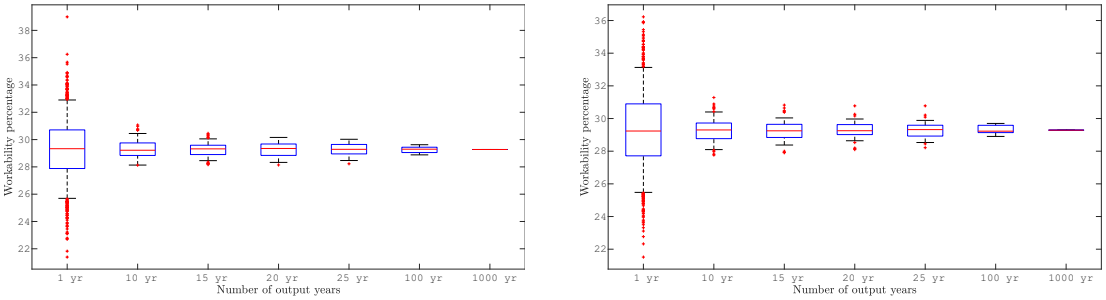

(a) Piece-wise time homogeneity **(b)** Non-time homogeneity

Figure E.9: The workability percentage of the North sea dataset subject to an operational limit $T_p \leq 6$ s for both (in)homogeneities and 1st-order measured for different bins of years. The whiskers of the box plot indicate the 95th percentiles and the red cross are its outliers.

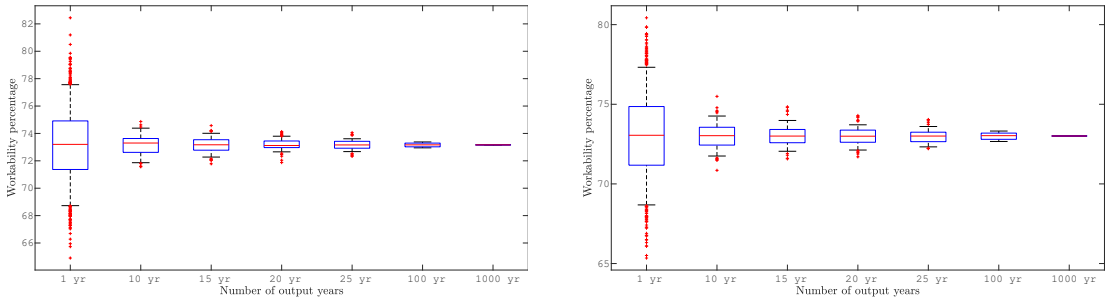

(a) Piece-wise time homogeneity **(b)** Non-time homogeneity

Figure E.10: The workability percentage of the North sea dataset subject to an operational limit $H_s \leq 2.5$ m for piece-wise time homogeneity and 1st-order measured for different bins of years. The whiskers of the box plot indicate the 95th percentiles and the red cross are its outliers.

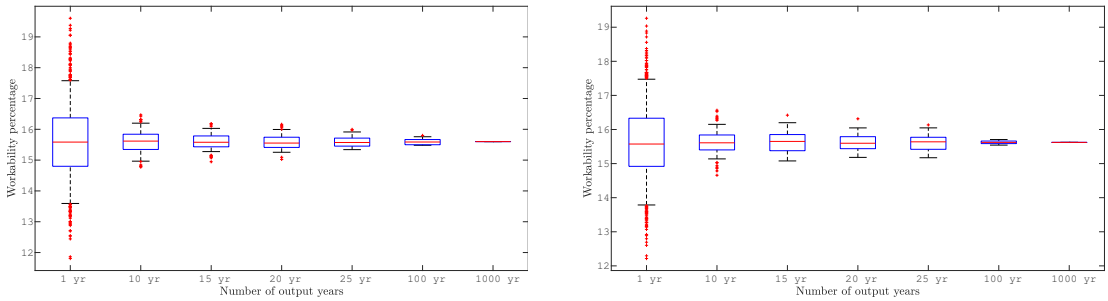

(a) Piece-wise time homogeneity **(b)** Non-time homogeneity

Figure E.11: The workability percentage of the Gulf of Guinea dataset subject to an operational limit $H_s \leq 1$ m for both (in)homogeneities and 1st-order measured for different bins of years. The whiskers of the box plot indicate the 95th percentiles and the red cross are its outliers.

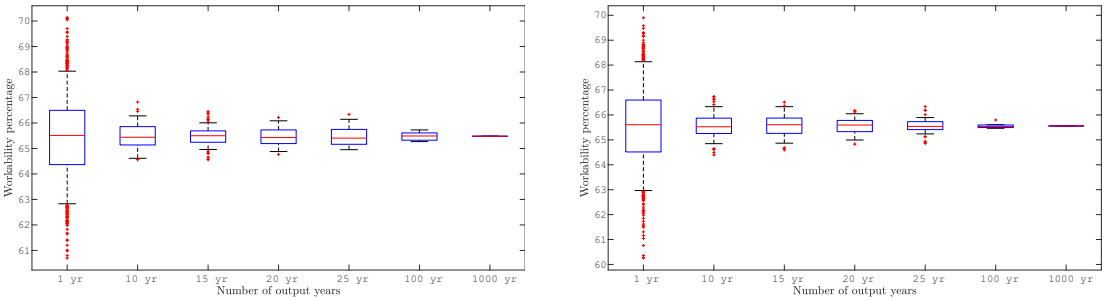

(a) Piece-wise time homogeneity **(b)** Non-time homogeneity

Figure E.12: The workability percentage of the Gulf of Guinea dataset subject to an operational limit $U \leq 5$ m/s for both (in)homogeneities and 1st-order measured for different bins of years. The whiskers of the box plot indicate the 95th percentiles and the red cross are its outliers.

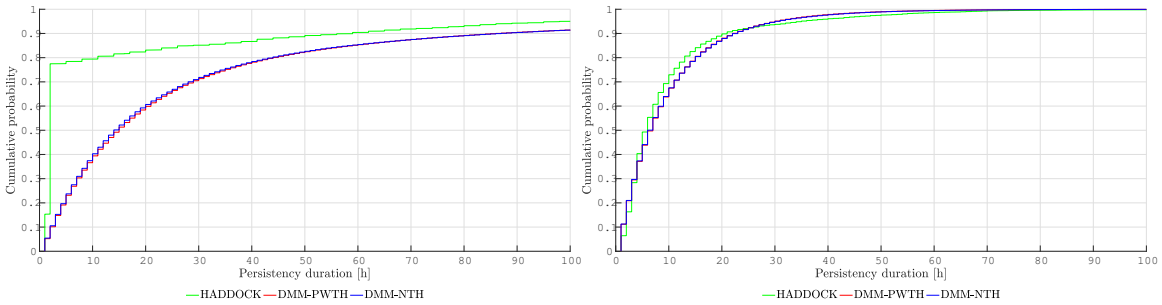

(a) Operational limit: $H_s \leq 1$ m **(b)** Operational limit: $U \leq 5$ m/s

Figure E.13: The cumulative distribution of persistency for the Gulf of Guinea subject to a set operational limit with 1st-Order and both homogeneities.

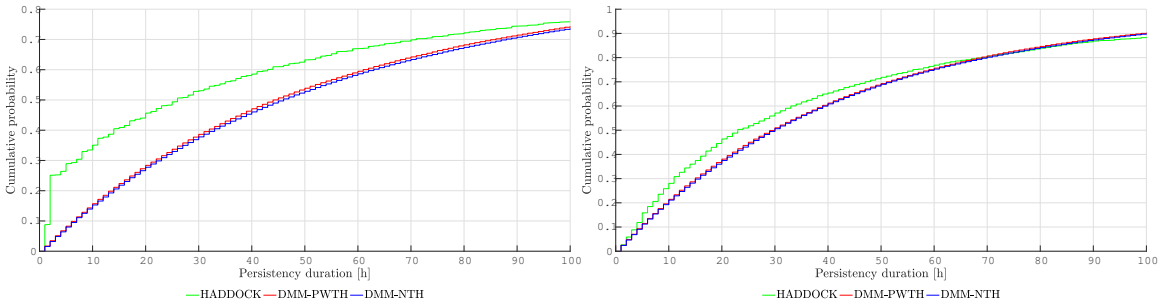

(a) Operational limit: $H_s \leq 1$ m **(b)** Operational limit: $T_p \leq 6$ s

Figure E.14: The cumulative distribution of persistency for the North sea subject to a set operational limit with 1st-Order and both homogeneities.

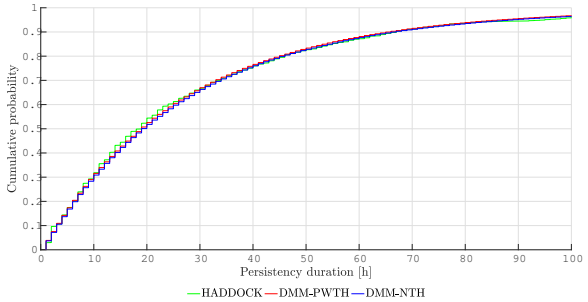

Figure E.15: The cumulative distribution of persistency for the North sea subject to an operational limit of $H_s \leq 2.5$ m, with 1st-Order and both homogeneities.

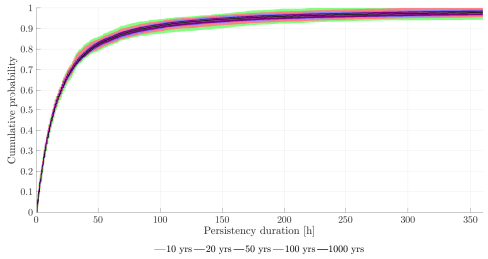

(a) Operational limit: $H_s \leq 1$ m

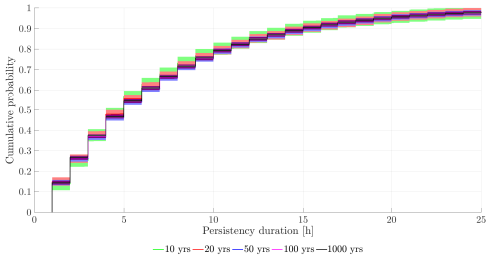

(b) Operational limit: $U \leq 5$ m/s

Figure E.16: The cumulative distribution of persistency for the Gulf of Guinea subject to a set operational limit with confidence bands determined with an α-value of 0.05. 1st-Order and non-time homogeneity.

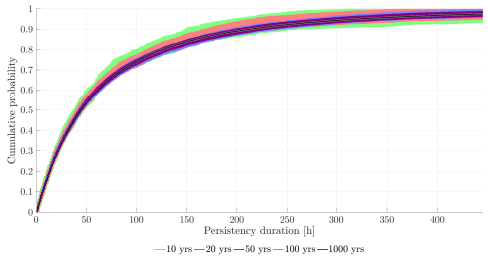

(a) Operational limit: $H_s \leq 1$ m

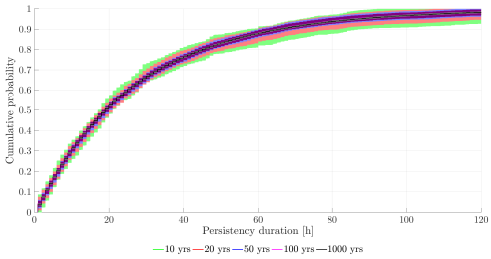

(b) Operational limit: $H_s \leq 2.5$ m

Figure E.17: The cumulative distribution of persistency for the North sea subject to a set operational limit with confidence bands determined with an α-value of 0.05. 1st-Order and non-time homogeneity.

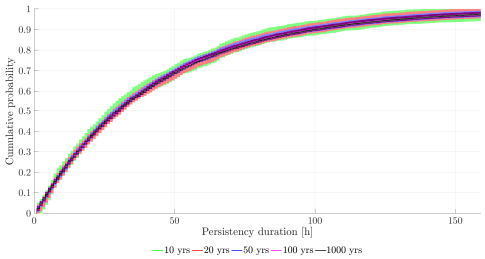

Figure E.18: The cumulative distribution of persistency for the Gulf of Guinea subject to a set operational limit with confidence bands determined with an α-value of 0.05. 1st-Order and non-time homogeneity.

E.7 Black-box validation

E.7.1 Different project

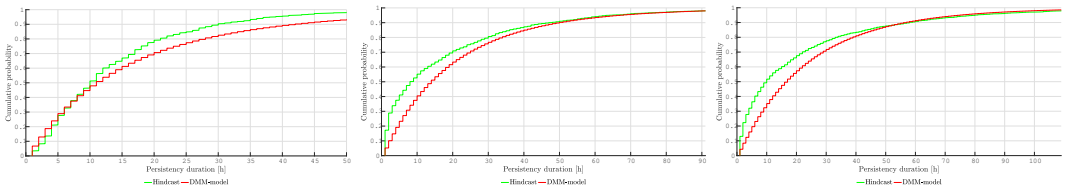

Figure E.19: The workable persistency duration distribution of the original (hindcast) and DMM-model generated 1000 years datasets are presented for the operation the first three operations in the hypothetical project in Table 6.10.

E.7.2 Different data

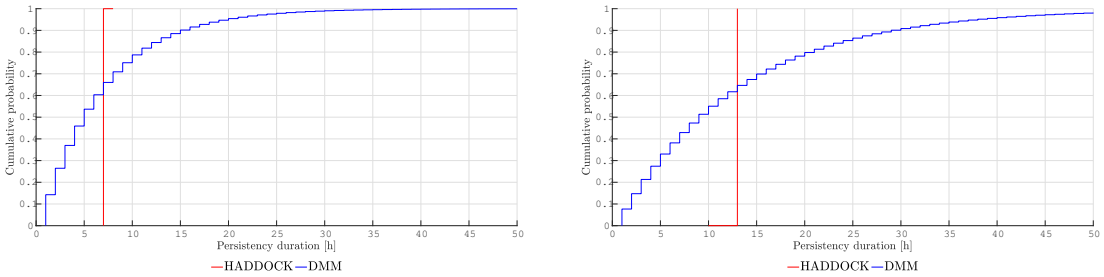

(a) Operational limit: $H_s \leq 1.5$ m **(b)** Operational limit: $H_s \leq 2$ m

Figure E.20: The persistency duration distribution of the original (hindcast) and DMM-model generated 1000 years datasets are presented for the sinus subject to two operational limits.

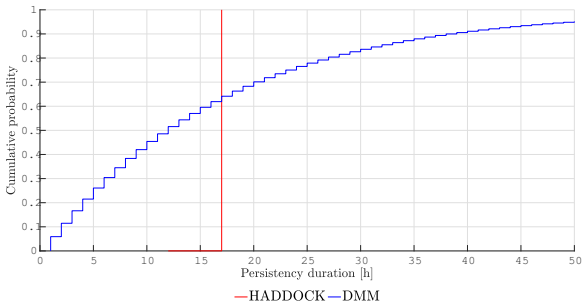

Figure E.21: The persistency duration distribution of the original (hindcast) and DMM-model generated 1000 years datasets are presented for the sinus subject to the limit of $H_s \leq 2.5$ m.

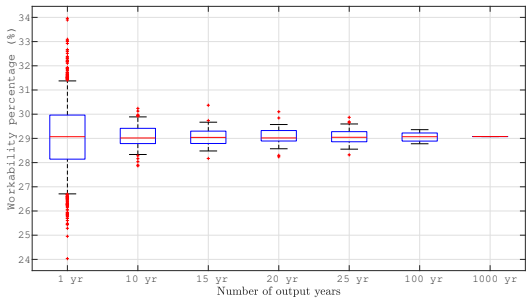

Figure E.22: The workability percentage of the harmonic sinusoidal motion subject to an operational limit $H_s \leq 1.5$ m for piece-wise time homogeneity and 1st-order measured for different bins of years. The whiskers of the box plot indicate the 95th percentiles and the red cross are its outliers.

F Extensions & Improvement

F.1 New coding method: Persistency

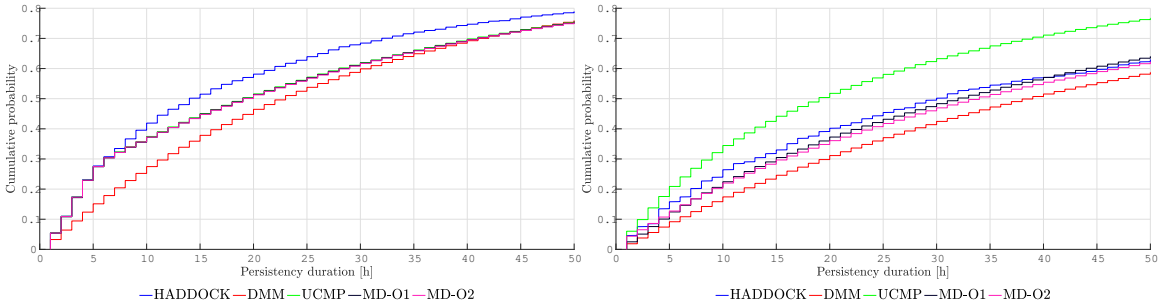

(a) Operation A **(b)** Operation B

Figure F.1: The cumulative distribution of persistency for the North sea subject to a set operational limit of $U \leq 10$ m/s (left) and $H_s \leq 2.5$ m (right).

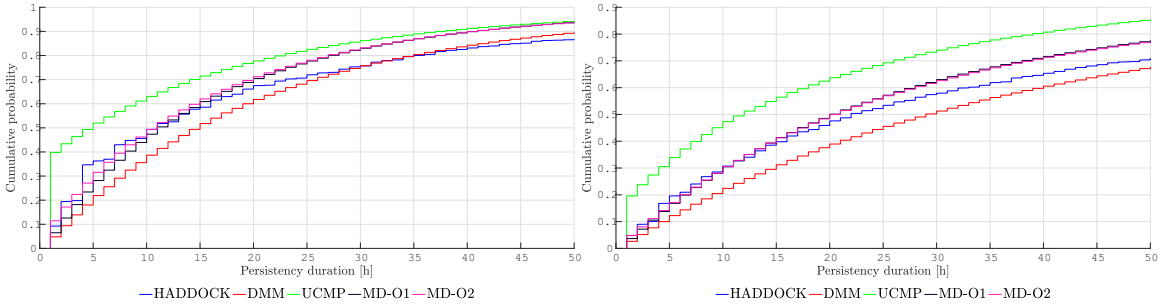

(a) Operation C **(b)** Operation D

Figure F.2: The cumulative distribution of persistency for the North sea subject to a set operational limit of $H_s \leq 1$ m, $U \leq 10$ m/s (left) and $H_s \leq 2$ m (right).

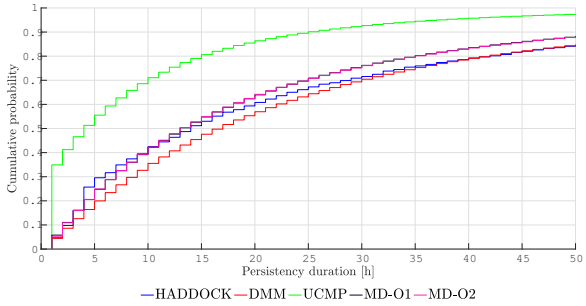

Figure F.3: The cumulative distribution of persistency for the North sea subject to a set operational limit of $T_p \leq 7$ s (Operation E).

F.2 New coding method: Workability

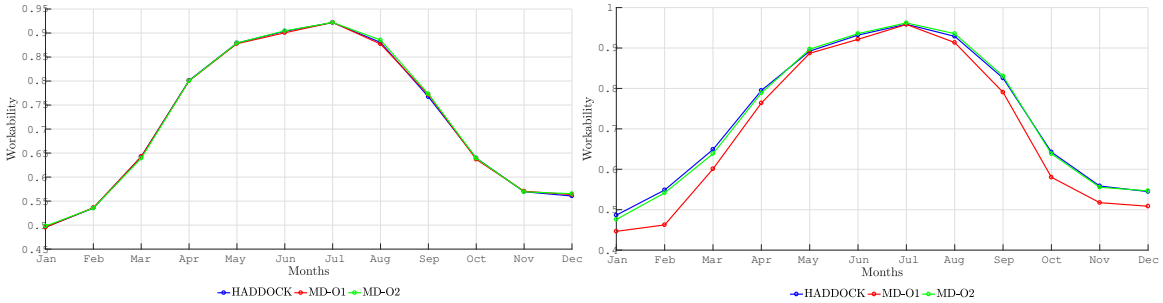

(a) Operation A **(b)** Operation B

Figure F.4: The workability throughout the year for the North sea subject to a set operational limit of $U \leq 10$ m/s (left) and $H_s \leq 2.5$ m (right).

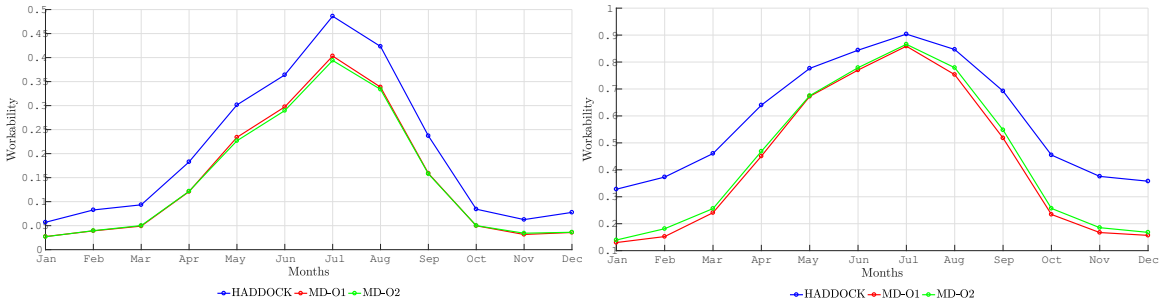

(a) Operation C **(b)** Operation D

Figure F.5: The workability throughout the year for the North sea subject to a set operational limit of $H_s \leq 1$ m, $U \leq 10$ m/s (left) and $H_s \leq 2$ m (right).

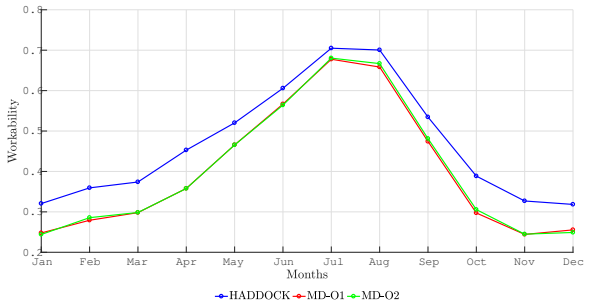

Figure F.6: The workability throughout the year for the North sea subject to a set operational limit of $T_p \leq 7$ s (Operation E).

F.3 Increasing Markov chain order: Persistency

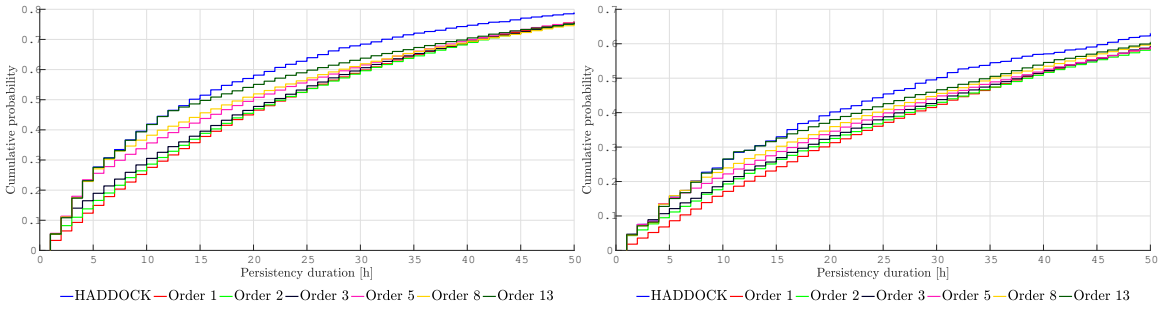

(a) Operation A **(b)** Operation B

Figure F.7: The cumulative probability distribution of the persistency based on Operation A and Operation B in Table 7.2 with the North sea dataset and start date 1-May.

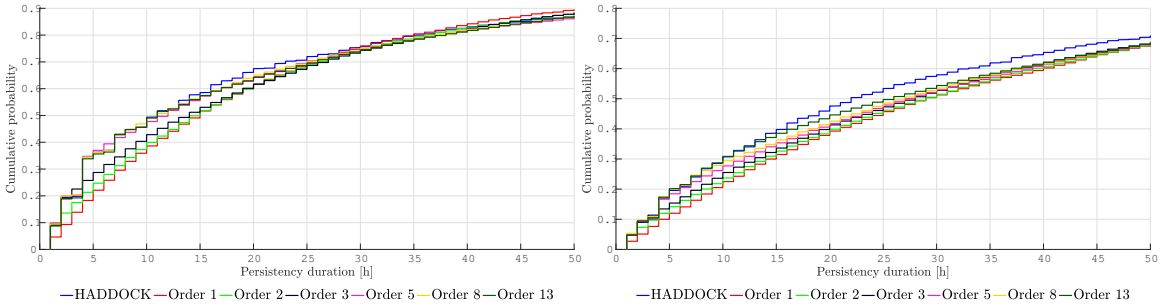

(a) Operation C **(b)** Operation D

Figure F.8: The cumulative probability distribution of the persistency based on Operation C and Operation D in Table 7.2 with the North sea dataset and start date 1-May.

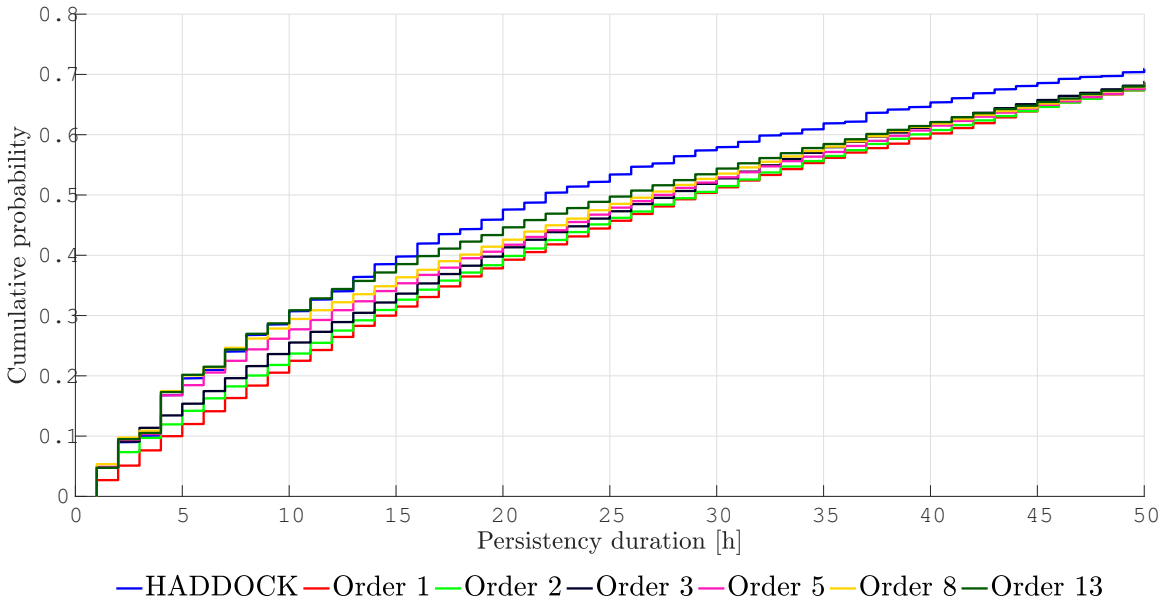

Figure F.9: The cumulative probability distribution of the persistency based on Operation E in Table 7.2 with the North sea dataset and start date 1-May.

Bibliography

[1] P. Ailliot, M. Prevosto, T. Soukissian, C. Diamanti, A. Theodoulides, C. Politis, et al. Simulation of sea state parameters process to study the profitability of a maritime line. In *The Thirteenth International Offshore and Polar Engineering Conference*. International Society of Offshore and Polar Engineers, 2003.

[2] D. Aldous and J. Fill. Reversible markov chains and random walks on graphs, 2002.

[3] K. Anastasiou and C. Tsekos. Operability analysis of marine projects based on markov theory. *Applied ocean research*, 18(6):329–352, 1996.

[4] T. W. Anderson and L. A. Goodman. Statistical inference about markov chains. *The Annals of Mathematical Statistics*, pages 89–110, 1957.

[5] A. H. S. Ang, A. A. Chaker, and J. Abdelnour. Analysis of activity networks under uncertainty. *Journal of the Engineering Mechanics Division*, 101(4):373–387, 1975.

[6] I. Babuska and J. T. Oden. Verification and validation in computational engineering and science: basic concepts. *Computer Methods in Applied Mechanics and Engineering*, 193(36):4057–4066, 2004.

[7] D. Bakan. *The test of significance in psychological research*. 66. Psychological Bulletin, 1966.

[8] P. Bartlett. *Introduction to Time Series Analysis. Lecture 3.* University of California, Berkeley., 2014.

[9] B. W. Boehm. Verifying and validating software requirements and design specifications. *IEEE software*, 1(1):75, 1984.

[10] L. E. Borgman and N. W. Scheffner. *Simulation of time sequences of wave height, period, and direction*. US Army Engineer Waterways Experiment Station, 1991.

[11] G. E. P. Box. All models are wrong, but some are useful. *Launer, RL*, 1979.

[12] G. E. P. Box, G. M. Jenkins, G. C. Reinsel, and G. M. Ljung. *Time series analysis: forecasting and control*. John Wiley & Sons, 2015.

[13] R. Castro. Lecture notes in applied statistics (tu eindhoven), lecture 1-introduction and the empirical cdf, 2013.

[14] D. R. DelBalzo, J. R. Schultz, and M. D. Earle. Stochastic time-series simulation of wave parameters using ship observations. *Ocean engineering*, 30(11):1417–1432, 2003.

[15] F. Douard, C. Domecq, and W. Lair. A probabilistic approach to introduce risk measurement indicators to an offshore wind project evaluation–improvement to an existing tool ecume. *Energy Procedia*, 24:255–262, 2012.

[16] G. D'Amico, F. Petroni, and F. Prattico. Wind speed and energy forecasting at different time scales: A nonparametric approach. *Physica A: Statistical Mechanics and its Applications*, 406:59–66, 2014.

[17] B. Efron. Missing data, imputation, and the bootstrap. *Journal of the American Statistical Association*, 89(426):463–475, 1994.

[18] C. K. Enders. Maximum likelihood estimation. *Encyclopedia of statistics in behavioral science*, 2005.

[19] S. Fouques, D. Myrhaug, and F. G. Nielsen. Seasonal modeling of multivariate distributions of metocean parameters with application to marine operations. *21st International Conference on Offshore Mechanics and Arctic Engineering*, 2, 2004.

[20] K. S. Hickmann, J. M. Hyman, and S. Y. Del Valle. Quantifying uncertainty in stochastic models with parametric variability. *arXiv preprint arXiv:1503.01401*, 2015.

[21] M. Hosseini, D. Pratas, and A. J. Pinho. A survey on data compression methods for biological sequences. *Information*, 7(4):56, 2016.

[22] Z. Huang and Z. S. Chalabi. Use of time-series analysis to model and forecast wind speed. *Journal of Wind Engineering and Industrial Aerodynamics*, 56(2-3):311–322, 1995.

[23] W. S. Jäger and O. Morales-Nápoles. A vine-copula model for time series of significant wave heights and mean zero-crossing periods in the north sea. *ASCE-ASME Journal of Risk and Uncertainty in Engineering Systems, Part A: Civil Engineering*, 3(4), 2017.

[24] O. D. Jimoh and P. Webster. The optimum order of a markov chain model for daily rainfall in nigeria. *Journal of hydrology*, 185(1-4):45–69, 1996.

[25] R. W. Katz. On some criteria for estimating the order of a markov chain. *Technometrics*, 23(3):243–249, 1981.

[26] R. L. Keeney. Decision analysis: an overview. *Operations research*, 30(5):803–838, 1982.

[27] M. C. Kennedy and A. O'Hagan. Bayesian calibration of computer models. *Journal of the Royal Statistical Society: Series B (Statistical Methodology)*, 63(3):425–464, 2001.

[28] U. Lall and A. Sharma. A nearest neighbor bootstrap for resampling hydrologic time series. *Water Resources Research*, 32(3):679–693, 1996.

[29] G. Leontaris, O. Morales-Nápoles, and A. R. M. Wolfert. Probabilistic scheduling of offshore operations using copula based environmental time series–an application for cable installation management for offshore wind farms. *Ocean Engineering*, 125:328–341, 2016.

[30] B. MacCartney. Nlp lunch tutorial: Smoothing, 2005.

[31] O. Makarynskyy, A. A. Pires-Silva, D. Makarynska, and C. Ventura-Soares. Artificial neural networks in wave predictions at the west coast of portugal. *Computers & Geosciences*, 31(4):415–424, 2005.

[32] A. Maria. Introduction to modeling and simulation. In *Proceedings of the 29th conference on Winter simulation*, pages 7–13. IEEE Computer Society, 1997.

[33] M. L. Menéndez, D. Morales, L. Pardo, and K. Zografos. Statistical inference for finite markov chains based on divergences. *Statistics & probability letters*, 41(1):9–17, 1999.

[34] V. Monbet, P. Ailliot, and M. Prevosto. Survey of stochastic models for wind and sea state time series. *Probabilistic engineering mechanics*, 22:113–126, 2007.

[35] V. Monbet and P. Marteau. Non parametric resampling for stationary markov processes: The local grid bootstrap approach. *Journal of statistical planning and inference*, 136(10):3319–3338, 2006.

[36] C. Z. Mooney. *Monte carlo simulation*, volume 116. Sage Publications, 1997.

[37] A. More and M. C. Deo. Forecasting wind with neural networks. *Marine structures*, 16(1):35–49, 2003.

[38] K. P. Murphy. *Machine learning: a probabilistic perspective*. MIT press, 2012.

[39] R. Nerzic, C. Frelin, M. Prevosto, V. Quiniou-Ramus, et al. Joint distributions of wind/waves/current in west africa and derivation of multivariate extreme i-form contours. In *The Seventeenth International Offshore and Polar Engineering Conference*. International Society of Offshore and Polar Engineers, 2007.

[40] F. Noé. Statistical inefficiency of markov model count matrices. *Preprint, http://publications. mi. fu-berlin. de/1699*, 2015.

[41] F. M. O'Carroll. Weather modelling for offshore operations. *The Statistician*, pages 161–169, 1984.

[42] S. D. Pethel and D. W. Hahs. Exact significance test for markov order. *Physica D: Nonlinear Phenomena*, 269:42–47, 2014.

[43] W. Press, S. Teukolsky, and W. Vetterling. B. flannery," numerical recipes in c, 1992.

[44] B. Rajagopalan, U. Lall, and D. G. Tarboton. Nonhomogeneous markov model for daily precipitation. *Journal of Hydrologic Engineering*, 1(1):33–40, 1996.

[45] J. Rip. Probabilistic downtime analysis for complex marine projects. Master's thesis, Delft University of Technology, December 2015.

[46] S. Robinson. Simulation model verification and validation: increasing the users' confidence. In *Proceedings of the 29th conference on Winter simulation*, pages 53–59. IEEE Computer Society, 1997.

[47] S. M. Ross. *Introduction to probability models*. Academic press, 2010.

[48] A. D. Şahin and Z. Şen. First order markov chain approach to wind speed modeling. *Wind Engineering and Industrial Aerodynamic*, 89(3-4):263–270, 2001.

[49] R. G. Sargent. Verification and validation of simulation models. In *Proceedings of the 37th conference on Winter simulation*, pages 130–143. winter simulation conference, 2005.

[50] K. A. Schouhamer Immink. Block-decodable runlength-limited codes via look-ahead technique. *Philips J. Res.*, 46(6):293–310, 1992.

[51] M. G. Scotto and C. Guedes Soares. Modelling the long-term time series of significant wave height with non-linear threshold models. *Coastal Engineering*, 40(4):313–327, 2000.

[52] B. Tan and K. Yilmaz. Markov chain test for time dependence and homogeneity: An analytical and empirical evaluation. *Elsevier*, 137(3):524–543, 2002.

[53] B. W. Taylor III, C. R. Bector, S. K. Bhatt, and E. S. Rosenbloom. *Introduction to management science, Module F: Markov Analysis*. New Jersey: Prentice Hall, 1996.

[54] H. Tong. Determination of the order of a markov chain by akaike's information criterion. *Journal of Applied Probability*, 12(03):488–497, 1975.

[55] A. C. Trahan. Effects of seasonality on the estimation of environmental extremes: A study of non-homogeneous methods for estimating environmental extremes. Master's thesis, Delft University of Technology, July 2013.

[56] G. van der Salm, S. Lucas, and B. Cezard. *Hydronamic metocean & data engineering presentation*. Royal Boskalis Westminster N.V., 2017.

[57] P. H. A. J. M. Van Gelder. *Statistical Methods for the Risk-Based Design of Civil Structures*. PhD thesis, Delft University of Technology, 2000.

[58] D. Vannak, M. S. Liew, and G. Z. Yew. Time domain and frequency domain analyses of measured metocean data for malaysian waters. In *Proceedings of World Academy of Science, Engineering and Technology*, page 670. World Academy of Science, Engineering and Technology (WASET), 2013.

[59] T. L. Walton Jr and L. E. Borgman. Simulation of nonstationary, non-gaussian water levels on great lakes. *Journal of waterway, port, coastal, and ocean engineering*, 116(6):664–685, 1990.

[60] D. S. Wilks and R. L. Wilby. The weather generation game: a review of stochastic weather models. *Progress in physical geography*, 23(3):329–357, 1999.

[61] W. Xie, B. Nelson, and R. Barton. Statistical uncertainty analysis for stochastic simulation. Technical report, Special Interest Group on Simulation and Modeling, 2014.

[62] X. Yang and Q. Zhang. Joint probability distribution of winds and waves from wave simulation of 20 years (1989-2008) in bohai bay. *Water Science and Engineering*, 6(3):296–307, 2013.

[63] J. Z. Yim, C. Chou, and P. Ho. A study on simulating the time series of significant wave heights near the keelung harbor. *The Twelfth International Offshore and Polar Engineering Conference*, 2002.

List of Figures

1 A 1st-order Markov chain example with 2 states and the transition probabilities P_{ij} . . . 2
2 The new breakdown of the DMM-model for complex marine projects based on Rip [45]. . . . 5

1.1 From deterministic to probabilistic project planning to project execution [45] 8
1.2 An example of how to get from an operational limit to a workability sequence 9
1.3 Hypothetical example of a single weather window project with a net duration of 4 time steps adopted from Rip [45] . . . 10
1.4 Hypothetical example of a complex project with a coupled operation 1 and uncoupled operation 2 and a warranty window provided for operation 3 [56] . 11
1.5 Hypothetical example of the cumulative distribution of downtime of a project (P50 and P80 indicated) . . . 12
1.6 Hypothetical example of the purpose of the DMM-model; by enlarging the dataset, the simulation uncertainty reduces . . . 13
1.7 Framework of the methodology of this thesis combined with the chapter layout. The red line indicates the same methodology can be applied for further research. The blue encircled numbers indicate the steps from above. 15

2.1 A first-order Markov chain example with 2 states and the transition probabilities P_{ij} . . . 18
2.2 2-Step schematization of transition probabilities from $X_t = 1$, hence the summation of the workable states equal $P_{11}^{(2)}$ and the summation of the non-workable states equal $P_{10}^{(2)}$ in Equation 2.8 . . . 21
2.3 Comparison between the piece-wise time homogeneous and the non-time homogeneous processes (with different bandwidths (h)) for the transition probability P_{01} extracted from Rip [45]. . . . 25
2.4 An example of two influence periods (D_1 and D_2) for an operational limit $H_s \leq 0.5$ m following operational limit $H_s \leq 1$ m; extracted from Rip [45] . 26
2.5 An exceedance probability curve of the influence period $D(H_s \leq 0.5$ m, $H_s \leq 1$ m) . . . 26
2.6 Schematizations of a type 1 (above) and a type 2 (below) parallel operations 28

2.7 By increasing the sample size n the maximum distance between $\hat{F}_n(x)$ and $L(x)$ or $U(x)$ decreases for multi α-values 30
2.8 Visual clarification of the DMM-model simulation procedure with a hypothetical project. 30
2.9 Breakdown of the DMM-model for complex marine projects extracted from Rip [45] 33

3.1 Classification of different types of uncertainty [57], with the main uncertainties of the DMM-model assigned to their corresponding uncertainty classification. 40

4.1 Schematized map of relation between real world, concept and computer model. Blue lines indicate how a model is built. Green lines indicate the verification phase. Red lines indicate the validation phase. 48
4.2 The cyclic software-testing process of the DMM-model. 49
4.3 Schematization of the verification process, where A B C D denote the different modules. 50
4.4 Schematization of the validation process, where A B C D denote the different modules. 51

5.1 Schematization of the non-existing transitions (indicated with the arrow) in between different years for the same month for the piece-wise time homogeneous method. The blue boxes depict workability sequences for January over multiple years. 54
5.2 Schematization of the non-workable influence period, where the periods D are defined by the passages of the 0/1 boundary of operation 1 and the 0/1 boundary of operation 2. 56
5.3 A hypothetical situation where the non-workable influence period overlaps the state that is generated by the cross-transition probability. 56
5.4 Hypothetical project simulation of a coupled operation and its succeeding operation, where the influence period should overlap the a generated state. 58
5.5 Schematization of the last transition of the month 59

6.1 The H_s, T_p scatter (left) and the sample autocorrelation (right) for the Gulf of Guinea dataset. 66
6.2 The H_s, T_p scatter (left) and the sample autocorrelation (right) for the Tasman sea dataset. 66
6.3 The H_s, T_p scatter (left) and the sample autocorrelation (right) for the North sea dataset. 66
6.4 Seasonality effects on both hemispheres presented with transition probability P_{01} subject to operational limit $H_s \leq 1.5$ m. Piece-wise time homogeneous method is indicated in blue and the non-time homogeneous method is performed with different kernel bandwidths h. 68

6.5 The workability percentage of the North sea dataset subject to an operational limit $H_s \leq 1$ m for non-time homogeneity and 1st-order measured for different bins of years. The whiskers of the box plot indicate the 95th percentiles and the red cross are its outliers. 75
6.6 The cumulative distribution of persistency for the North sea subject to an operational limit of $H_s \leq 1$ m and 1st-order and both homogeneity. 78
6.7 The cumulative distribution of persistency for the Gulf of Guinea subject to a set operational limit: $H_s \leq 1$ m with 1st-order and both homogeneities. . 82
6.8 The cumulative probability distributions of the downtime on the Gulf of Guinea dataset with start date January 1. The duration is computed with HADDOCK and with the DMM-model simulated 1000 years. 82
6.9 The cumulative probability distributions of the downtime on the North sea dataset with start date January 1. The duration is computed with HADDOCK and with the DMM-model simulated 1000 years. 83
6.10 The cumulative probability distributions of the downtime on the Tasman sea dataset with start date January 1. The duration is computed with HADDOCK and with the DMM-model simulated 1000 years. 83
6.11 H_s, T_p-scatter of a dataset that has been collected at the North sea $(53.91°N, 2.15°E)$. The red line indicates a combination of operational limits: ($H_s \leq 2$ m, $T_p \leq 7$ s), ($H_s \leq 1.5$ m, $T_p \leq 9$ s). 84
6.12 The cumulative probability distributions of the downtime on the given North sea dataset with start date January 1. The duration is computed with HADDOCK (original) and with the DMM-model simulated 1000 years. . . 85
6.13 Wave height modelled as a sinusoidal harmonic motion with three operational limits schematized for 1 day. 86
6.14 2-Hourly measured workability sequences per operational limit presented for 24 hours corresponding to Figure 6.13. 86
6.15 The persistency duration distribution of the original (hindcast) and DMM-model generated 1000 years datasets are presented for operation 2 (limit of $H_s \leq 2$ m). 87
6.16 The cumulative distribution of persistency for both 1000 years datasets with operational limit: $H_s \leq 1$ m. The 1000 years output is the regenerated workability sequence. 88

7.1 Exceedance probability of the influence period $D(H_s \leq 1$ m, $H_s \leq 2.5$ m) with a zoom in at the reasonably smallest influence period (approximately 5 hours) at an exceedance probability of 0.98. 92
7.2 A hypothetical project simulation with 2 operations (p and q), where operation q encounters the influence period. Method 1 denotes the reasonably smallest and method 2 denotes a randomly chosen influence period from the exceedance curve. 93

7.3 Increasing the Markov chain order the cumulative distribution of persistency converges to the hindcast data (persistency of 13 hrs). An operational limit of $H_s \leq 2$ m is used on the harmonic sinusoidal motion. 94
7.4 Increasing the Markov chain order the cumulative distribution of persistency converges to the hindcast data. An operational limit of $H_s \leq 2$ m is used on the North sea dataset. The red markers indicate the splitting points where the generated dataset splits off the hindcast dataset. 94
7.5 A hypothetical non-existing transition possibility, where the first state of the next month (February) is based on the last states of January with 8th-order. 95
7.6 A hypothetical workability sequence generation with 14th-order, with the result that every transition probability is equal to 1. Thus, hindcast data is exactly copied. 96
7.7 The cumulative probability distribution of the downtime on the North Sea dataset computed with HADDOCK, DMM-model and the improved DMM-model. 98
7.8 The cumulative probability distribution of the downtime on the Gulf of Guinea dataset computed with HADDOCK, DMM-model and the improved DMM-model. 98
7.9 The cumulative probability distribution of the downtime on the Tasman Sea dataset computed with HADDOCK, DMM-model and the improved DMM-model. 98
7.10 A hypothetical schematization of the project generation in the new coding method after step 3. 101
7.11 An hypothetical workability sequence for 2 operations to clarify the Markov dependency, where the transitions $1 \rightarrow 1$ are indicated with arrows. At these time steps the transition probabilities are determined for operation q. . . . 105
7.12 Time-shifting visualized for the Markov Dependency method, where backward-, no- and forward-shifting are indicated with blue, red and green brackets respectively. 106
7.13 The cumulative distribution of persistency for the North sea subject to a set operational limit of $U \leq 10$ m/s (left) and $H_s \leq 2.5$ m (right) 110
7.14 The cumulative probability distribution of the downtime, based on the project in Table 7.2 and the North sea dataset with start date 1-May. The durations are computed with HADDOCK, DMM, UCMP, MD-O1 and MD-O2 models. 111
7.15 Comparison between HADDOCK, MD-O1 and MD-O2 methods with the P50 and the P80 values, based on the hypothetical project in Table 7.2 and the North sea dataset. 112
7.16 The cumulative probability distribution of the downtime, based on the project in Table 7.2 and the North sea dataset with start date 1-December. The durations are computed with HADDOCK, MD-O1 and MD-O2 models. The P50 and P80 values indicated with green markers. 113

7.17 The cumulative probability distribution of the downtime based on the project in Table 7.2 and the North sea dataset with start date 1-May. 113
7.18 The bar chart per operation with the total downtime encountered of all the 1000 generated projects. 114
7.19 The cumulative probability distribution of the persistency based on Operation C in Table 7.2 with the North sea dataset and start date 1-May. 114

A.1 A schematization of the algorithm for constructing workability sequences of marine projects with the improved 'Downtime Modular Markov' model. . . 123
A.2 A schematization of the algorithm for constructing workability sequences of marine projects with the 'Updated Conditional Markov probabilities' method. 124
A.3 A schematization of the algorithm for constructing workability sequences of marine projects with the 'Markov Dependency' method. 125

C.1 Example of the derivation of N_{11}^{pq} 129
C.2 Clarification for Equation C.22 with an example of operations p and q . . . 132

D.1 Chi-squared distribution, with χ^2 on the x-axis and the p-value on the y-axis 138

E.1 Seasonality effects on both hemispheres presented with transition probability P_{01} subject to operational limit $H_s \leq 1.5$ m. Piece-wise time homogeneous method is indicated in blue and the non-time homogeneous method is performed with different kernel bandwidths h. 139
E.2 Seasonality effects in the Gulf of Guinea presented with transition probability P_{01} subject to operational limit $H_s \leq 1.5m$. Piece-wise time homogeneous method is indicated in blue and the non-time homogeneous method is performed with different kernel bandwidths h. 139
E.3 Exceedance probability of influence periods $D(p, q)$ for operational limit $H_s \leq 1$ m (left) and $H_s \leq 2$ m (right) in the North Sea 143
E.4 Exceedance probability of influence periods $D(p, q)$ for operational limits $H_s \leq 2.5$ m (left) and $U \leq 10$ m/s (right) in the North Sea 143
E.5 Exceedance probability of influence periods $D(p, q)$ for operational limit $T_p \leq 7$ s (left) and $H_s \leq 2$ m, $U \leq 10$ m/s (right) in the North Sea 144
E.6 The cross-transition probability P_{01}^{pq} of the hypothetical project in Table 6.3 presented over the year with monthly stationarity in the North sea (left) and the Tasman sea (right) 144
E.7 The cross-transition probability P_{01}^{pq} of the hypothetical project in Table 6.3 presented over the year with monthly stationarity in the Gulf of Guinea . . 144
E.8 The workability percentage of the North sea dataset subject to an operational limit $H_s \leq 1$ m for both (in)homogeneities and 1st-order measured for different bins of years. The whiskers of the box plot indicate the 95th percentiles and the red cross are its outliers. 145

E.9 The workability percentage of the North sea dataset subject to an operational limit $T_p \leq 6$ s for both (in)homogeneities and 1st-order measured for different bins of years. The whiskers of the box plot indicate the 95th percentiles and the red cross are its outliers. 145
E.10 The workability percentage of the North sea dataset subject to an operational limit $H_s \leq 2.5$ m for piece-wise time homogeneity and 1st-order measured for different bins of years. The whiskers of the box plot indicate the 95th percentiles and the red cross are its outliers. 146
E.11 The workability percentage of the Gulf of Guinea dataset subject to an operational limit $H_s \leq 1$ m for both (in)homogeneities and 1st-order measured for different bins of years. The whiskers of the box plot indicate the 95th percentiles and the red cross are its outliers. 146
E.12 The workability percentage of the Gulf of Guinea dataset subject to an operational limit $U \leq 5$ m/s for both (in)homogeneities and 1st-order measured for different bins of years. The whiskers of the box plot indicate the 95th percentiles and the red cross are its outliers. 147
E.13 The cumulative distribution of persistency for the Gulf of Guinea subject to a set operational limit with 1st-Order and both homogeneities. 147
E.14 The cumulative distribution of persistency for the North sea subject to a set operational limit with 1st-Order and both homogeneities. 147
E.15 The cumulative distribution of persistency for the North sea subject to an operational limit of $H_s \leq 2.5$ m, with 1st-Order and both homogeneities. . . 148
E.16 The cumulative distribution of persistency for the Gulf of Guinea subject to a set operational limit with confidence bands determined with an α-value of 0.05. 1st-Order and non-time homogeneity. 148
E.17 The cumulative distribution of persistency for the North sea subject to a set operational limit with confidence bands determined with an α-value of 0.05. 1st-Order and non-time homogeneity. 148
E.18 The cumulative distribution of persistency for the Gulf of Guinea subject to a set operational limit with confidence bands determined with an α-value of 0.05. 1st-Order and non-time homogeneity. 149
E.19 The workable persistency duration distribution of the original (hindcast) and DMM-model generated 1000 years datasets are presented for the operation the first three operations in the hypothetical project in Table 6.10. 149
E.20 The persistency duration distribution of the original (hindcast) and DMM-model generated 1000 years datasets are presented for the sinus subject to two operational limits. 149
E.21 The persistency duration distribution of the original (hindcast) and DMM-model generated 1000 years datasets are presented for the sinus subject to the limit of $H_s \leq 2.5$ m. 150

E.22 The workability percentage of the harmonic sinusoidal motion subject to an operational limit $H_s \leq 1.5$ m for piece-wise time homogeneity and 1st-order measured for different bins of years. The whiskers of the box plot indicate the 95th percentiles and the red cross are its outliers. 150

F.1 The cumulative distribution of persistency for the North sea subject to a set operational limit of $U \leq 10$ m/s (left) and $H_s \leq 2.5$ m (right). 151
F.2 The cumulative distribution of persistency for the North sea subject to a set operational limit of $H_s \leq 1$ m, $U \leq 10$ m/s (left) and $H_s \leq 2$ m (right). . . . 151
F.3 The cumulative distribution of persistency for the North sea subject to a set operational limit of $T_p \leq 7$ s (Operation E). 152
F.4 The workability throughout the year for the North sea subject to a set operational limit of $U \leq 10$ m/s (left) and $H_s \leq 2.5$ m (right). 152
F.5 The workability throughout the year for the North sea subject to a set operational limit of $H_s \leq 1$ m, $U \leq 10$ m/s (left) and $H_s \leq 2$ m (right). . . 152
F.6 The workability throughout the year for the North sea subject to a set operational limit of $T_p \leq 7$ s (Operation E). 153
F.7 The cumulative probability distribution of the persistency based on Operation A and Operation B in Table 7.2 with the North sea dataset and start date 1-May. 153
F.8 The cumulative probability distribution of the persistency based on Operation C and Operation D in Table 7.2 with the North sea dataset and start date 1-May. 153
F.9 The cumulative probability distribution of the persistency based on Operation E in Table 7.2 with the North sea dataset and start date 1-May. 154

List of Tables

2.1 Transition matrix of 2nd-order Markov chain 20
2.2 A hypothetical example of a 'workability-array', where the first column represents the time steps and all the other columns represent the binary workability sequences for all operations. 24
2.3 Workability states for a coupled operation 27

5.1 The amount of transition probabilities by varying the Markov chain order (first column) and the number of sequentially coupled operations (first row), which can be determined by $\mathcal{O}(4^{n+1})^u$. 58
5.2 Comparison of the numbered days in the DMM-model and reality 60
5.3 Summarized conclusions per module of the verification process 63

6.1 Summarized results of the seasonality (chi-squared) hypothesis tests, where NTH means non-time homogeneous and PWTH means piece-wise time homogeneous. 71
6.2 Summarized results of the order hypothesis tests, where the lowest order is reported in case the test was not rejected. The - denotes that all tests were rejected for orders 1 to 6. 71
6.3 The operations used for the white-box validation of the influence period and the cross-transition probability (Module C). 72
6.4 The simulation of 6 small hypothetical projects, wherein the other modules are adapted. Abbreviations: O = Order, PWTH = Piece-Wise Time Homogeneous, NTH = Non-Time Homogeneous, * = Coupled operation . . 73
6.5 The results of the χ^2 statistic test for the North sea dataset, with the homogeneous method and 1st Markov chain order. α-value of 0.05 is used for the test. 76
6.6 The results of RMSE for the workability of North sea and Gulf of Guinea datasets are given. Solely the homogeneous methods are regarded, with 1st-order Markov chain. 77
6.7 Statistic test results of the two-sample Kolmogorov-Smirnov test, with the datasets of the North sea and the Gulf of Guinea for several operational limits. 1st Markov chain order is used for all operations. The significance level is set on 5%. Abbreviations: PWTH = Piece-Wise Time Homogeneous, NTH = Non-Time Homogeneous, O = Original 78

6.8 The maximum distances of the two-sample Kolmogorov-Smirnov statistic test, with the datasets of the North sea and the Gulf of Guinea for several operational limits. Non-time homogeneity and 1st Markov chain order is used for all operations, * indicates homogeneous. 79
6.9 Planned installation cycle and operational limits on Pacific Orca with the warranty windows, extracted from Rip [45]. 80
6.10 Planned installation cycle and operational limits of a hypothetical project. . 84
6.11 The workability percentage and the persistency presented of the harmonic sinusoidal motion subject to the three operations of the hindcast data (HADDOCK) and only the workability percentage of the 1000 years generated with the DMM-model. 87
6.12 Summarized conclusions of the validation process 90

7.1 Workability states for 2 sequentially coupled operations (operation A and operation B) and the subsequent operation C. 96
7.2 A hypothetical project to validate the new coding method. 109
7.3 The settings belong to the hypothetical project from Table 7.2 to validate the new coding method. 109
7.4 The workability percentage per operation of the new coding method with the Updated Conditional Markov Probabilities (UCMP) and with the Markov Dependency (MD) compared with the hindcast data (HADDOCK). 109

C.1 The values of N_i^p,N_i^q and N_{ij}^{pq} for the sequence of Figure C.1 129

E.1 The results of the hypothesis chi-square test ($\alpha = 0.05$) for 7 different operational limits in the Gulf of Guinea with first-order Markov chain . . . 140
E.2 The results of the hypothesis chi-square test ($\alpha = 0.05$) for 7 different operational limits in the North sea with first-order Markov chain 140
E.3 The results of the hypothesis chi-square test ($\alpha = 0.05$) for 7 different operational limits in the Tasman sea with first-order Markov chain 141
E.4 The results of the hypothesis test ($\alpha = 0.05$) for 7 different operational limits in the Gulf of Guinea 141
E.5 The results of the hypothesis test ($\alpha = 0.05$ for 7 different operational limits in the Gulf of Guinea 141
E.6 The results of the hypothesis test ($\alpha 0.05$) for 7 different operational limits in the North sea 142
E.7 The results of the hypothesis test ($\alpha = 0.05$) for 7 different operational limits in the North sea 142
E.8 The results of the hypothesis test ($\alpha = 0.05$) for 7 different operational limits in the Tasman sea 142
E.9 The resulted p-values of the hypothesis test for 7 different operational limits in the Tasman sea 143